ISSN 1980-9743

Soils and Rocks Volume 34, N.2 2011

Soils and Rocks

Soils and Rocks

An International Journal of Geotechnical and Geoenvironmental Engineering

ABMS

G

Volume 34, N. 2
May-August 2011

SOILS and ROCKS

An International Journal of Geotechnical and Geoenvironmental Engineering

Editor André Pacheco de Assis - University of Brasilia, Brazil

Co-editor Ricardo Oliveira - COBA, Portugal

Soils and Rocks publishes papers in English in the broad fields of Geotechnical Engineering, Engineering Geology and Geo-environmental Engineering. The Journal is published in April, August and December. Subscription price is US$ 90.00 per year. The journal, with the name "Solos e Rochas", was first published in 1978 by the Graduate School of Engineering, Federal University of Rio de Janeiro (COPPE-UFRJ). In 1980 it became the official magazine of the Brazilian Association for Soil Mechanics and Geotechnical Engineering (ABMS), acquiring the national character that had been the intention of its founders. In 1986 it also became the official Journal of the Brazilian Association for Engineering Geology and the Environment (ABGE) and in 1999 became the Latin American Geotechnical Journal, following the support of Latin-American representatives gathered for the Pan-American Conference of Guadalajara (1996). In 2007 the journal acquired the status of an international journal under the name of Soils and Rocks, published by the Brazilian Association for Soil Mechanics and Geotechnical Engineering (ABMS), Brazilian Association for Engineering Geology and the Environment (ABGE) and Portuguese Geotechnical Society (SPG). In 2010, ABGE decided to publish its own journal and left the partnership.

Soils and Rocks

1978,	1 (1, 2)
1979,	1 (3), 2 (1,2)
1980-1983,	3-6 (1, 2, 3)
1984,	7 (single number)
1985-1987,	8-10 (1, 2, 3)
1988-1990,	11-13 (single number)
1991-1992,	14-15 (1, 2)
1993,	16 (1, 2, 3, 4)
1994-2010,	17-33 (1, 2, 3)
2011,	**34 (1, 2**

ISSN 1980-9743 CDU 624.131.1

ISSN 1980-9743

SOILS and ROCKS
An International Journal of Geotechnical and Geoenvironmental Engineering

Publication of
ABMS - Brazilian Association for Soil Mechanics and Geotechnical Engineering
SPG - Portuguese Geotechnical Society
Volume 34, N. 2, May-August 2011

Table of Contents

Articles

Soils and Rocks
v. 34, n. 2

Kinetic Mass Transfer Model for Contaminant Migration in Soils

Adriana de Souza Forster Araújo, Izabella Christynne Ribeiro Pinto Valadão,
José Adilson de Castro, Alexandre José da Silva, Elizabeth Ritter

Abstract. This work studied the transport phenomena in the soil of the Gramacho MSW landfill located in Rio de Janeiro, Brazil. A model was proposed to determine the mass transfer rate of the leachate contaminant ions to the soil particles. Previous researchers have focused on the diffusion and sorption phenomena using simple relations that do not completely explain the data of overall mass transfer obtained by laboratory experiments. Thus, this work proposes a modified rate equation implemented into MPHMTP software that takes into account the combined mechanisms of advection and diffusion in the leachate and sorption at the particle surface followed by diffusion in the interior of the soil particle. The model predictions were compared with laboratory-measured data and presented better agreement compared to those obtained using the commercial POLLUTE software.

Keywords: diffusion, sorption, chemical kinetic, leachate, landfill, mass transfer.

1. Introduction

In Brazil, the system of management for urban solid residue uses the landfill as an economically suitable solution for the final solid waste disposal. Landfill leachate is produced by the degradation of waste and the movement of rainwater that occurs within disposed layers. When it is drained from the landfill, the leachate contains dissolved and suspended materials that interact with soil particles, depending on the soil physical and chemical characteristics. The leachate properties vary depending on the waste and the age of the landfill, which makes it difficult to treat because it may contain many chemical compounds that, under the influence of natural agents (rain and microorganisms), generate contaminants that are difficult to mitigate.

According to some authors (Bear, 1972; Gelhar, 1993; Domenico & Schwartz, 1998; Fetter, 1999), the groundwater transport of contaminants has been one of the most important research topics in hydrology and engineering in the recent decades. Such studies aimed to find methodologies able to reduce possible social and ecological impacts due to waste disposal. To date, the fate of contaminants into soil is still receiving considerable attention due to the impact on several ecosystems.

The migration of contaminant ions into the soil is influenced by several processes that can be physical (advection and hydrodynamic dispersion), chemical (sorption, complexation and precipitation) and biological (degradation by biotic or abiotic factors). Several researchers have addressed the contamination phenomenon by different techniques (Goodall & Quigley, 1977, Rowe, 1988, Barone *et al.*, 1989, Schakelford & Daniel, 1991, Mitchell, 1994, Ehrlich *et al.*, 1994, Barbosa *et al.*, 1996, Boscov *et al.*, 1999, Leite & Paraguassu, 2002, Azevedo *et al.*, 2003). Mostly, the focus of these studies has been the pollutant transport mechanisms through artificial barriers or natural soil with the aims of elucidating the complex phenomena and developing new technologies to mitigate or minimize environmental impacts.

The study of contaminant transport into the soil has, so far, been carried out based on the assumption that hydraulic conductivity is the main phenomenon responsible for the infiltration of the contaminant. However, experimental investigations have evidenced that the molecular diffusion process is a significant transport mechanism and, for practical applications, cannot be neglected (Crooks & Quigley, 1984, Quigley *et al.*, 1987, Johnson *et al.*, 1989). Depending on the contaminant species, the chemical process may be relevant, and complex chemical reactions will take place. To take into consideration and identify the relevant phenomena coupled with fluid flow and mass transfer, comprehensive mathematical models have been developed. However, most of the models treat individual and simplified phenomena (Liu *et al.*, 2000). Therefore, mathematical formulations that consider complex transport mechanisms and chemical kinetics (Ehrlich and Ribeiro, 1995) have yet to be developed. In this paper a mathematical model to pre-

Adriana de Souza Forster Araújo, D.SC., Fellow of the National Post Doctorate/CAPES, Universidade Federal Fluminense, Volta Redonda, RJ, Brazil. e-mail: adriana@metal.eeimvr.uff.br.
Izabella Christynne Ribeiro Pinto Valadão, D.SC., Fellow of the National Post Doctorate/CAPES, Universidade Federal Fluminense, Volta Redonda, RJ, Brazil. e-mail: izabella@metal.eeimvr.uff.br.
José Adilson de Castro, Ph.D., Associate Professor, Universidade Federal Fluminense, Volta Redonda, RJ, Brazil. e-mail: adilson@metal.eeimvr.uff.br.
Alexandre José da Silva, Dr. Ing., Associate Professor, Universidade Federal Fluminense, Volta Redonda, RJ, Brazil. e-mail: ajs@metal.eeimvr.uff.br.
Elizabeth Ritter, D.SC., Associate Professor, Universidade do Estado do Rio de Janeiro, Rio de Janeiro, RJ, Brazil. ritter@uerj.br.
Submitted on April 30, 2010; Final Acceptance on October 27, 2010; Discussion open until December 30, 2011.

dict the mass transport within the landfill soil is proposed and validated with experimental data.

Studies carried out on the soil and leachate of the Gramacho Municipal solid waste (MSW) located at Duque de Caxias city, Rio de Janeiro State, Brazil, have considered only the mechanisms of sorption and diffusion of ions from leachate to the soil and vice versa (Barbosa, 1994; Ritter, 1998, Ritter *et al.*, 1999, Ritter & Campos, 2006). The experimental data from diffusion tests with non-reactive chloride and sodium ions and reactive potassium and ammonium ions have shown a good fit with the POLLUTE software (Rowe & Booker, 1994), which bases the calculations on isothermal sorption theory. In contrast, experiments carried out with calcium ion have not yielded a good fit, indicating that these mechanisms are not the predominant ones.

This research focuses on the transport process and aims to predict the kinetics of mass transfer in a landfill soil (Araújo, 2006). It is expected that phenomenological models will better reproduce the behavior of contaminants in these environments. A software termed MPHMTP (Multi Phase Heat and Mass Transfer Program), developed by Castro (2000), was used in this study. The software allows the implementation of transport equations of contaminants in the soil, taking into consideration the coupled mass transfer phenomena (advection, diffusion, sorption and chemical reactions).

The model proposed in this work was applied to the experimental data obtained by Ritter & Gatto (2003) and compared with simulation results presented by Pinto (2004).

2. Experimental Data

2.1. Experimental program history

The Gramacho Metropolitan Landfill occupies an area of 1.2 km^2 and is situated in a region of mangroves on the shores of the Guanabara Bay, close to the Sarapuí and Iguaçu rivers, over an organo-saline clay deposit, permanently submerged. The Gramacho MSW has been under recuperation since 1996, and several remediation actions to avoid contamination have been implemented. These actions are mainly a lateral channel that receives the leachate and a lateral trench, filled with the local organic clay, in the perimeter of the landfill, to compose a leachate collection system (Ritter & Campos, 2006). The trench was excavated very deeply to reach the local foundation organic clay. Tables 1 and 2 show, respectively, the experimentally determined parameters for the soil and leachate from the landfill (Barbosa, 1994, Ritter *et al,* 2004).

Previous studies emphasized the importance of salinity on the transport of contaminants through the landfill foundation (Barbosa, 1994 and Barbosa *et al.* 1996). It was identified by diffusion experiments with leachate that the leachate establishes a flow of chemical species in both directions (for the soil leachate and vice versa). Chloride, sodium, calcium and magnesium diffuse from soil to leachate because these ions have high concentrations in the saline organic soil (see Table 2); conversely, potassium has a higher concentration in the leachate compared to landfill soil. Barbosa (1994) evaluated the diffusion process in the soil of Gramacho's landfill using the software POLLUTE, where the effective diffusion coefficients of most important ions were estimated. It was verified that the Cl^- and SO_4^{2-} anions can be considered conservative species. The results for Na^+ and Mg^{2+}, assuming no sorption for these ions, agreed well with experimental data obtained in sorption and diffusion experiments carried on a laboratory scale. For K^+ and Ca^{2+}, using Pollute software, the model predictions showed large divergence from experimental ones, indicating that sorption theory may not be applicable to predict the migration of these ions.

Table 1 - Characterization of soil.

Fraction < 5 μm (%)	70
Moisture content (%)	140 a 170
Liquid limit (%)	167
Plasticity limit (%)	77
Porosity	~0.70 a 0.80
Density of grains	2.41
Plasticity index (PI) (%)	90

Table 2 - Chemical composition of the leachate and pore water.

Chemical analysis	Leachate	Pore water
pH	7.9	8.26
Conductivity ($mS.cm^{-1}$)	24.4	22.1
Cl^- ($mg.L^{-1}$)	4367	6105
Na^+ ($mg.L^{-1}$)	3089	4475
K^+ ($mg.L^{-1}$)	1681	543
NH_4^+ (mg/L)	1815	92
Ca^{+2} (mg/L)	203	365
Mg^{+2} (mg/L)	92	850

3. Model Formulation

In a multiphase flow, the chemical species are mixed, and thus, it is possible to describe the presence of each ion by its molar or mass fractions. A general transport equation that takes into account the contaminant concentration within the soil and leachate is presented by Eq. (1):

$$\frac{\partial(\rho_i \varepsilon_i \phi_k)}{\partial t} + \frac{\partial}{\partial x_j}(\rho_i \varepsilon_i u_j \phi_k) = \frac{\partial}{\partial x_j}\left(\Gamma_{\phi_k} \frac{\partial \phi_k}{\partial x_j}\right) + S_{\phi_k} \qquad (1)$$

The indexes i and k represent the phases and chemical species, respectively, while j indicates the spatial coordinates. ρ and u are the phase density and velocity components, respectively. Γ is the effective ion diffusion into the phase. ϕ_k is the mass fraction of the species, ε_i is the phase volume fraction of each phase, t is time and x is the spatial coordinate. A typical control volume showing the coexistence of both phases, solid and interstitial liquid, with their respective ions is schematically presented in Fig. 1a.

Equation (1) represents the mass conservation for each of the ions present in an individual phase, solid or liquid. The first term on the left side of the equation is the mass fraction accumulation rate, while the second one is the convective contribution due to phase motion. The first term on the right side is the contribution due to ion diffusion. S_{ϕ_k} is the so-called source or sink term, which accounts for ion exchange due to chemical and physical phenomena at the phase interfaces or within the phase by neutralization or chemical reactions. In this investigation, the source term is used to calculate the mass transfer from solid to liquid phases and vice-versa, including sorption, desorption and all other solid-liquid ion interactions.

To establish a consistent model of the ion transport in both phases, this investigation assumed that local equilibrium holds at the interfaces of solid and liquid leachate, and therefore, the ion exchange can be modeled by considering three distinct resistance steps to the mass transfer as follows: 1) transport of the contaminant in the liquid phase to the surface of the particle (advection, diffusion and dispersion), 2) sorption / desorption of the contaminant at the surface of the solid particle and 3) diffusion of the contaminant inside the particle of soil These three mechanisms are schematically shown in Fig. 1b, which represents an amplified view of the particle surface and the interactions of ions belonging to the solid particle and the interstitial liquid. As depicted in the Fig. 1b, the equilibrium concentrations of the ions in the particle and in the liquid boundary layer are not the same due to internal and external interactions. There exists a concentration gradient in the liquid phase, which forms a boundary layer, while another internal gradient is established in the vicinity of the particle surface. In the interior of the particle there are ions and compounds with the ability to attach or react with the contaminants and absorb them permanently or vice-versa. These phenomena can occur by physical or chemical affinity. To construct a model capable of quantifying these mass and ion transfers, it is important to image the equilibrium profiles of the contaminant concentration in the system and formulate transport resistances for each of these phenomena. Inside of the particles, the stationary diffusive phenomenon is predominant due to the concentration gradient imposed by near-surface interactions, and the parameter that controls this inner diffusion can be obtained by batch test equilibrium experiments, which characterize the particular system as solid-liquid. On the surface, which is in contact with the contaminant, advection and diffusion simultaneously occur, forming hydrodynamic and concentration boundary layers. At the interface, the sorption phenomenon occurs in the active sites. The solid particle geometry obviously affects the values of equilibrium concentrations in the solid liquid system.

To account for these phenomena, a rate equation that is able to account for the simultaneous resistance of the boundary layers and differences in the ion equilibria at the particle surface is presented in Eq. (2). According to this formulation, the source term can be modeled by introducing a coefficient or specific rate of transfer, β_f, which represents the specific rate proportional to the equilibrium driving force for ion transfer. This formulation is general and can represent several transport resistances, depending on the mass transfer coefficient formulation. In this investi-

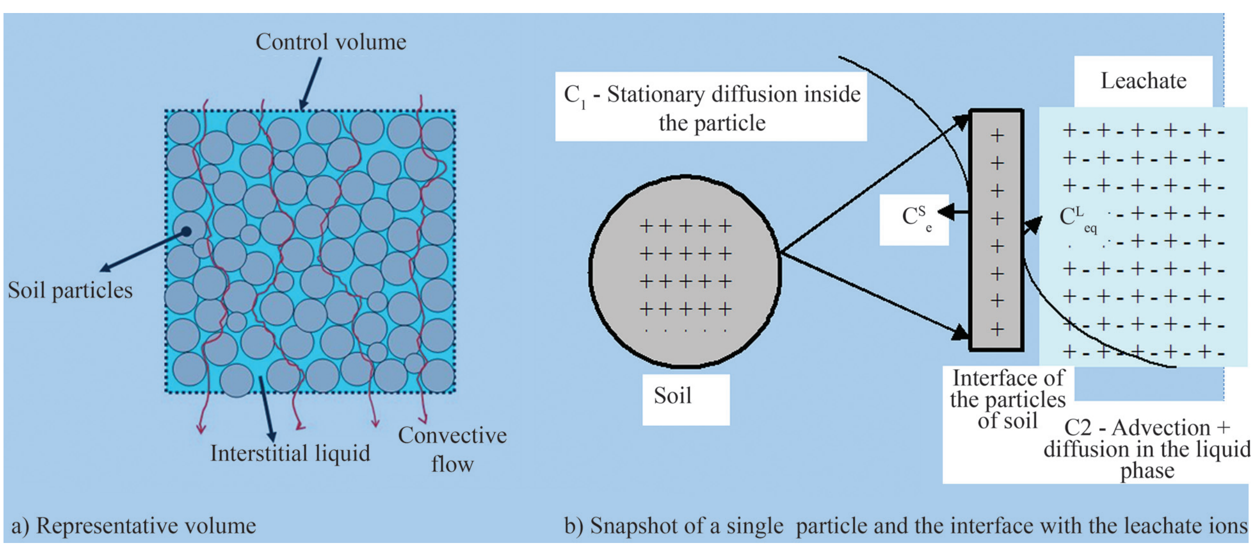

Figure 1 - Mechanism for the formulation of the kinetics of mass transfer of ions between the leachate and soil.

gation a kinetic rate constant is introduced to account for the mass transfer resistance at the particle surface and chemical control. This is equivalent to the linear sorption isotherm when the exponent of the driving concentration is unitary and the equilibrium concentration at the interface is constant. Thus, it is possible to consider a general isotherm formulation. Therefore, in this model, the general rate equation for mass transfer is proposed, as follows:

$$S_{\phi_k} = k_{\phi_k} \beta_{\phi_k} A_{s-l} [\rho_l \varepsilon_l][\phi_k - \phi_k^*]^n \quad (2)$$

where k_{ϕ_k} is the kinetic constant for the transfer of k ion, A_{s-l} is the interfacial area between solid and liquid, β_{ϕ_k} is the effective mass transfer coefficient of the k ion and ϕ_k^* is the interface equilibrium concentration of the k ion. The exponent coefficient in Eq. (2) represents a generalization for the description of the equilibrium behavior at the interface; in the particular case where $n = 1$ it will represent the classical formulation for the linear sorption rate. These parameters can be numerically optimized to reproduce the experimental data and thus can be used to predict temporal and spatial contamination profiles. The contact between solid particles and interstitial liquid and the effective mass transfer coefficient can be determined by Eqs. (3) and (4):

$$A_{s-l} = \frac{6\varepsilon_s}{d_s \phi_s} \quad (3)$$

$$\beta_{\phi_k} = \frac{Sh D_{\phi_k}^l}{d_s \phi_s} \quad (4)$$

in which, *Sh,* the Sherwood number, is given by

$$Sh = 1.17 (R_e)^{0.585} (Sc_{\phi_k})^{1/3} \quad (5)$$

with Reynolds and Schmidt numbers given by Eqs. (6) and (7),

$$R_e = \frac{\rho_l \varepsilon_l |\vec{U}_l - \vec{U}_s| (d_s \phi_s)}{\mu_l} \quad (6)$$

$$Sc_{\phi_k} = \frac{\mu_l}{\rho_l D_{\phi_k}^l} \quad (7)$$

The variables and symbols used in the above equations are listed in Table 3.

3.1. MPHMTP Software

The software (MPHMTP – Multi Phase Heat and Mass Transfer Program) was developed by Castro (2000), coded in Fortran 90/95. The software uses different module interfaces for input data, geometry construction, phase properties, boundary, initial condition settings and output data customizations. The rate transfer equations are implemented into a specific module with flexibility for user supply expression for rate transfer depending on the ion considered. The user interfaces are subroutines that must be implemented and customized by the user. The software solves the complete transport equation for a generic species or ion, and the transfer coefficients together with the source terms are calculated interactively by an external subroutine furnished by the user. The numerical solution is based on the Finite Volume Method (FVM), and the time integration is based on the fully implicit formulation (Patankar, 1985). The solution is obtained for a generalized coordinate system, which allows perfect adjustment of the calculation domain to complex geometries of the soil layers in the landfill. The discrete algebraic equations are solved using the ADI-TDMA algorithm (Alternate Direction Iteration Tri-Diagonal Matrix algorithm). The properties and source term definitions subroutine allows the user to consider every kind of media, such as non-uniform soil or different configurations of soils layers with different properties. In the source term module, the user can add new routines to calculate the local mass transfer rates of each control volume within the domain.

Table 3 - Variables and symbols used in the above equations.

Variables	Units	
ε_s		Solid phase volumetric fraction
ε_l		Liquid phase volumetric fraction
ds	m	Soil particles average diameter
φs		Soil particles form factor
β_{ϕ_k}	$m.s^{-1}$	Mass transfer coefficient
$D_{\phi_k}^l$	$m^2.year^{-1}$	Chemical species diffusion coefficient *i*, in the liquid phase
R_e		Reynolds number changed between the liquid and solid phases
Sc_{ϕ_k}		Schmidt number
ρ_l	$kg.m^{-3}$	Liquid phase density
U_l	$m.s^{-1}$	Velocity in the liquid phase
U_s	$m.s^{-1}$	Velocity in the solid phase
μ_l	Pa.s	Liquid phase viscosity

4. Results and Discussions

As discussed in the model features, experimental data were used to determine the model parameters accounting for the mass transfer phenomena. Two laboratory scale experiments were performed: the equilibrium batch tests and diffusion tests. The equilibrium experiments were used to determine the equilibrium concentration of each soil-leachate system. Using the MPHMTP software, the input parameters obtained from laboratory diffusion tests, the geometry of the experimental apparatus and the initial conditions, the simulations were carried out for each ion to obtain the best fit for the model parameters. Table 4 presents the results of the equilibrium tests and model parameters determined in this study. The results presented in Table 4 were obtained by iterative refinement until the numerical

Table 4 - Best fitting of model parameters obtained by numerical simulations.

Ion	k	ϕ_k^* (mg/L)	n	D_e (m^2/year)
Cl^-	$2*10^{-6}$	5372.4	1.05	0.064
Na^+	$3*10^{-9}$	5012.0	1.50	0.035
Ca^{+2}	$9.58*10^{-8}$	332.15	1.54 / 1.51	0.025
Mg^{+2}	$8*10^{-6}$	467.5	2.00	0.086
K^+	$1.05*10^{-5}$	434.4	1.32	0.062
NH_4^+	$2.50*10^{-2}$	754.4	1.75	0.062

and experimental results showed close agreement, with the exception of D_e, which assumed the values of D_0 for a free dilute solution in water (Lerman, 1979). Therefore, in this model effective diffusion coefficients were not used; on the contrary, all the effects of ions interactions with the media were regarded as source terms. This was done due to the ability of the model to deal with specific phenomena. This approach has the advantage of quantifying the separate process. In the numerical procedure, the criterion used to stop the calculations was the lowest global error for all species considered. The experiments were carried out for 72 h for diffusion cells and 48 h for bath equilibrium experiments. The model was used to reproduce the whole experimental procedure, and the final concentrations were compared for each ion prediction.

The model predictions were divided into reactive and non-reactive ones. The non-reactive ions can be accurately predicted by linear sorption isotherms, while the reactive ones usually present a complex behavior. This model was intended to show that both behaviors can be accurately predicted by this formulation.

4.1. Non-reactive ions

Figures 2a and 2b show the profiles of ion diffusion in the experimental Barone cell for Cl^- and Na^+, regarded as non-reactive ions for comparisons with experimental data and previous models used in POLLUTE software and sorption isotherms. In these figures are also shown the reference concentration values for soil and leachate that are assumed as initial conditions for the calculations. The POLLUTE software can predict only the soil domain; in contrast, the MPHMTP considers both connected domains, the soil and reservoir, and does not need to impose boundary conditions on the soil reservoir interface, as required by POLLUTE. This software feature avoids additional assumptions regarding the surface boundary conditions. Although in the case of non-reactive ions the formulations for both software are essentially the same, due to the more realistic treatment of the interface between soil and reservoir, the MPHMTP presents closer agreement with the experimental data considering both formulations, sorption isotherms (UFF sorption model) and present formulation (UFF kinetic model). Inside of the reservoir, the diffusion of ions occurs in free solution, and the ion concentration profile is determined by the diffusion into the liquid phase until the equilibrium condition is achieved at the soil reservoir interface. Although the liquid concentration gradients were not measured, the present model seemed to better reproduce the liquid concentration profile and did not present discontinuity in the interstitial liquid concentrations at the soil reservoir interface. For the chloride ion, the value of the effective diffusion coefficient (D_e) was assumed to be equal the diffusion coefficient in free solution (D_0) for ions in aqueous solution at 25 °C, according to the literature (0.064 m^2/year). In this

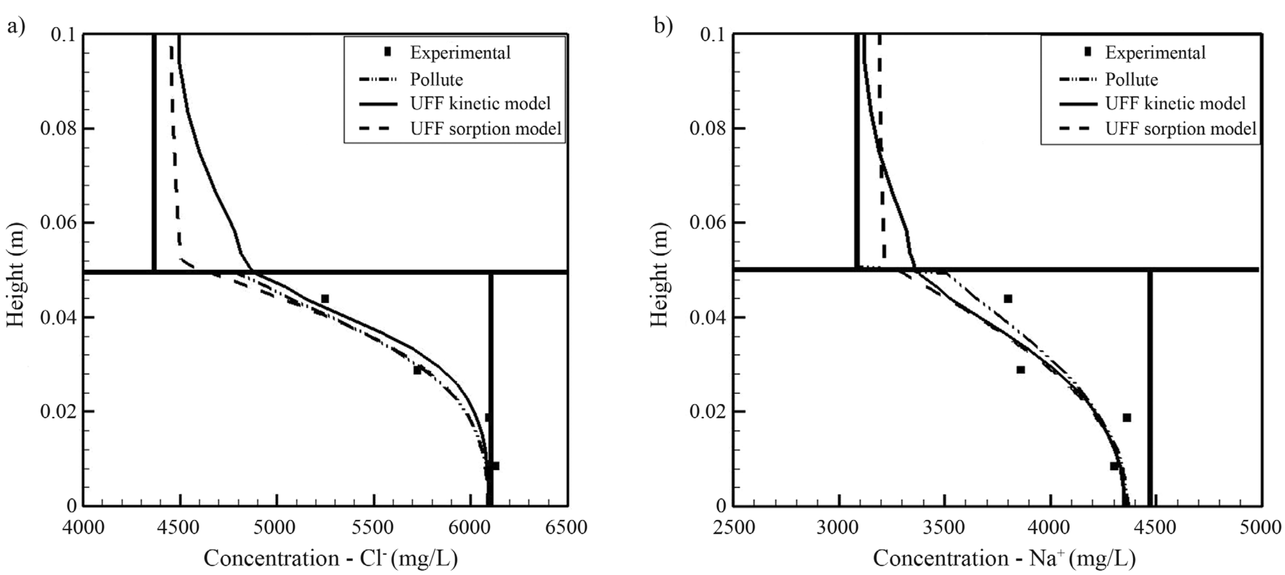

Figure 2 - Profile of molecular diffusion for chloride ions (a) and sodium (b) using the experimental results of 2003 (duration of test 72 h).

study the diffusion coefficient for sodium ions assumed the value of 0.035 m^2/year.

Figures 3 (a) and (b) show the comparison for model predictions and experimental data for the Ca^{2+} and Mg^{2+} ions. For both ions, the present model showed closer agreement with experimental measurements. The experimental measurements for Ca^{2+} showed an atypical behavior that cannot be represented by sorption isotherms and distribution coefficients, k_d, because the intrinsic solution for these models does not allows signal changes in the derivative of the concentration curves. This atypical behavior can only be traced by a kinetic model, as presented in this study. For the Mg^{2+} ion, all models presented the same pattern; however, the present model was able to get closer to the experimental results. An excellent agreement was obtained with the kinetic model, which is credited to its ability to consider local changes in the mass transfer rates depending upon local non-equilibrium conditions, which is not possible by constant effective diffusion coefficients formulations or retardations terms, as considered in the partition coefficients formulations such as k_d. The diffusion coefficients assumed those values for aqueous solution at 25 °C, according to the literature (0.025 m^2/year for Ca^{2+} and 0.086 m^2/year for Mg^{2+}). For these four ions, both the measured and calculated results indicated that the ions are transferred from soil to the leachate liquid because the landfill soil is rich in these ions and allows leaching phenomena, as can be observed in Figs. 2 and 3.

4.2. Reactive ions

The NH_4^+ and K^+ ions are usually referred to as reactive ones due to their typical behavior in the equilibrium batch tests. Figure 4 shows the profiles for ammonium (Fig. 4a) and potassium (Fig. 4b) with the soil and leachate reference values shown as constants, as used in the setting initial conditions for all models. It was observed that the mass transfer model presented better agreement with experimental measurements compared with both POLLUTE and UFF- sorption predictions. For both ions, the D_e value used in the simulation was 0.010 m^2/year for K^+ and 0.020 m^2/year for NH_4^+. In contrast to the ions presented in the last section, ammonium and potassium were transferred from the leachate to the soil with consequent contamination of the soil landfill.

Table 5 presents a comparison of values for the effective diffusion coefficients, D_e, used in the simulations and the reference values for the aqueous solution at 25 °C, D_0, according to the literature (Lerman, 1979). In this table, the D_e values estimated by Pinto, 2004 (UFF sorption model), by Ritter and Gatto (2003) using Pollute and by the present model are presented. Notably, the effective coefficients far from the reference values usually indicate strong interactions of the ions and the solid leachate system and usually cause larger deviations for the isotherm sorption models or distribution coefficients formulations. In this study, only Cl^- did not confirm this general trend because the experimental profile presented a typical behavior for diffusion-like phenomena; therefore, for this particular behavior it is always possible to represent the concentration curves by an equivalent solution of the diffusion equation, as the literature indicates (Incropera, & Wiit, 1990).

4.3. Transient results

Figures 5, 6 and 7 show the profiles of transient ion diffusion considered in the leachate and soil landfill used in this study. The figures present the temporal evolution of the concentration profiles numerically predicted (18, 36, 54 and 72 h). The numerical values at 72 h, which are coinci-

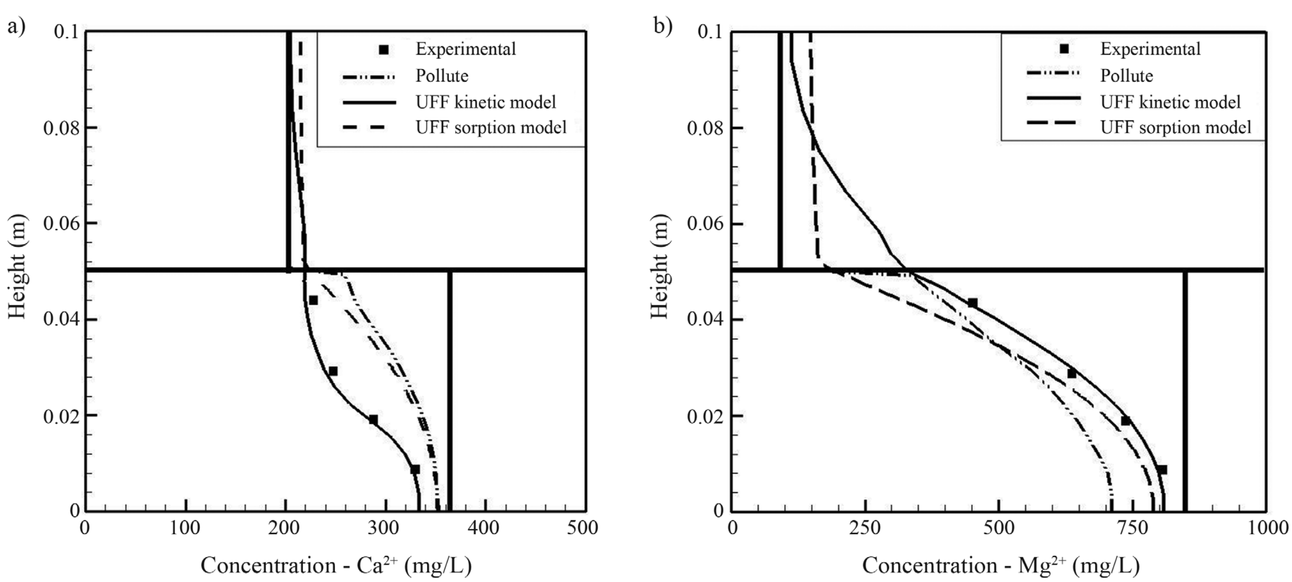

Figure 3 - Profile of molecular diffusion for calcium (a) and magnesium (b) ions using the experimental results of 2003.

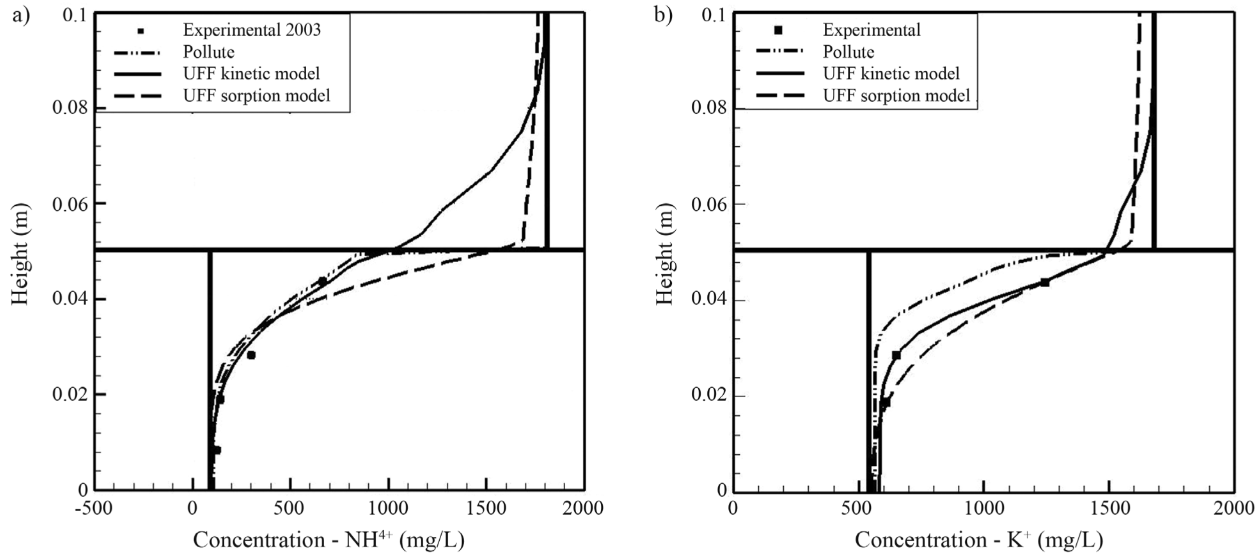

Figure 4 - Profile of molecular diffusion for ammonium ions (a) and potassium (b) using the experimental results of 2003.

Table 5 - Comparison of effective diffusion coefficients determined in this simulation: UFF sorption model, POLLUTE, present model and D_0 for ion in aqueous solution at 25 °C according the literature.

Ion	D_e (m²/year)[(a)]	D_e (m²/year)[(b)]	D_e (m²/year)[(c)]	D_0 (m²/year)[(d)]
Cl^-	0.020	0.020	0.064	0.064
Na^+	0.040	0.040	0.035	0.042
Ca^{+2}	0.040	0.040	0.025	0.025
Mg^{+2}	0.040	0.060	0.086	0.086
K^+	0.020	0.020	0.010	0.062
NH_4^+	0.010	0.070	0.020	0.062

(a) UFF-sorption (b) POLLUTE (c) Present model and (d) the diffusion coefficient in free solution (D_0) according to the literature.

dent with the measured time, were those used to validate the model. It is interesting to note the behavior of calcium, which indicated that the ion transfer mechanism changed with time, evidenced by the changing the sign of the curves derivatives. For Na^+, the experimental results showed larger variations probably due to inaccurate measurements; however, it was possible to get intermediate predictions across the measured results.

Figures 8 to 10 show the average concentration temporal evolution for interstitial leachate throughout the experimental procedure. The predicted results show the changes in ions concentrations with time and represent a measure of soil contamination with the ions and vice versa. It was observed that for Cl^- the concentration profile reached a saturation point during the experiment time, while the same was not predicted for Mg^{2+}, Ca^{2+} or Na^+.

Figure 9 shows the profiles of calcium (Fig. 9a) and sodium (Fig. 9b) ions, in which it can be noticed that stabilization was not achieved.

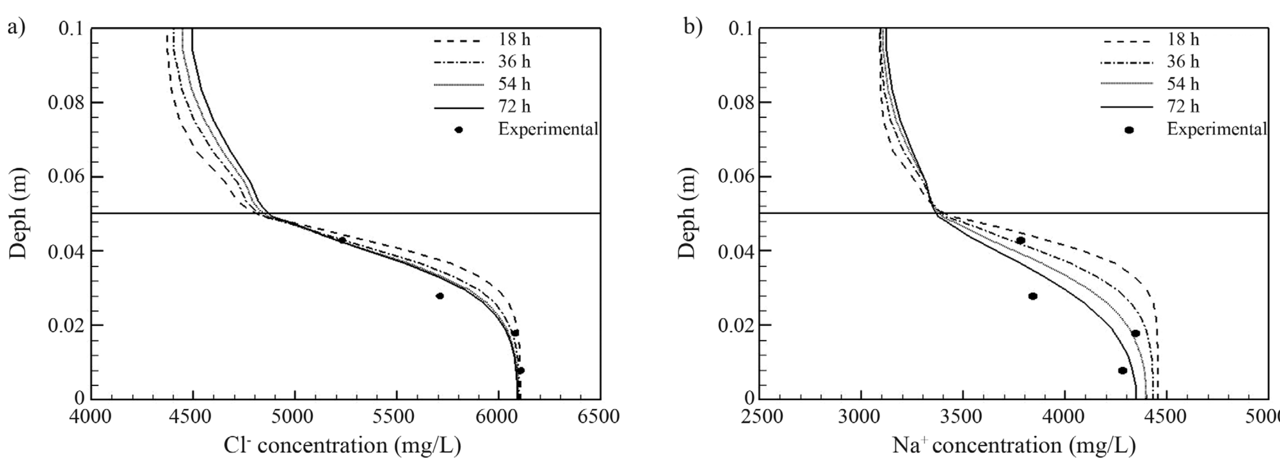

Figure 5 - Profile of transient molecular diffusion for chloride ions (a) and sodium (b) using 18, 36, 54 and 72 h for simulation.

In contrast to the above ions, for NH_4^+ and K^+, the concentrations in the soil increased with time, indicating that these ions were transferred from leachate to soil. For both ions, the model indicated that the experimental time was not sufficient to saturate the liquids.

According to the characterization tests of the soil from the Gramacho landfill (Ritter & Gatto, 2003), the ammonium and potassium ions are in lower concentration in the soil, and the soil has large capability to absorb this ions compared to calcium, sodium, chloride and magnesium.

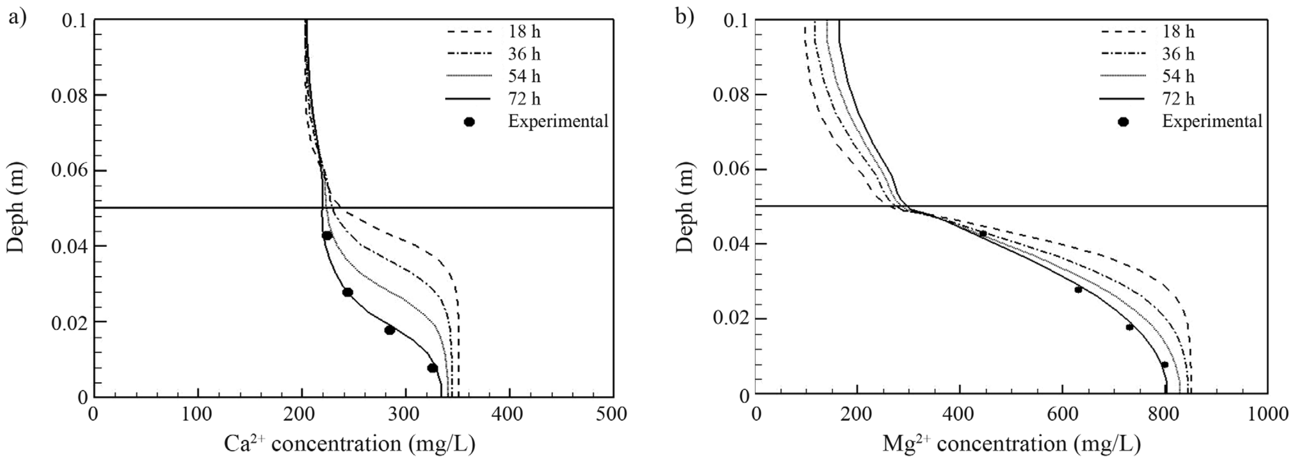

Figure 6 - Profile of transient molecular diffusion for calcium (a) and magnesium (b) ions using 18, 36, 54 and 72 h for simulation.

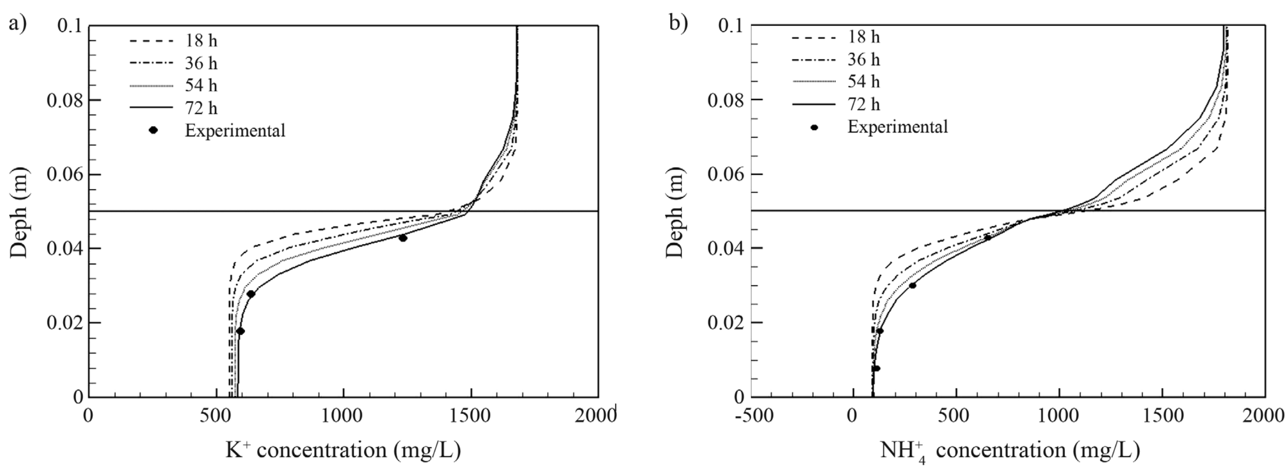

Figure 7 - Profile of transient molecular diffusion for potassium (a) and ammonium (b) ions using 18, 36, 54 and 72 h for simulation.

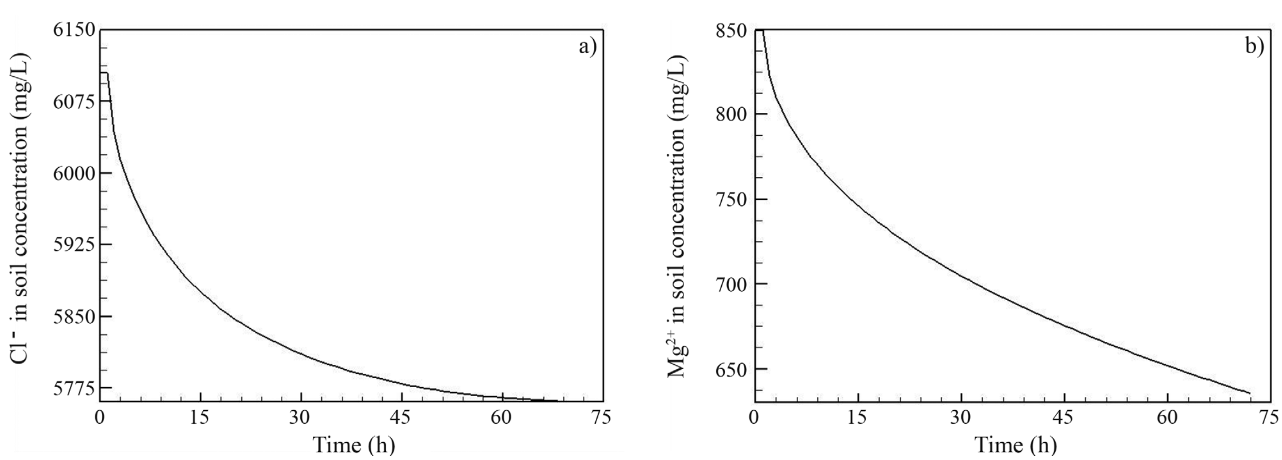

Figure 8 - Profile of concentration versus time for chloride (a) and magnesium (b) ions.

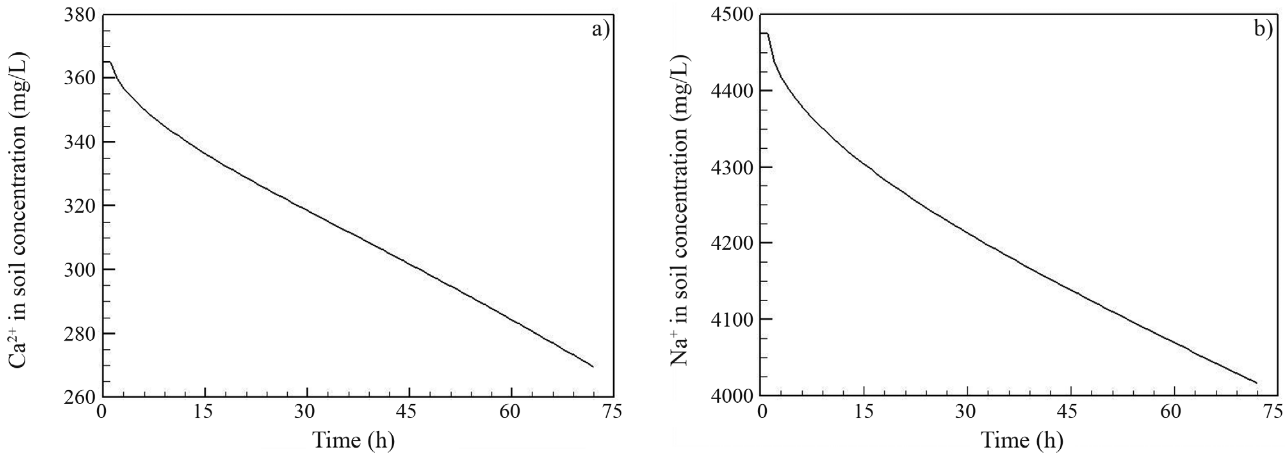

Figure 9 - Profile of concentration versus time for calcium (a) and sodium (b) ions.

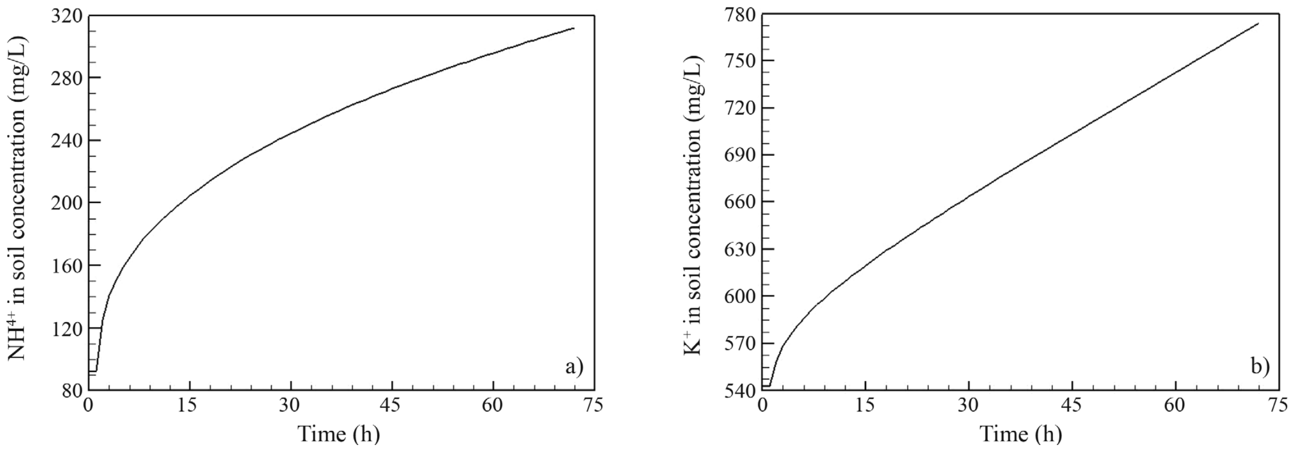

Figure 10 - Profile of concentration versus time for ammonium ions (a) and potassium (b).

Figures 11, 12 and 13 show the rate of mass transfer of the soil interstitial liquid to the soil particles for chloride, sodium and magnesium ions. The figures show the total rate of mass transfer (a) and in the medium point inside the experimental cell (b). For both ions, the rate of mass transfer rapidly increased at the beginning of the experiment and indicated that the maximum rate could not be achieved within the experimental time and that saturation conditions were beyond of the experimental time in this study.

In contrast with Cl^{+} and Na^{+}, presented in Figs. 11 and 12, the Mg^{2+} rate of mass transfer reached the maximum values and slowly decreased. However, the saturation con-

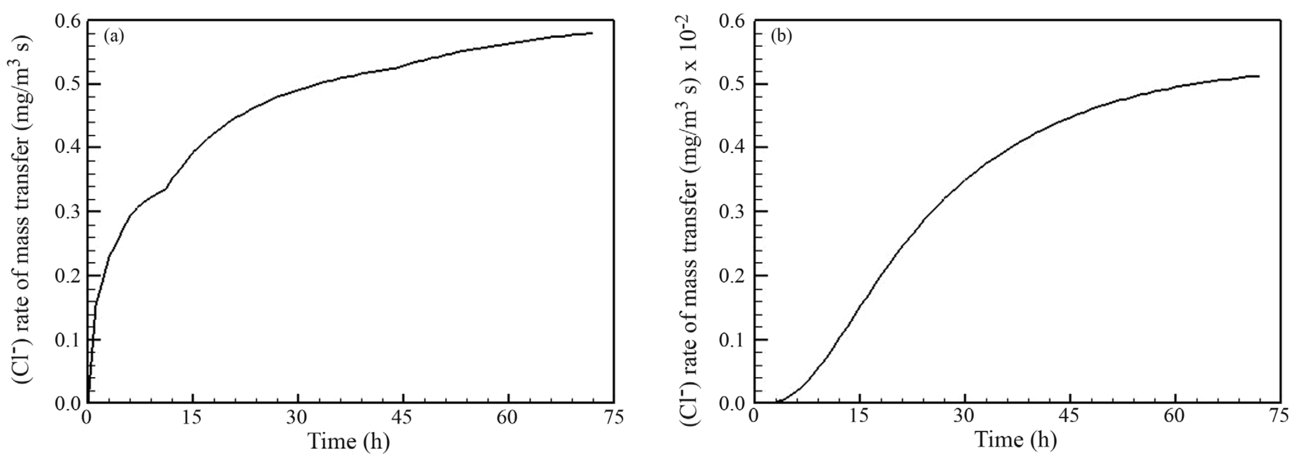

Figure 11 - Profile of the rate of mass transfer for the (a) total and (b) medium point for chloride ion.

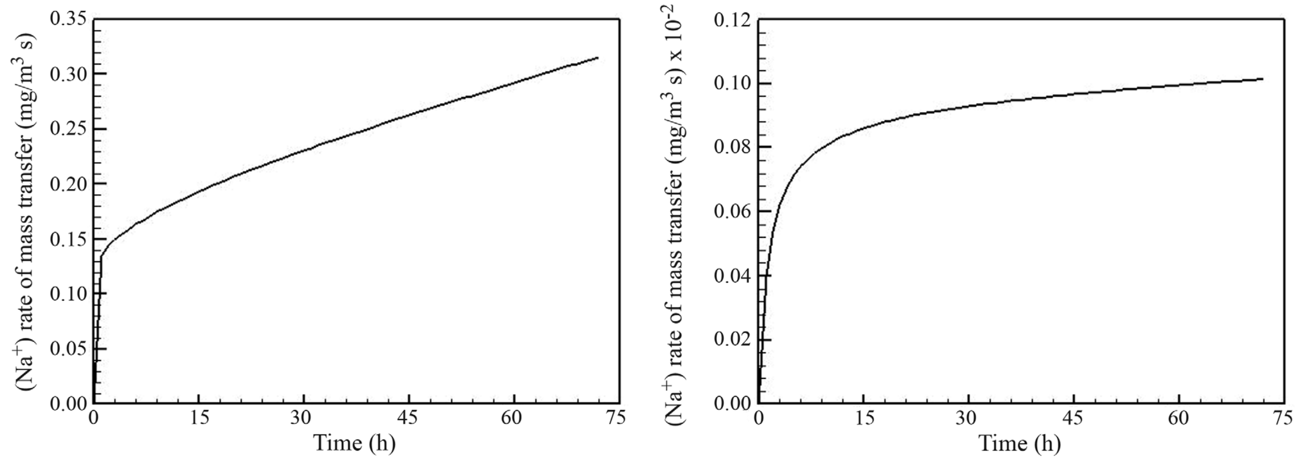

Figure 12 - Profile of the rate of mass transfer for the (a) total and (b) medium point for sodium ion.

centration was still beyond the experimental time considered in this study, although the results indicated that the beginning of the saturation process was achieved (Figs. 13a and 13b).

Figures 14 and 15 show the rate of mass transfer of the soil particles to the interstitial liquid for the ammonium and potassium ions. The figures show the calculated total mass transfer rate (a) and the rate at the point inside the experimental cell in the vicinity of the interface soil reservoir interface (b). It can be observed that, at the beginning of the calculation, the mass transfer rate was very rapid for NH_4^+ and the inversion point was rapidly achieved, initiating the saturation process. For K^+, the initial stage was also rapid, and almost linear growth was observed. For both ions, the saturation concentrations were not achieved in the interval of the experimental time.

The transient calculations presented in this section can be used to predict the long-term contamination profile, although it is not shown in this study. The rate of mass transfer predicted in these calculations could be used to estimate plume contamination within the soil landfills, and therefore it is a useful tool to analyze environmental impacts on the soil. The aim of this study was to estimate model parameters and confront model formulations with experimental measurements. Features of the model such as soil saturation time and plume contamination were not explored in this study. The next step of this study is under development and consists of the application of the formulation discussed here for large-scale landfills simulations. However, due to large computation times and a need to accurately represent large domains, the MPHMTP software is being improved by implementing parallel computation techniques suitable for use in a computer cluster, which will provide spatial and time-scale calculations compatible with landfills with reasonable computation times.

5. Conclusions

In this paper, a model based on mass transfer formulations was presented and discussed in light of previous models and experimental results for laboratory scale experimental procedures. The main features of MPHMTP (Multi-Phase Heat and Mass Transfer Program) were dis-

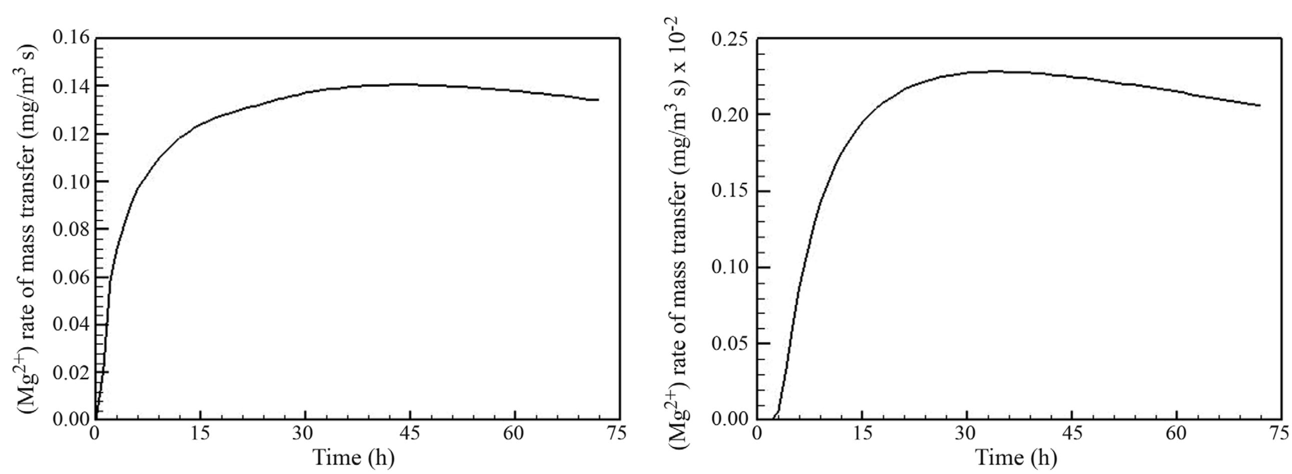

Figure 13 - Profile of the rate of mass transfer for the (a) total and (b) medium point for magnesium ion.

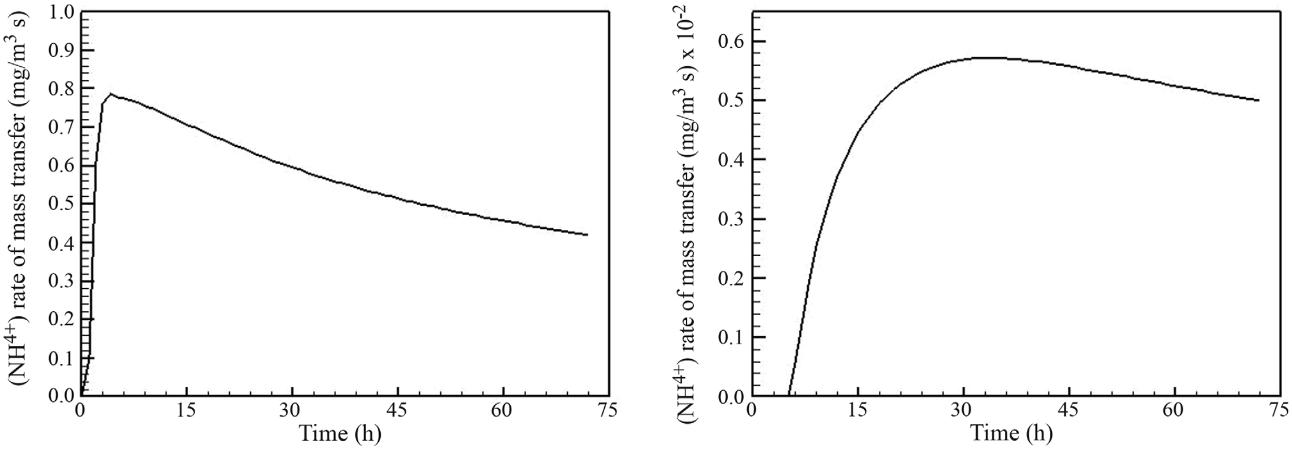

Figure 14 - Profile of the rate of mass transfer for the (a) total and (b) medium point for ammonium ion.

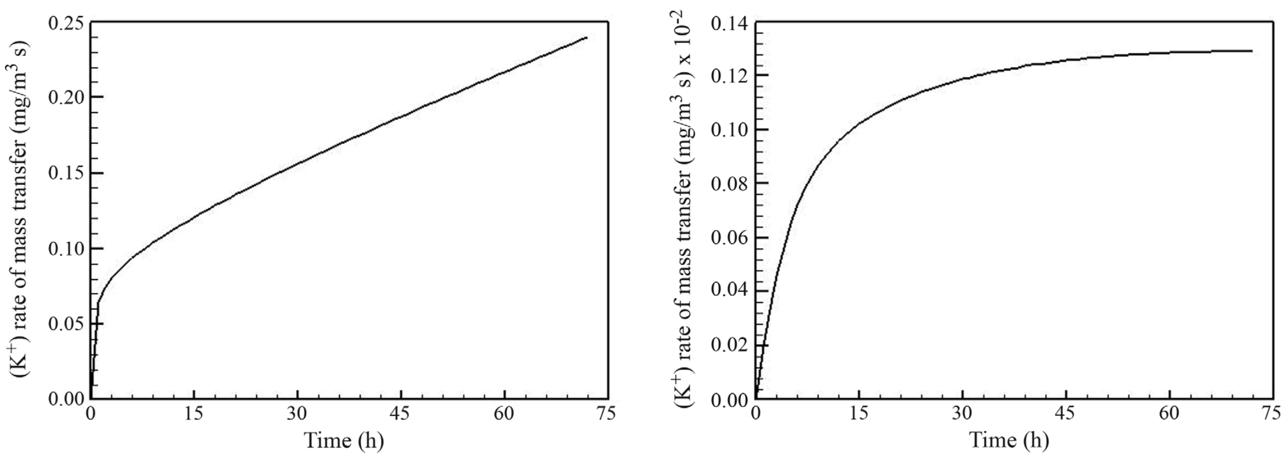

Figure 15 - Profile of the rate of mass transfer for the (a) total and (b) medium point for potassium ion.

cussed. The model was based on general transport equations of ions within the soil media and can handle several kinds of soil and barrier structures by considering the ion concentration evolution in both soil and interstitial liquids. The model predictions were compared to previous models and showed closer agreements with experimental data obtained in the Barone experimental cell using soil from the Gramacho landfill. As a baseline, the chloride, sodium, calcium, magnesium, ammonium and potassium ions were selected as representative of medium to high sorption rates in an organic soil such as that from the Gramacho landfill.

As a general trend, the model predicted results closer to the experimental measurements compared to the commercial POLLUTE software and a previously developed model based on distribution coefficients (UFF-sorption model). In the specific case of the calcium ion, strong agreement was observed regardless of the atypical behavior presented by this ion in the experimental measurements.

The results of the simulation carried out in this work confirmed that the migration process of inorganic ions from the leachate into the soil can be explained by taking into account three basic mechanisms: advection and diffusion in the liquid phase (leachate), sorption in the soil/leachate interface and diffusion in the soil particles. In contrast with previous models, this model accurately predicted the behavior of all ions presented in the diffusion experiments and showed potential for application to large time and spatial scale predictions of ion contamination in landfills.

Acknowledgments

The authors thank CAPES, CNPq and FAPERJ for financial support of this research.

References

Araújo, A.S.F. (2006) Simulação Computacional e Validação da Migração de Íons do Chorume no Solo Através de um Modelo Baseado nos Fenômenos de Transferência de Massa. Dissertação de Mestrado, Escola de Engenharia Industrial Metalúrgica de Volta Redonda, 100 pp.

Azevedo, I.C.D.; Nascentes, C.R.; Azevedo, R.F.; Matos, A.T. & Guimarães, L.M. (2003) Coeficiente de difusão hidrodinâmico e fator de retardamento de metais pesados em solo residual compactado. Solos e Rochas, v. 26:3, p. 229-249.

Barbosa, M.C. (1994) Investigação Geoambiental do Depósito de Argila sob o Aterro de Resíduos Sólidos de Gramacho-RJ. Tese de Doutorado, Programa de Engenharia Civil, Universidade Federal do Rio de Janeiro, 342 pp.

Barbosa, M.C.; Almeida, M.S.S. & Ehrlich, M. (1996) Ions diffusion through an organic saline clay soil. Proceedings of the Second International Congress on Environmental Geotechnics, Osaka, Japan, pp. 7-12.

Barone, F.S., Yanful, E.K., Quigley R.M. & Rowe, R.K. (1989) Effect of multiple contaminant migration on diffusion and adsorption of some domestic waste contaminants in a natural clay soil. Canadian Geotechnical Journal, v. 26, p. 189-198, 10.1139/t89-028.

Bear, J. (1972) Dynamics of Fluids in Porous Media. American Elsevier, American Elsevier Publishing Company, Inc., USA, 1972, 764 pp.

Boscov, M.E.; Oliveira, E.; Ghilardi, M.P. & Silva, M.M. (1999) Difusão de metais através de uma argila laterítica compactada. Proc. 4° Congressso Brasileiro de Geotecnia Ambiental, REGEO'99, São José dos Campos, pp. 323-330.

Castro, J.A. (2000) A Multi-Dimensional Transient Mathematical Model of Blast Furnace Based on Multi-Fluid Model. Ph.D. Thesis, Institute for Advanced Materials Processing, Tohoku University.

Crooks, V.E. & Quigley, R.M. (1984) Saline leachate migration through clay: A comparative laboratory and field investigation. Geotechnical Journal, Canadian, v. 21, p. 349-362, 10.1139/t84-035.

Domenico, P.A. & Schwartz, F.W. (1998) Physical and Chemical Hydrogeology. John Wiley & Sons, New York, 824 pp.

Ehrlich, M.; Almeida, M.S.S. & Barbosa, M.C. (1994) Pollution control of Gramacho Municipal landfill. Proc. First Int. Congress on Environmental Geotechnics, Edmonton, Canadá, pp. 657-664.

Ehrlich, M. & Ribeiro, S.G.S. (1995) Análise numérica da migração de contaminantes no solo utilizando um modelo hidrogeoquímico. Anais do III Simpósio sobre Barragens de Rejeitos e Disposição de Resíduos, REGEO'95, Ouro Preto, pp. 441-452.

EPA (1992) Batch-Type Procedures for Estimating Soil Adsorption of Chemicals. Technical Resource Document, 100 pp.

Fetter, C.W. (1999) Contaminant Hydrogeology. 2nd ed. Prentice-Hall, Upper Saddle River, 501 pp.

Gelhar, L.G. (1993) Stochastic Subsurface Hydrology. Prentice-Hall, Englewood Cliffs.

Goodall, D.C. & Quigley, R.M. (1977) Pollutant migration for two sanitary landfill site near Sarnia, Ontário. Canadian Geotechnical Journal, v. 14, p. 223-236, 10.1139/t77-023.

Incropera, F.P. & Wiit, D.P. (1990) Fundamentos de Transferência de Calor e de Massa. Livros Técnicos e Científicos Editora S.A., Rio de Janeiro, 494 pp.

Johnson, R.L.; Cherry, J.A. & Pankov, J.F. (1989) Diffusive contaminant transport in natural clay: a field example and implications for clay-lined waste disposal sites. Environmental Science Technology, v. 23:3, p. 340-349, DOI: 10.1021/es00180a012.

Kawasaki, N.; Kinoshita, H.; Oue, T.; Nakamura, T. & Tanada, S. (2004) Study on adsorption kinetic of aromatic hydrocarbons onto activated carbon in gaseous flow method. Journal of Colloid and Interface Science, v. 275:1, p. 40-43.

Leite, A.L. & Paraguassu, A.B. (2002). Diffusion of inorganic chemicals in some compacted tropical. Proc. IV International Congress on Environmental Geotechnics, IV ICEG, Rio de Janeiro, pp. 39-45.

Lerman, A. (1979) Geochemical Process. Water and Sediment Environments. John Wiley & Sons, New York, 481 pp.

Liu, C.; Szecsody, J.E.; Zachara, J.M. & Ball, W.P. (2000) Use of the generalized integral transform method for solving equations of solute transport in porous media. Advances in Water Resources, v. 23:5, p. 483-492.

Mitchell,J.K. (1994) Physical Barriers for waste containment. First International Congress on Environmental Geootechnics , Canada, pp. 951-961.

Patankar, S.V. (1985) Numerical Heat Transfer and Fluid Flow. Hemisphere Publishing Company, Washington, 197 pp.

Pinto, I.C.R. (2004) Modelamento e Simulação Computacional da Migração dos Íons do Chorume em Meio Poroso. Dissertação de Mestrado, Universidade Federal Fluminense, 81 pp.

Poirier, D.R. & Geiger, G.H. (1994) Transport Phenomena in Materials Processing, TMS, 509 pp.

Quigley, R.M.; Yanfull, E.K. & Fernandez, F. (1987). Ion Transfer by Diffusion Trough Clay Barriers. In: Geotechnical Practice for Waste Disposal'87. ASCE, Geot. Spec. Publication, nº 13, pp. 137-158.

Ritter, E. (1998) Efeito da Salinidade na Difusão e Sorção de Alguns Íons Inorgânicos em um Solo Argiloso Saturado. Tese de Doutorado, Universidade Federal do Rio de Janeiro, 229 pp.

Ritter, E.; Ehrlich, M. & Barbosa, M.C. (1999) Difusão e sorção em soluções simples e múltiplas em solos argilosos salinos e não salinos. Anais do IV Congresso Brasileiro de Geotecnia Ambiental, REGEO'99, São José dos Campos, pp. 331-338.

Ritter, E.; Leite, A E.B. & Machado, V.F. (2001) Avaliação da capacidade de mitigação da argila orgânica presente na fundação e nas valas de contenção lateral para o chorume gerado no Aterro Metropolitano de Gramacho

– Rio de Janeiro. Anais do XXVII Congresso Brasileiro de Engenharia Sanitária e Ambiental, João Pessoa, CD-Rom, 9 pp.

Ritter, E.; Campos, J.C. & Giordano, G (2002) Sorption of inorganic ions from leachateand organic soil of M.S.W. Gramacho Landfill. Proc. IV International Congress on Environmental Geotechnics, IV ICEG, Rio de Janeiro, pp. 165-170.

Ritter, E. & Gatto, R.L. (2003) Relatório Interno (PIBIC/UERJ), Rio de Janeiro.

Ritter, E.; Campos, J.C. & Gatto, R.L. (2004). The contamination level through an organic soil of Gramacho MSW. Proc ISC-2 on Geotechnical and Geophysical Site Characterization, Viana da Fonseca & Mayne (eds), Milpress, Rotterdam, pp. 1339-1343.

Ritter, E. & Campos, J.C. (2006) Avaliação da sorção e difusão molecular de íons inorgânicos do chorume e da argila orgânica do aterro metropolitano de Gramacho (RJ). Solos e Rochas, v. 29:1, p. 77-88.

Rowe, R.K. (1988) Contaminant migration through groundwater – The role of modeling in the design of barriers. Canadian Geotecchnical Journal, v. 25:4, p. 778-798.

Rowe, R.W. & Booker, J.R. (1983) Program POLLUTE – ID Pollutant Migration Analysis Program. Geotechnical Research Center, Faculty of Engineering Science, The University of Westem Ontario, London, Ont. Canadá.

Schackelford, C. & Daniel, D. (1991) Diffusion in saturated soil II: Results for compacted clay. Journal of Geotechnical Engineering, v. 117:3, p. 485-506.

Yagi, J.I. (1993) Mathematical modeling of the flow of four fluids in a packed bed. ISIJ International, v. 33:6, p. 619-639.

A Study on the Effects of MSW Fiber Content and Solid Particles Compressibility on its Shear Strength Using a Triaxial Apparatus

Sandro Lemos Machado, Mehran Karimpour-Fard

Abstract. It is commonly accepted that the shear strength of Municipal Solid Waste (MSW) is enhanced by the reinforcement effect of its fibrous constituents. However, most papers in the technical literature do not systematically evaluate the effect of the MSW fibers on its stress-strain-strength response. This paper presents results of a series of laboratory triaxial tests performed to evaluate the effect of the MSW fiber content and solid particle compressibility on its mechanical behavior. The variation in the MSW shear strength and shear strength parameters with fiber content and axial strain are analyzed, the effective parameters obtained from CD and CU tests are compared and the applicability of Terzaghi's equation for MSW materials discussed. Test results were used to calculate the Factor of Safety, FS, for some slope geometrical configurations and the results were used to create some charts relating FS, fiber content and the slope geometry. The authors believe this subject could be of interest to landfill management companies, especially considering the new trend in plastic material recycling for energy recovery purposes.

Keywords: MSW, MSW fibers, solid particles compressibility, shear strength, triaxial tests, slope stability.

1. Introduction

The stress-strain-strength response of Municipal Solid Waste (MSW) is a matter of concern for the design and operation of landfills as well as when post-closure behavior and re-use or mining of old landfills areas are considered. It is commonly stated that MSW can stand very high values of shear stress due to the reinforcement effect of the fibrous materials it contains (Kavazanjian *et al.* 1999, Athanasopoulos *et al.* 2008). However, the number of papers that have systematically evaluated the effect of the fibrous waste components on the MSW mechanical response of MSW is limited.

Landava and Clark (1990), as a part of their extensive work, performed direct shear tests using a large apparatus with horizontal dimensions of 434 x 287 mm. According to their findings, the shear strength of old waste is clearly higher than that of fresh waste. They concluded that the low strength of fresh waste, which was shredded, was because fibrous and elongated particles have been found to align themselves in a horizontal direction, which is coincident with the shearing plane in direct shear tests. The presence of these sliding planes led to a reduction in the MSW shear strength. In the case of natural and old waste, there is no preferential alignment of the fibers which results in higher shear strengths.

Kölsch (1995) stated that triaxial and direct shear tests do not describe adequately the MSW shearing behavior, because in these test arrangements the anisotropy of waste is not sufficiently recorded. To quantify the tensile strength of MSW and evaluate the reinforcement characteristics of MSW materials, he developed an equipment for tensile test which was enable to apply tensile stress to MSW samples by pulling one half of the box and increasing the horizontal deformation slowly until the applied tensile force reaches a maximum. Typical results of tensile tests on MSW samples can be visualized in Fig. 1. In this figure the slope of the envelopes represents the angle of internal tensile forces. The higher this angle, the higher the reinforcement component in shearing behavior of MSW. As can be observed in this graph, the angle of internal tensile forces in the case of fresh waste is lower than aged waste, which could be attributed to the higher fiber content in old waste due to decomposition processes.

Zekkos (2005) performed large triaxial tests on the MSW materials from San Francisco bay and showed that the effect of the waste composition on the stress-strain-strength response of the MSW materials is significant. He also reported the results of large direct shear tests performed on the same materials by (2005) and showed that the type of mechanical response of MSW materials is dependent on the shear mechanisms. According to Georgiopoulos (2005), the direction of the fibers inside the samples could affect the mechanical response of these materials during shearing. In the case of samples in which the direction of the fibers were perpendicular to the shear plane, the response was similar to the samples sheared in triaxial apparatus, showing an upward concavity in their stress-strain

Sandro Lemos Machado, Ph.D., Associate Professor, Departamento de Ciência e Tecnologia de Materiais, Universidade Federal da Bahia, Salvador, BA, Brazil. e-mail: smachado@ufba.br.
Mehran Karimpour-Fard, Visiting Researcher, Departamento de Ciência e Tecnologia de Materiais, Universidade Federal da Bahia, Salvador, BA, Brazil.
Submitted on June 8, 2010; Final Acceptance on November 23, 2010; Discussion open until December 30, 2011.

curves due to the reinforcement effect of the fibrous material (Fig. 2).

In a similar work, Athanasopoulos *et al.* (2008) performed several large direct shear tests on MSW materials with varying fiber directions and concluded that the optimum angle of fiber which leads to a higher shear strength is 60 degrees, taking the horizontal plane as reference (Fig. 3).

Despite these valuable contributions, the number of experimental works focusing on the effect of the fiber content on the mechanical response of MSW remains incipient. One of the first attempts in this field was performed in the Geo-environmental Laboratory at the Federal University of Bahia (GEOAMB) by Karimpour-Fard (2009) using a large triaxial apparatus which is presented in the following sections.

2. Materials, Apparatus and Experimental Work

The MSW samples used in this research were collected at the disposal front of the Metropolitan Center

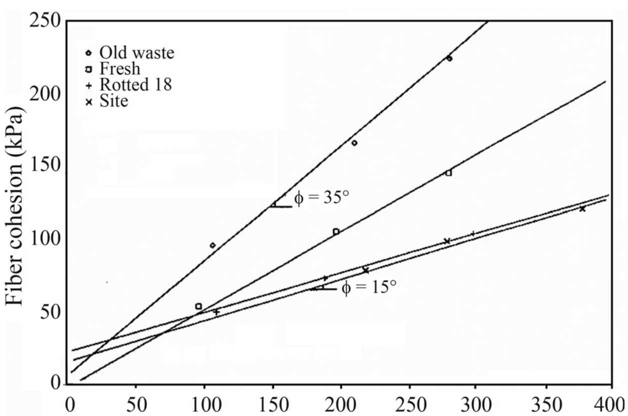

Figure 1 - MSW cohesion due to fiber reinforcement effect. Kölsch (1995).

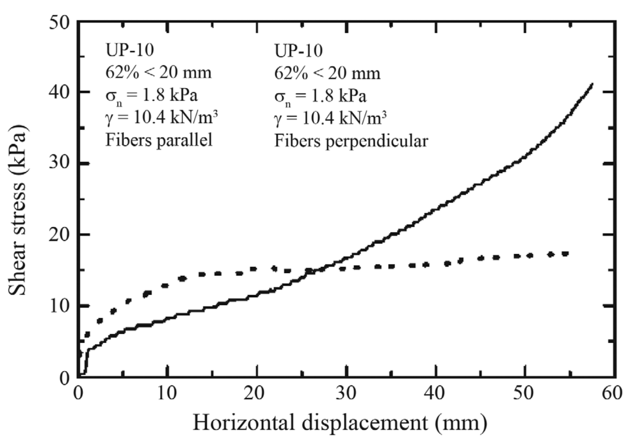

Figure 2 - The effect of the direction of the fibers on the mechanical response of MSW materials Georgiopoulos (2005).

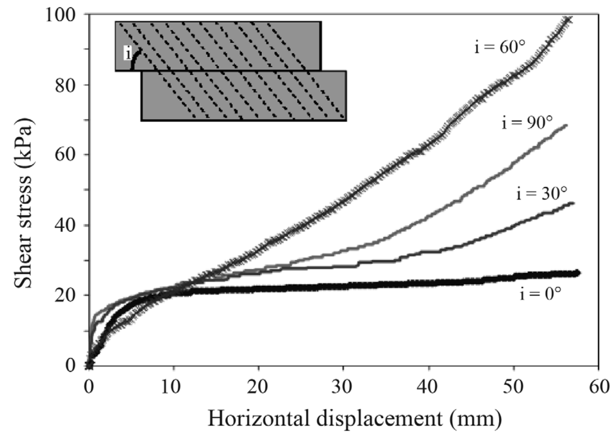

Figure 3 - Changing the shear strength of MSW materials with variation in the direction of the fibers, Athanasopoulos *et al.* (2008).

Landfill, MCL, located approx. 20 km from Salvador. The results of the composition analysis of the MSW in the MCL according to the reports represented by GEOAMB in March 2010, are presented in Table 1.

As can be observed, the main elements which could act as a reinforcement element, plastic and textiles, make up about 25% of all the waste (dry basis). Other planar elements such as paper and cardboard, sometimes referred to as the fiber elements in the literature, in this research were assumed paste material as as having a negligible influence on MSW reinforcement.

This is justified by the high water content found in this material (around 100%, dry basis) which leads to a loss of tensile strength of such waste components. All the samples used in this work can be considered as fresh waste with a negligible soil content. Considering the data presented in Table 1 and the considerations made above, the maximum fiber content used in the compacted samples was assumed to be 25% by dry weight.

The water content of samples used in this work varied from 115 to 125%. Particles larger than 5 cm were removed from the waste or were reduced in size. Figure 4 illustrates the stages of sampling and treatment.

Considering a maximum fiber content of 25%, intermediate fiber contents of 12.5, 6.25 and 0 percent were chosen to compact the samples. To reach the desired value of fiber content in each sample the first step was to remove all the plastics and textiles from the MSW. After that, the desired amount of fibers was added to the waste, which was mixed and homogenized in order to obtain the samples to be used in the tests.

Figure 5 shows the apparatus used and the preparation steps of the sample. As can be seen, a large triaxial test apparatus was used to evaluate the mechanical behavior of the MSW materials. This apparatus includes a loading frame with a capacity of 300 kN and a set of hardware and software to perform stress/strain controlled triaxial tests. The

Table 1 - The composition of fresh MSW material in MCL (Machado *et al.*, 2010).

Component	Average composition – dry basis			Average composition – wet basis		
	Average (%)	S.D. (%)	Cov.	Average (%)	S.D. (%)	Cov.
Wood	5.92	3.04	0.51	5.19	3.39	0.65
Stone/Ceramic	10.89	6.56	0.60	5.88	3.84	0.65
Textile	3.66	1.78	0.49	4.19	2.25	0.54
Rubber	0.44	0.45	1.01	0.29	0.27	0.95
Plastic	20.11	4.92	0.24	18.74	3.99	0.21
Glass	3.78	1.55	0.41	1.65	0.75	0.46
Metal	2.90	1.59	0.55	1.49	0.71	0.48
Paper/Cardboard	17.12	5.17	0.30	19.70	4.27	0.22
Paste	35.18	6.64	0.19	42.86	7.27	0.17

S.D. : Standard Deviation, Cov. : Coefficient of variance.

size of the triaxial chamber and the nominal size of the samples were 50x100 and 20x35 cm, respectively. Samples were compacted statically to reach a nominal density of 8 kN/m^3 similar to that obtained in field after waste disposal. The loading frame was used to compress the samples to the height of 30 cm. Samples were left pressed for 2 h and then released to rebound. The height of the samples at the end of the process was about 35 cm.

A test program was scheduled based on the short and long term behavior of MSW materials so both drained and undrained tests were carried out to evaluate the effect of the fiber content on the waste shear strength. Table 2 lists the tests performed.

Samples were saturated with water. The saturation techniques used were upward flow (using an effective confining pressure of 10 kPa) and back-pressure. The flow stage lasted for a minimum of two hours until stationary flow was reached. The back-pressure technique used confining pressure increments of 50 kPa and a minimum value of B = 0.9 was adopted.

After saturation, the samples were consolidated until a negligible rate of volume change was observed. To correct the cross section of the samples after consolidation, a non-isotropic deformation assumption was used (Eq. (1)),

Figure 4 - Sample preparation (a) Sampling (after quartering, particles larger than 5 cm were removed) (b) removing plastic and textiles (c) and (d) cutting and processing the particles larger than 5 cm.

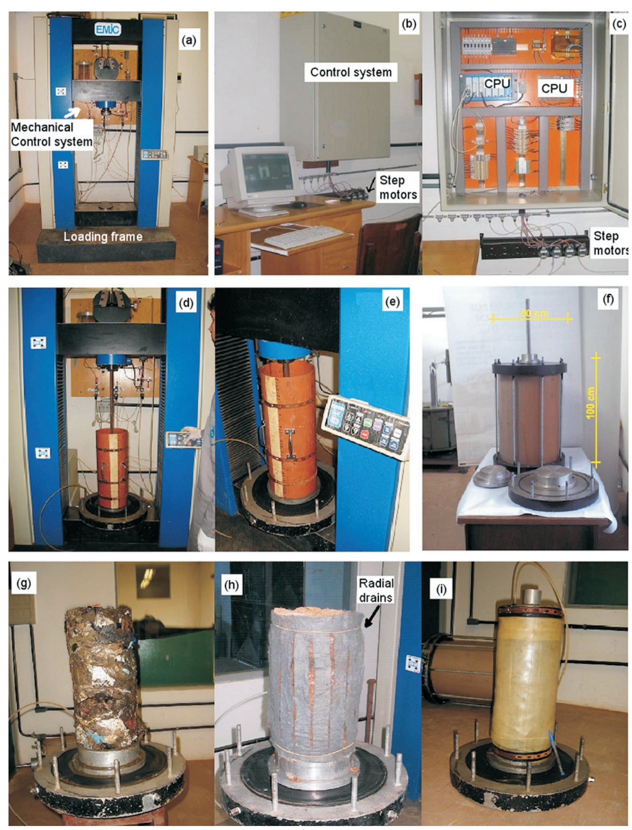

Figure 5 - (a) Loading frame (b) and (c) control system (d) and (e) compacting the sample (f) triaxial chamber (g) sample after compaction (h) Radial geotextile drains (i) sample before test.

Table 2 - List of performed tests.

No.	Test type	F.C. (%)	$\Delta\sigma_3$ (kPa)	γ_0 (kN/m^3)
1	TX-CD	0	50	8.4
2	TX-CD	0	150	8.55
3	TX-CD	0	300	8.32
4	TX-CU	0	50	8.32
5	TX-CU	0	150	8.42
6	TX-CU	0	300	8.15
7	TX-CD	6.25	50	8.26
8	TX-CD	6.25	150	8.23
9	TX-CD	6.25	300	8.38
10	TX-CU	6.25	50	8.44
11	TX-CU	6.25	150	8.48
12	TX-CU	6.25	300	8.46
13	TX-CD	12.5	50	8.05
14	TX-CD	12.5	300	8.41
15	TX-CU	12.5	50	8.32
16	TX-CU	12.5	300	8
17	TX-CD	25	50	7.83
18	TX-CD	25	300	8.1
19	TX-CU	25	50	8.52
20	TX-CU	25	300	8.12

TX. Triaxial Test, CD. Consolidated-Drained. CU. Consolidated-Undrained, F.C. Fiber Content. $\Delta\sigma_3$. Consolidation stress, γ_0. Initial density.

as suggested by Shariatmadari *et al.* (2009) who used samples collected at the same place.

The recorded volume changes during the consolidation phase were used in conjunction with the changes in the sample height (measured using the free length of the loading ram) to calculate the sample radial strain and the sample cross section prior to shearing. According to the authors, the ratio of axial to radial strain (which should be equal to one in isotropic materials) varied from 1.65 to 3.48, with an average of 2.4. This means that the assumption of isotropic deformation leads to a smaller cross section and therefore to higher values of axial stress and shear strength. In Eq. (1) ε_r, ε_a and ε_v are the radial, axial and volumetric strains, respectively.

$$\varepsilon_r = 1 - \sqrt{\frac{1-\varepsilon_V}{1-\varepsilon_a}} \tag{1}$$

The apparatus shown in Fig. 5 had two different chambers to measure volume change. The rst chamber (chamber No. 1), common in triaxial apparatus, measures the changes in the volume of water inside the samples (or the changes in the volume of the samples, in the case of saturated specimens with incompressible particles). The second one, chamber No. 2, connected to the conning stress water supply line, was used to measure the overall sample volume change (please refer to Fig. 6).

In the case of the second chamber, the measured volume values were corrected in order to take into account the triaxial cell deformation. Triaxial cell deformation was small compared to the volume change of the samples even for low conning pressures. Chamber 2 always showed higher volume changes than chamber 1 and this difference was believed to be due to the compressibility of the waste particles.

Tests were performed using a loading rate of 0.8 mm/min. The shearing phase lasted until the sample reached 30% of axial strain. Tests were performed according to procedures suggested by Head (1986) and ASTM D4767 (2004).

3. Results and Analysis

Figures 7 and 8 present the results of the triaxial tests performed using confining pressures of 50 and 300 kPa. As can be observed, almost all the curves are concave upward, without presenting any evidence of rupture, which is in agreement with the results presented by researchers such as Grisolia & Napoleoni (1995), Jessberger & Kockel (1993), Carvalho (1999), Machado *et al.* (2002, 2008), Towhata *et al.* (2004), Zekkos (2005), Nascimento (2007) and Karimpour-Fard (2009). With increasing fiber content, the MSW shear strength increased in both drained and undrained tests. Although not shown in this paper, even in the case of the use of the maximum obliquity criteria, $(\sigma'_1/\sigma'_3)_{max}$, it is not possible to detect failure of the MSW samples.

Analyzing Fig. 8b it is possible to observe that the pore water pressure at the end of the shearing phase is almost equal to the confining stress. These results are similar to those obtained by Carvalho (1999) and Nascimento (2007). On the one hand, this means that if the effective stress equation proposed by Terzagui is used, the effective confining stress will approach zero. Despite this, however, the samples continue to present strain hardening, and absolutely no evidence of liquefaction can be found in the tests results. On the other hand, the use of the Terzaghi equation in such conditions leads to very high friction angles and almost null cohesion intercepts which is physically contradictory with the ability of the samples to sustain high deviatoric stress levels in almost unconfined conditions.

Shariatmadari *et al.* (2009) analyzed the results obtained from drained and undrained triaxial tests and concluded that the compressibility of the MSW particles leads to a contact area that is not negligible compared to the total cross section area of the samples, which is the most important assumption of Terzaghi's effective stress equation. According to the authors, instead of the effective stress equation proposed by Terzaghi, Eq. (2) originally proposed

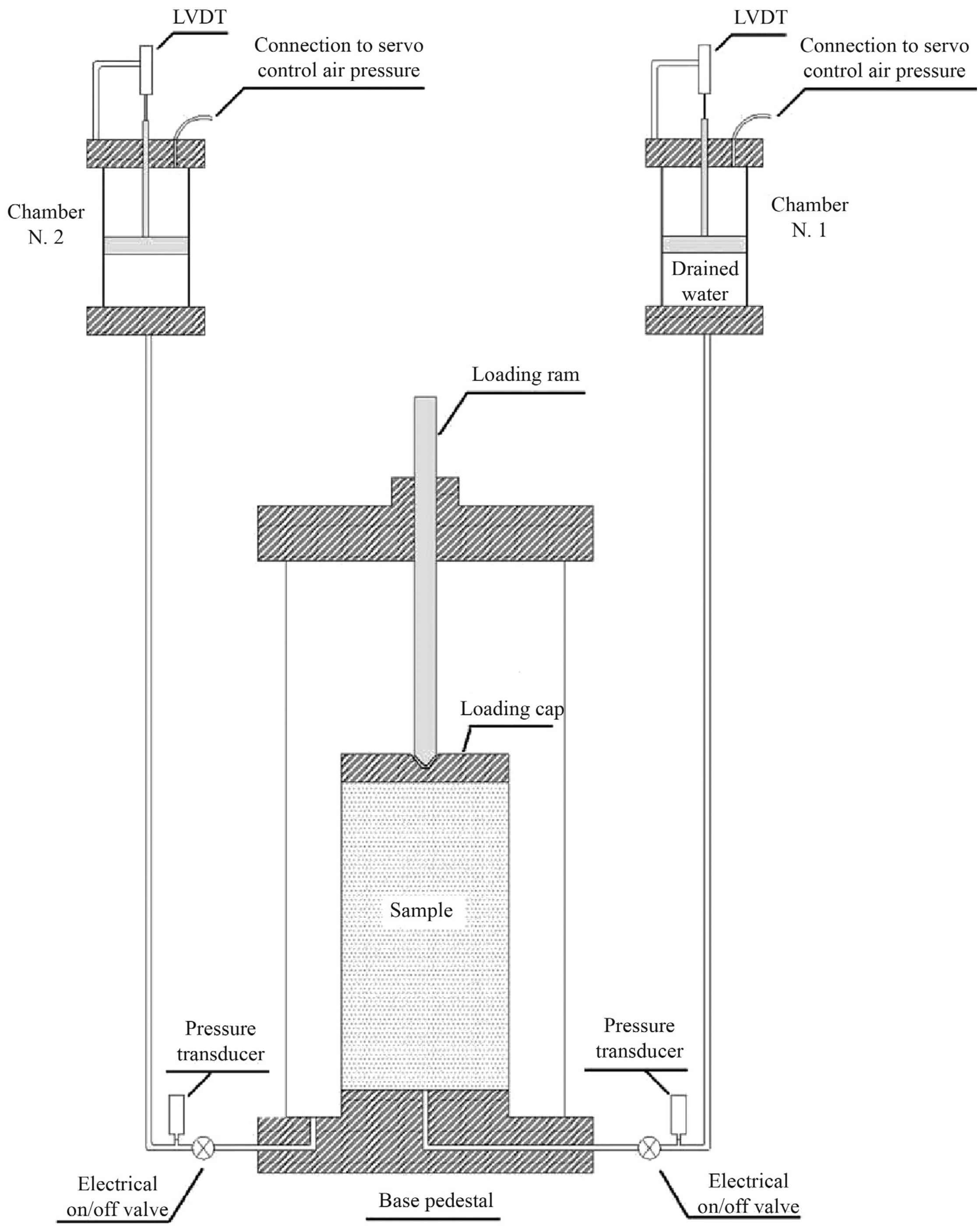

Figure 6 - A schematic view of triaxial apparatus used.

by Skempton (1961) should be used when analyzing the undrained behavior of MSW:

$$\sigma' = \sigma - Au \qquad (2)$$

where σ' and σ are the effective and total normal stresses. *A* is the pore pressure (*u*) reduction coefficient, a function of the ratio between the compressibility of MSW particles and the compressibility of the MSW as a whole (Eq. (3)).

$$A = 1 - \frac{C_s}{C} \qquad (3)$$

where C_s is the compressibility of the waste particles and C is the compressibility of the waste as a whole.

Figure 9 shows the variation of A with mean pressure (*p*) for MSW samples with different fiber contents. According to Shariatmadari *et al.* (2009) the use of the *A* factor to

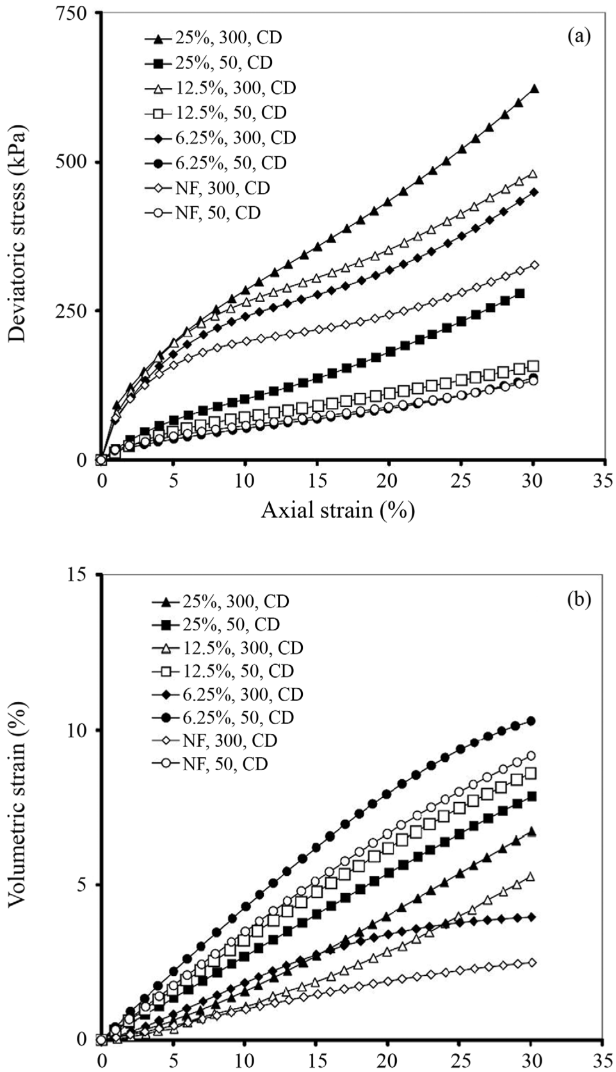

Figure 7 - Typical CD triaxial test results.

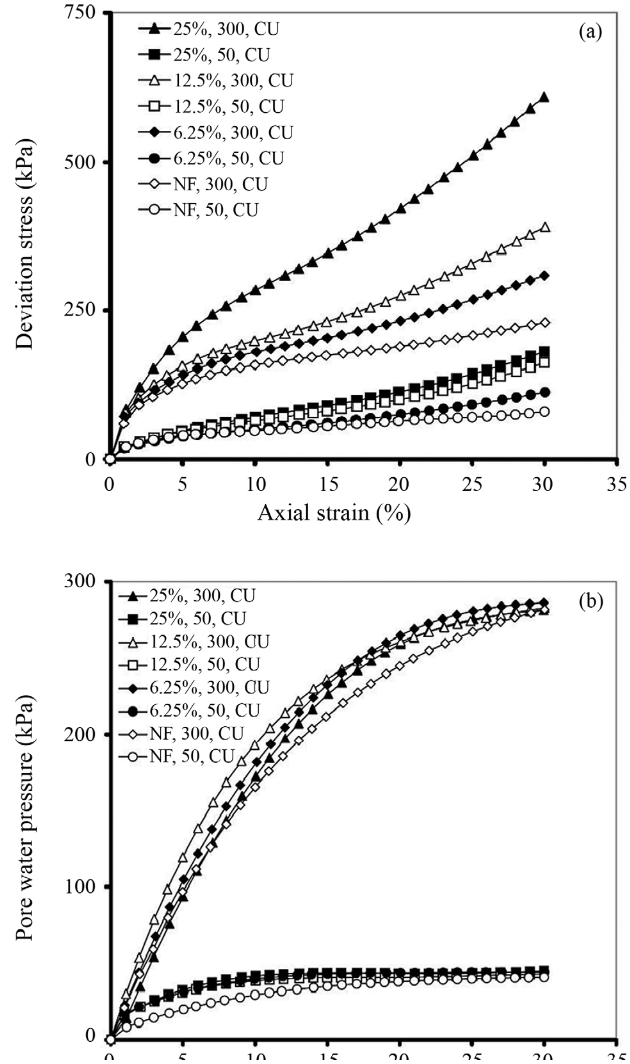

Figure 8 - Typical CU triaxial test results.

compute the pore water pressure contribution in the effective stress equation resulted in a signicant improvement in the compatibility between the effective parameters obtained from CU and CD tests.

Figure 10 presents the effective stress paths followed by the samples in CD and CU tests. In the case of the effective stress paths obtained in CU tests, two equations were used for effective stress calculation: one is the classic Terzaghi equation ($A = 1$) and the other is Eq. (2) ($A < 1$).

To evaluate the effect of the fiber content on the MSW shear strength parameters, the results were analyzed using the Mohr-Coulomb shear strength envelope. Because of the strain hardening nature of MSW (it was not possible to detect any trend of failure in the performed tests) the shear strength parameters were calculated for axial strain values of 5, 10, 15 and 20%.

The use of the Mohr-Coulomb shear strength envelope in MSW materials is a controversial. As presented by

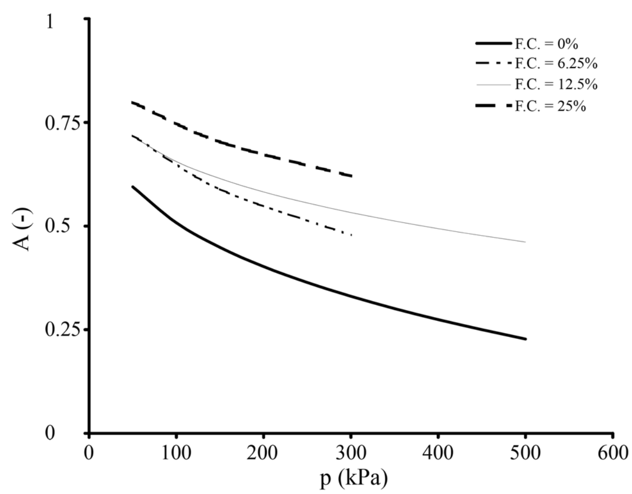

Figure 9 - Values of A parameter for varying fiber contents and mean stress.

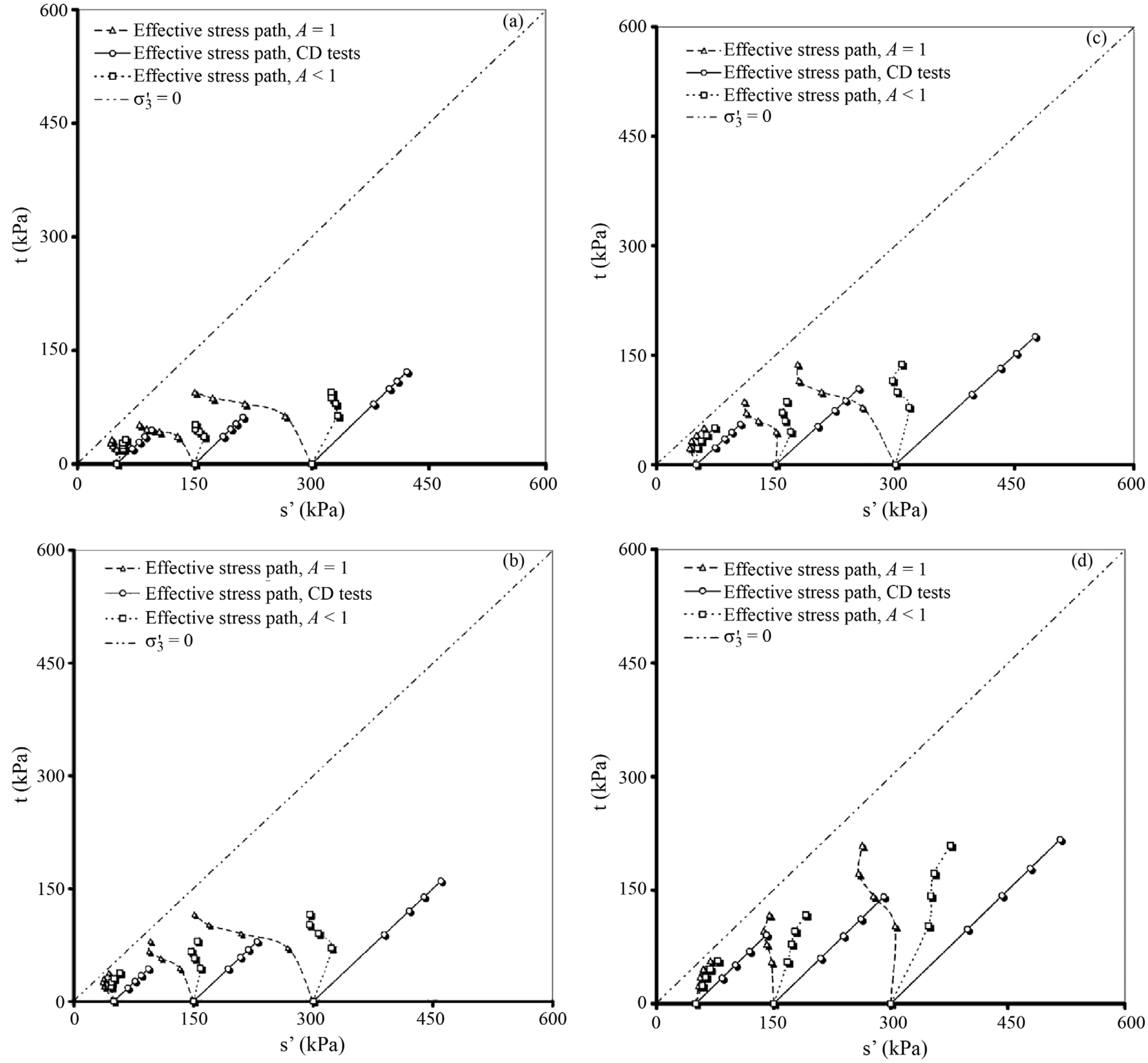

Figure 10 - Stress path of MSW samples with varying ber content (a) 0%, (b) 6.25%, (c) 12.5% and (d) 25%.

Machado *et al.* (2002) and Machado *et al.* (2008), MSW short and long term mechanical behavior can be modeled as a composite material of two phases each with its own constitutive model. However, the use of such complex elastoplastic models is not possible in most of the available commercial slope stability software and these models require a number of parameters which is not usually available in the field. Besides this, the capacity of landfill structures such as gas and leachate collection systems and cover layers to sustain horizontal and vertical displacements without losing serviceability can be used to define maximum strain levels and thus makes it possible and defensible to use the Mohr-Coulomb shear strength envelope in slope stability analysis in landfills.

Figure 11 presents the shear strength envelopes for each fiber content and drainage condition adopted in the experimental program (20% of axial strain). Tables 3 and 4 present the obtained MSW friction angle and cohesion intercept for the different levels of axial strain. Figure 12 summarizes the obtained results graphically.

As can be noted, there are different patterns of shear strength mobilization in the CU and CD tests. In the case of the CD tests, Fig. 12b and Table 4, fiber content affects cohesion intercepts much more than friction angles. Despite the 6.25% fiber content there is a decrease in the obtained value of cohesion. After 6.25% the effect of the fiber content on the friction angle seems negligible.

Table 3 - Evolution of the MSW shear strength parameters with axial strain for different fiber contents. CU tests.

Axial strain (%)	Fiber content (%)							
	0		6.25		12.5		25	
	ϕ	C (kPa)	ϕ	C (kPa)	ϕ	C (kPa)	ϕ	C (kPa)
5	9	9	10	9	10	10	14	6
10	11	9	12	12	12	16	17	10
15	11	11	13	15	13	20	20	14
20	12	14	14	21	15	26	22	17

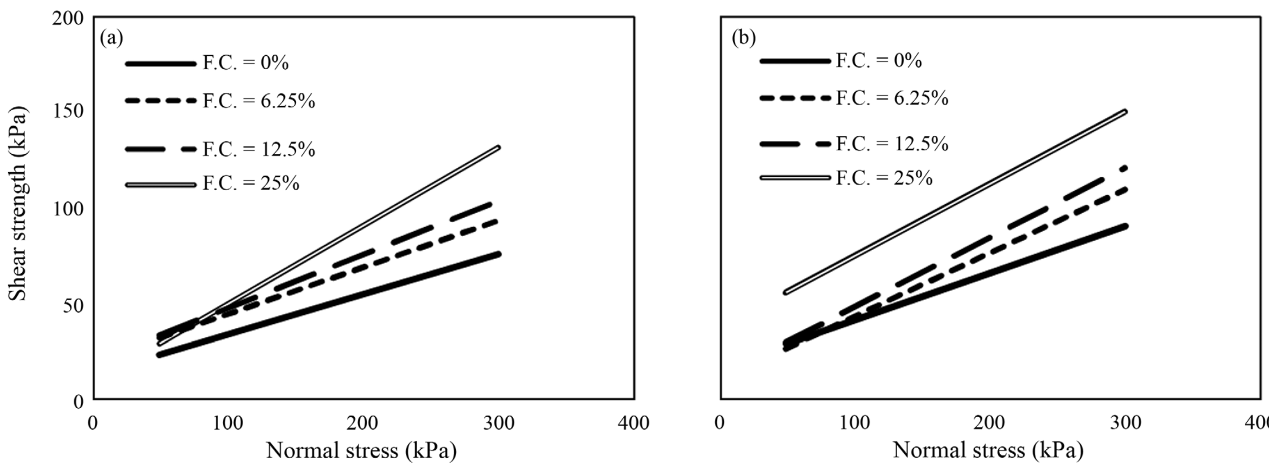

Figure 11 - The effect of the fiber content on the shear strength (a) undrained conditions (b) drained conditions.

In the case of CU tests, there is a monotonic increase in the friction angle with fiber content and the effect of the fiber content on the cohesion intercept seems to reach a maximum for a fiber content of 12.5%. One of the possible reasons for such behavior must be related to the high values of pore water pressure generated during the shear phase, which tends to reduce the anchoring conditions of the fibers inside the samples.

Figure 13 compares the effective stress results from CU and CD tests using Eq. (2) and Terzaghi's equation. In order to do this, shear strength envelopes were calculated for various levels of axial strain and fiber contents as well. Using the obtained shear strength envelopes and a 50 kPa of normal stress increments, shear strength ratios (β) for samples with the same fiber content were calculated as follows:

$$\beta = \frac{\tau_p}{\tau_r} \qquad (4)$$

where τ_r is the shear strength based on stress analysis of CD test results and τ_p is the shear strength based on effective stress analysis of CU tests.

The log normal distribution was used to perform a statistical analysis of the β values. The mean (μ) and standard deviation (σ_β) were evaluated using the natural logarithm of strength ratio as follows:

Table 4 - Evolution of the MSW shear strength parameters with axial strain for different fiber contents. CD tests.

Axial strain (%)	Fiber content (%)							
	0		6.25		12.5		25	
	ϕ	C (kPa)	ϕ	C (kPa)	ϕ	C (kPa)	ϕ	C (kPa)
5	11	4	13	2	13	7	12	17
10	13	8	16	4	16	12	16	25
15	13	13	17	8	18	17	18	34
20	14	18	19	11	19	22	20	46

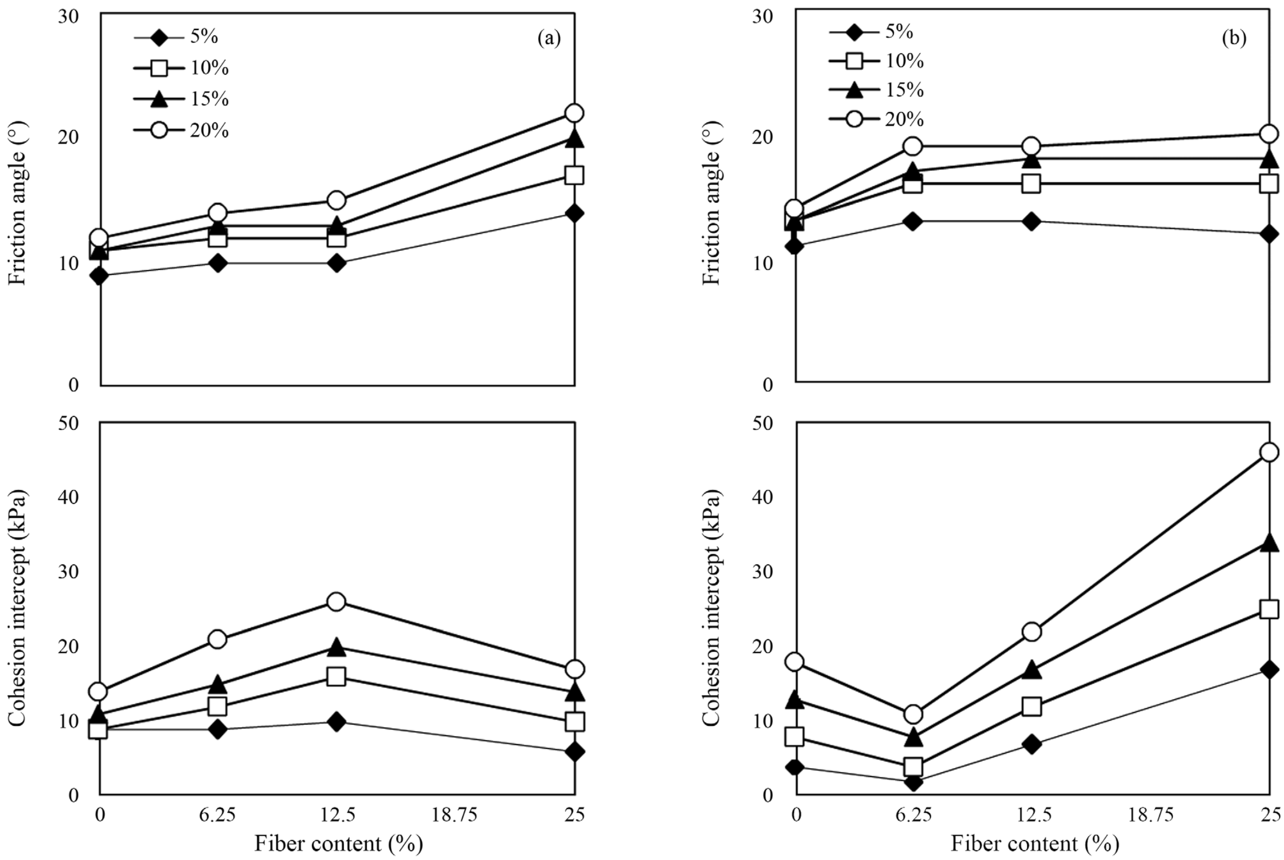

Figure 12 - Variation of shear strength parameter of MSW materials with varying fiber contents (a) undrained conditions (b) drained conditions.

$$\mu = \frac{1}{n}\sum_{i=1}^{n} \ln \beta_i \tag{5}$$

$$\sigma_\beta = \sqrt{\frac{1}{n-1}\sum_{i=1}^{n} (\ln \beta_i - \mu)^2} \tag{6}$$

the Log Normal distribution of the β values is given by

$$f(\beta) = \frac{1}{\sqrt{2\pi}\,\sigma_\beta\,\beta} \exp\left(-\frac{1}{2}\left(\frac{\ln(\beta)-\mu}{\sigma}\right)^2\right) \tag{7}$$

The function above produces a bell shaped distribution with a constant area, therefore increasing the peak value of $f(\beta)$ implies reducing the width and as a result the scatter of the prediction is lower. If the peak length is equal to 1, this means that the average value of shear strength is equal to unity or the average error is zero. If the peak length is greater than 1, the effective shear envelope derived from CU tests leads to an over estimation of shear strength compared to CD ones and vice-versa.

As can be seen in Fig. 13, the error analysis performed using the results of effective stress from the CU tests and assuming the results of CD tests as a reference showed that ignoring particle compressibility could cause an overestimation of up to 50% in the shear strength of MSW. Using Eqs. (2) and (3) this error was reduced to less than 15%.

In this paper, effective stress parameters were obtained using the results of CD tests. Although not the case in this paper, in the absence of CD tests, the authors suggest the use of Eq. (2) in order to obtain effective shear strength parameters from CU tests. The use of Terzaghi's equation may lead to an unacceptable overestimation of the MSW shear strength.

For illustrative purposes, some slope stability calculations were carried out to verify the effect of the fiber content on the factor of safety (FS) of some hypothetical slopes. The authors believe that this kind of information is worthwhile for designers as a preliminary approach to evaluate the effect of fiber removal on the MSW shear strength parameters and on the slope factor of safety. In this case only the shear parameters obtained for 20% of axial strains were used. Slopes were defined considering their height and inclination.

Due to the developments in computing, the use of several relatively new numerical methods for slope stability analysis are increasing in popularity. One such is the shear strength reduction technique (SSR). In this method, the factor of safety of one slope is computed by reducing the shear strength of soil, rock or any type of Geo-materials

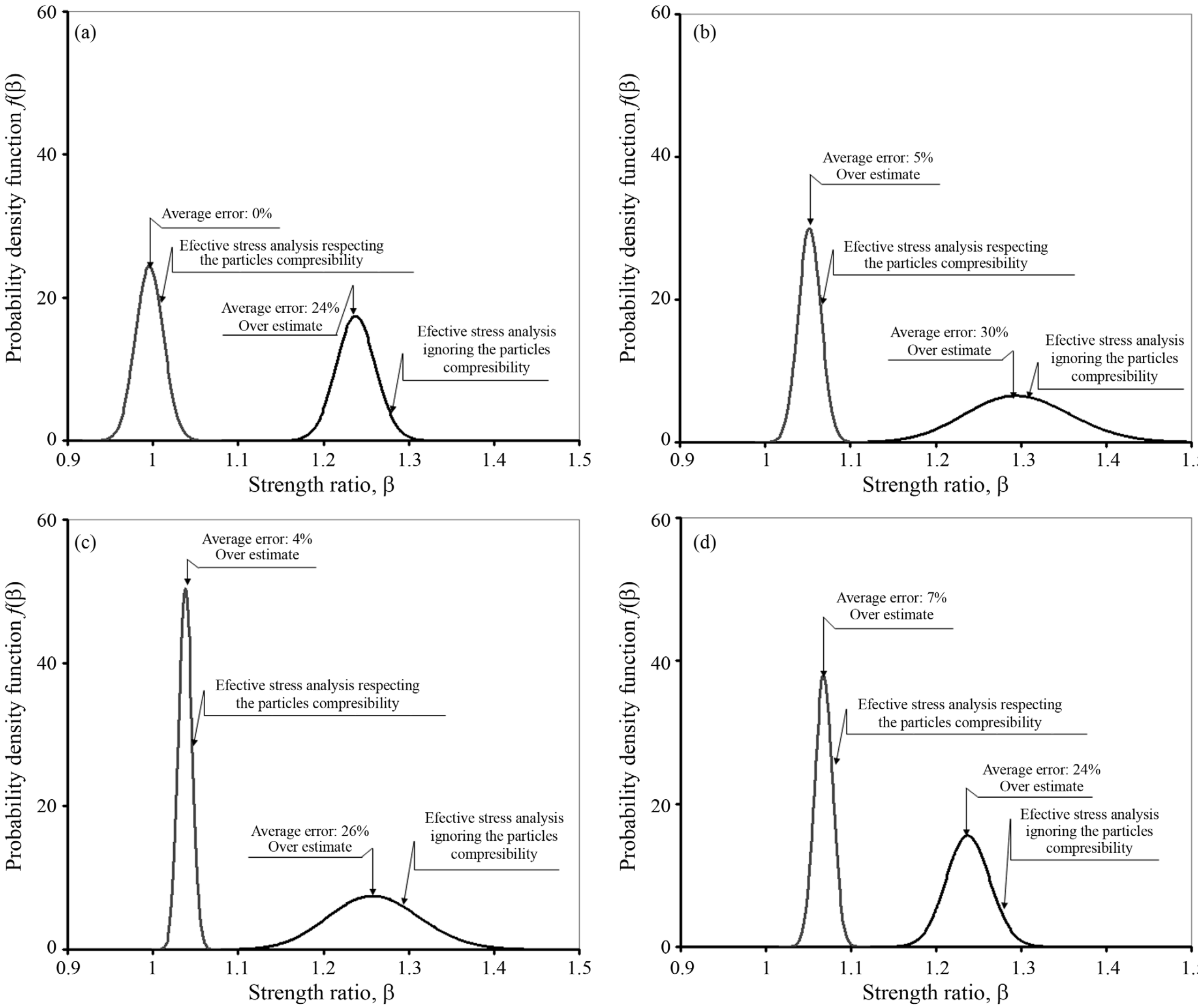

Figure 13 - Error analysis. (a) 0%, (b) 6.25%, (c) 12.5% and (d) 25% fiber content.

in stages, until the slope fails. For Mohr-Coulomb material shear strength is reduced by FS according to the equation:

$$\frac{\tau}{FS} = \frac{c'}{FS} + \frac{\tan(\varphi')}{FS} \quad (8)$$

Eq. (8) can be re-written as

$$\frac{\tau}{FS} = c^* + \tan(\varphi^*) \quad (9)$$

In this case, $c^* = c'/FS$ and $\phi^* = \arctan(\phi')/FS$ are the reduced Mohr-Coulomb shear strength parameters and these values can be input into an finite element or finite difference model and analyzed. For Mohr-Coulomb materials, the main steps for systematically searching for the critical FS, which brings a previously stable slope to the verge of failure, are described below:

Step 1: Develop a numerical model of a slope, using appropriated boundaries and the deformation and strength properties established for the slope materials. Run the model obtaining the values of stress and strain and recording the maximum total deformation in the slope.

Step 2: Increase the value of FS and calculate the reduced values of c’ and f ‘ as described above. Enter the new strength properties into the slope model and repeat Step 1.

Step 3: Repeat Step 2, using systematic increments of FS, until the numerical model does not converge with a solution (the displacement values become excessively high), *i.e.* continue to reduce material strength until the slope fails. The final FS value can be calculated as the one that leads to virtually infinite displacements. The FS steps must be reduced as the displacements become higher to approach an equilibrium limit situation.

The Finite Difference Method code FLAC (FLAC, 2000) enables the analysis of slope stability using the SSR technique. To evaluate the effect of fiber content on the slope stability using FLAC software, about 150 combina-

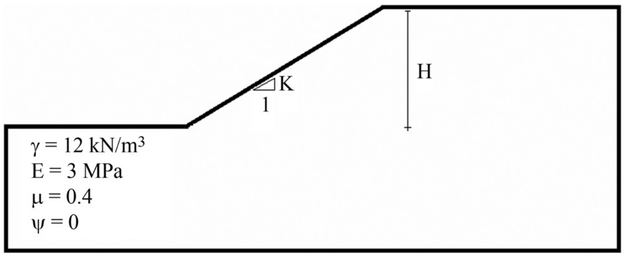

Figure 14 - Hypothetical slope section adopted for slope stability calculation.

tions of slope geometry and MSW shear strength parameters were used.

Figure 14 illustrates the general model of waste fill used for these analysis. It was assumed that the waste fill had been constructed on a foundation of waste materials of infinite depth (this is reasonable in the MCL case, as the cells are part excavated and part above the ground level). Besides this, critical surfaces (assumed as the regions of the mesh with higher displacements) were always located at shallow depths, passing near the toe of the slope. The model boundaries extend to the left and right far enough to have no effect on the values of the computed FS.

It was assumed that the leachate collection system works properly so that increasing levels of leachate (or gas pressure) inside the fill is not a matter concern. The authors believe that these are reasonable assumptions only in well managed landfills with the use of a compatible number of deep and superficial gas drains and an efficient leachate collection system. In slope stability analysis of waste fills, the authors suggest that the use of undrained parameters must be considered only in the absence of gas pressure or leachate level information.

According to the discussion presented above, only the results of the CD tests were used in the performed calculus. As said above, other values of strain may be chosen by the staff responsible for the landfill management, considering the interactions between the waste mass and the cover layer, drainage system, etc. Values of k were chosen in order to cover MSW slope inclinations normally found in the field for new and old MSW slopes. In the same way values of H cover most of the situations found in Brazilian landfills.

Table 5 presents the FS factors calculated by the software for various geometry and strength conditions. As can be observed, although most FSs are relatively high, there is a clear increase in FS values as the fiber content increases. The only exception occurs when comparing the results of the material without fibers with the results of the material with a fiber content of 6.5% for low slope heights. This can be explained by observing Figure 7 and Table 4. Samples without fibers presented higher cohesion and consequently higher shear strengths for low levels of confining stress. This is possibly due to this fact that in the absence of plastics, samples compact better (higher densities) resulting in better interlocking between particles which cause a higher strength at lower confining pressures.

In Table 5 FS values lower than 1.6 were highlighted in order to make clear that these values are considered unsatisfactory by the authors to guarantee to the overall stability of the MSW mass.

Fig 15 presents some charts with the variation of FS as a function of the slope height and fiber content.

4. Conclusions

The fibrous components of MSW play a key role in its mechanical behavior. The reinforcement action of these components and their effect on the shear strength is the main reason why the MSW shear-strain curves are concave upward and do not show evidence of failure even under high levels of stress and strain. Most of the fiber elements inside the MSW materials are plastics and most of these are plastic bags used by the population to provisionally store their MSW until it is collected by the refuse collection services from their residences.

The results clearly show that with increasing fiber content and/or plastic content the shear strength of MSW materials increases. This finding is compatible with the re-

Table 5 - Factor of safety of slopes with varying geometry and strength.

Fiber content (%)	k	H (m)						
		5	7	10	12.5	15	17.5	20
0	1	2.35	1.92	1.41	1.21	1.08	0.99	0.91
	2	2.94	2.33	1.86	1.64	1.49	1.37	1.28
	3	3.42	2.76	2.26	2.01	1.84	1.71	1.62
	4	3.90	3.17	2.63	2.38	2.19	2.06	1.96
	5	4.26	3.54	2.97	2.71	2.52	2.38	2.27
6.25	1	1.84	1.42	1.20	1.06	0.96	0.89	0.83
	2	2.49	1.99	1.72	1.56	1.44	1.36	1.29
	3	3.09	2.52	2.21	2.02	1.89	1.79	1.72
	4	3.58	2.97	2.69	2.48	2.34	2.23	2.15
	5	4.01	3.40	3.07	2.85	2.71	2.60	2.52
12.5	1	3.08	2.26	1.85	1.60	1.38	1.26	1.17
	2	3.83	2.92	2.45	2.16	1.96	1.81	1.70
	3	4.47	3.84	2.97	2.66	2.44	2.28	2.16
	4	5.05	4.03	3.49	3.16	2.93	2.75	2.62
	5	5.58	4.53	3.97	3.62	3.36	3.19	3.04
25	1	5.53	3.92	3.12	2.63	2.31	2.08	1.90
	2	6.56	4.53	3.92	3.62	3.01	2.76	2.53
	3	7.14	5.50	4.72	3.99	3.60	3.26	3.09
	4	8.05	6.13	5.38	4.72	4.49	3.84	3.61
	5	8.51	6.82	5.80	5.15	4.70	4.38	4.11

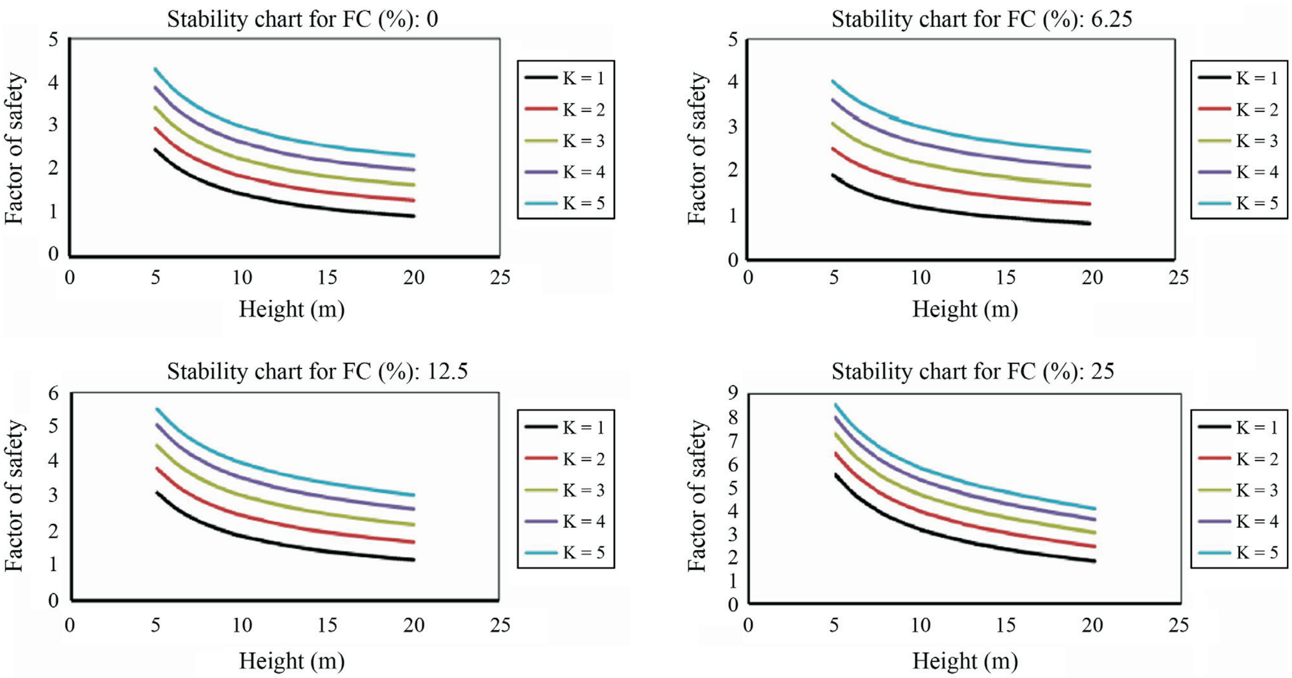

Figure 15 - Stability chart of slopes with varying geometries and fiber contents.

sults of the constitutive model presented for MSW materials by Machado *et al.* (2008) and Machado *et al.* (2002) and many other authors in the technical literature (Zekkos 2005, Georgiopoulos 2005, Athanasopoulos *et al.* 2008).

The error analysis performed using the results of effective stress from CU tests and assuming the results of CD tests as a reference showed that ignoring particle compressibility could cause an overestimation of up to 50% in the shear strength of MSW. Using Eqs. (2) and (3) this error was reduced to less than 15%.

The results of waste fill stability analysis have shown that decreasing the MSW fiber content the Factor of Safety also decreases. For a height of 20 m, reducing the fiber content from 25% to 0% results in a decrease in the Factor of Safety from 2.53 to 1.28, considering a slope of 1:2. For a slope of 1:3, these values change from 3.09 to 1.62.

Finally, there is a a new trend to recycle plastic material for energy recovery purposes instead of landfilling. The staff responsible for landfill management must be aware that this practice will imply a reduction in the storage capacity of the landfill in order to preserve adequate levels of security.

References

ASTM D4767 (2004) Standard Test Method for Consolidated Undrained Triaxial Compression Test for Cohesive Soils, doi:10.1520/D4767-04.

Athanasopoulos, G.; Grizi, A.; Zekkos, D.; Founta, P. & Zisimatou, E. (2008) Municipal solid waste as a reinforced soil: Investigation using synthetic waste, Proc. ASCE-Geoinstitute Geocongress. The Challenge of Sustainability in the Geoenvironment, Geotechnical Special Publication, Pub. No. 177, pp. 168-175.

Carvalho, M.F. (1999) Comportamento mecânico de resíduos sólidos urbanos. PhD Thesis. Geotechnical Department, University of São Paulo, 300 pp.

FLAC v. 4.0. (2000) Users Manual. Itasca Consulting Group Inc., Minneapolis, 124 pp.

Georgiopoulos, D. (2005) Direct Shear Tests on MSW Specimens from Tri-Cities Landfill, California, USA, Using a Large Shear Box. Diploma Thesis, University of Patras, 260 pp.

Grisolia, M.; Napoleoni, Q.; & Tangredi, G. (1995) The use of triaxial tests for the mechanical characterization of municipal solid waste. Proc. of the 5th International Landfill Symposium – Sardinia 95, Sardinia, pp. 761-767.

Head, K.H. (1986) Manual of Soil Laboratory Testing, v. 3: Effective Stress Tests. Pentech Press, London, 442 pp.

Jessberger, H.L. & Kockel, R. (1993) Determination and assessment of the mechanical properties of waste. Sarsby, R.W. (ed) Waste Disposal by Landfill – Green ‘93. Balkema, Rotterdam, pp. 313-322.

Karimpour-Fard, M. (2009) Mechanical behavior of MSW materials with different initial states. PhD Thesis, Iran University of Science and Technology. [in Persian].

Kavazanjian Jr., E.; Matasovic, N. & Bachus, R.C. (1999) Large-diameter static and cyclic laboratory testing of municipal solid waste. Proc. Sardinia `99-7th International Waste Management and Landfill Symposium, Cagliari, pp. 437-444.

Kölsch, F. (1995) Material values for some mechanical properties of domestic waste. Proc. of the 5th International Landfill Symposium in Sardinia, pp. 711-729.

Landva, A.O. & Clark, J.I. (1990) Geotechnics of waste fill. Geotechnics of waste fill, Theory and practice, STP 1070. Landva and Knowles (eds), ASTM, pp. 86-103.

Machado, S.L; Carvalho, M.F.; Nascimento, J.C.F. & Santos A.C. (2010) Characterization of the MCL Domestic Waste. MCL internal report, Salvador, 45 pp.

Machado, S.L.; Carvalho, M.F. & Vilar, O.M. (2002) Constitutive model for municipal solid waste. Journal of Geotechnical and Geoenvironmental Engineering, v. 128:11, p. 940-951.

Machado, S.L.; Vilar, O.M. & Carvalho, M.F. (2008) Constitutive model for long term municipal solid waste mechanical behavior. Computers and Geotechnics, v. 35:5, p. 775-790.

Nascimento, J.C.F. (2007) Comportamento mecânico de resíduos sólidos urbanos. Ms.C. Dissertation. Geotechnical Department, University of São Paulo, 150 pp.

Shariatmadari, N.; Machado, S.L.; Noorzad, A. & Karimpour-Fard, M. (2009) Municipal solid waste effective stress analysis. Waste Management (Elmsford), v. 29:12, p. 2918-2930.

Towhata, I.; Kawano, Y.; Yonai, Y. & Koelsh, F. (2004) Laboratory tests on dynamic properties of municipal wastes. Proc. 11th Conference in Soil Dynamics and Earthquake Engineering and 3rd International Conference on Earthquake Geotechnical Engineering, Berkeley, California, v. 1, pp. 688-693.

Zekkos, D.P. (2005) Evaluation of Static and Dynamic Properties of Municipal Solid-Waste. PhD Thesis, University of California, Berkeley, 578 pp.

List of Symbols

A – Pore water pressure reduction factor
B – Skempton pore water pressure parameter.
c' - MSW effective cohesion
c^* - MSW reduced or mobilized cohesion
C_s - Compressibility of the MSW the waste particles
C - Compressibility of the waste as a whole
CD – Consolidated Drained
CU – Consolidated Undrained
E – Modulus of elasticity
F.C.- Fiber Content
FS – Factor of Safety
H - Slope heigh
k - Slope inclination
MSW – Municipal Solid Waste
p - Mean normal stress
SSR – Shear strength reduction technique
TX – Triaxial Test
β - Shear strength ratio
μ - Mean of the natural logarithm values of β
σ_β - Standard deviation of the natural logarithm values of β
γ_0 - Initial density of the samples
ε_a - axial strain
ε_r - radial strain
σ_v - volumetric strains
σ_3 - Consolidation pressure
υ - Poisson coefficient
ϕ'- MSW effective friction angle
ϕ^* - MSW reduced or mobilized friction angle
τ - Shear strength, shear stress.
τ_r - Shear strength based on stress analysis of CD test results
τ_p - Shear strength based on effective stress analysis of CU tests
σ' - Effective normal stresses
σ - Total normal stresses

Long-Term Efficiency of Zero-Valent Iron - Pumice Granular Mixtures for the Removal of Copper or Nickel From Groundwater

N. Moraci, P.S. Calabrò, P. Suraci

Abstract. The use of Permeable Reactive Barriers (PRBs) for in situ remediation of contaminated groundwater represents an attractive technology for both economic and operational reasons. A reactive medium widely used in PRBs is the Zero-Valent Iron (ZVI) which, in several case studies, has proved highly efficient for the removal of both inorganic and organic contaminants. One of the major concerns related to ZVI PRBs is their long-term hydraulic conductivity, which often decreases during operation, potentially compromising the long-term efficiency and durability of the barrier. This paper proposes the use of granular mixtures of ZVI and natural pumice in various weight ratios with the aim of solving this problem. The experimental research was carried out using two different metallic contaminants (nickel and copper) in aqueous solution at two concentrations. The issues related with long-term efficiency of the PRB are examined on the basis of the results of the experimental activity carried out by means of long-term column tests. It is demonstrated how iron-pumice granular mixtures are efficient in contaminant removal and, at the same time, are able to maintain constant the permeability of the PRB.

Keywords: contaminated groundwater, heavy metals, hydraulic conductivity, permeable reactive barrier, pumice, zero-valent iron.

1. Introduction

The use of Permeable Reactive Barriers (PRBs) for in situ remediation of contaminated groundwater represents an attractive technology both for economic and operational reasons (Thiruvenkatachari *et al.*, 2008; USEPA, 2004; NTUA, 2000; USEPA, 1998). A Permeable Reactive Barrier consists of a permeable subsurface wall composed of various reactive media, commonly built as a continuous trench filled with the treatment material. The trench is perpendicular to and intercepts the contaminated groundwater plume. As the water flows through it under the natural hydraulic gradient, the reactive medium degrades or traps the contaminants, providing the remediation of the aquifer by means of physical, chemical, biological or mixed processes. A PRB does not need any energy input, because it uses the natural hydraulic gradient of groundwater (passive method).

The reactive medium in the barrier interacts with the contaminants according to the above mentioned processes, removing (degrading or trapping) the pollutants and preventing the flux of the contaminants downstream of the PRB location. For the correct design of a PRB, a detailed geotechnical and hydrogeologic site characterization and an accurate physical and chemical study of the contamination are required in order to select the reactive medium and the barrier dimensions and configuration.

A filling reactive material widely used in PRBs is the Zero-Valent Iron (ZVI), which has demonstrated, in several cases presented in the scientific literature, a very good efficiency, in particular for heavy metals (*e.g.* Cd, Cr, Cu, Ni, Pb, Zn) removal (*e.g.* Wilkin and Mc Neil, 2003; Morrison *et al.*, 2002), even if it has been extensively and successfully used for the removal of other organic and inorganic compounds (*e.g.* Cundy *et al.*, 2008; Thiruvenkatachari *et al.*, 2008; Blowes *et al.*, 2000; NTUA, 2000; USEPA, 1998).

Notwithstanding its flexibility and good performance, the use of ZVI alone demonstrated some drawbacks regarding to the long-term efficiency of the PRB especially in terms of permeability (Li *et al.*, 2006; Li *et al.*, 2005; Liang *et al.*, 2005; Vogan *et al.* 1999; Mackenzie *et al.*, 1999), given its natural tendency for corrosion. In fact, the accumulation of precipitates (mainly hydroxides and salts such as carbonates) resulting from iron corrosion modifies the efficiency and especially the permeability of the barrier in time. Such a phenomenon can eventually lead to the generation of preferential paths towards zones outside the barrier (characterized by higher permeability), making the contaminated groundwater flow bypass the barrier itself.

N. Moraci, Mechanics and Materials Department, Faculty of Engineering, Mediterranean University of Reggio Calabria, Reggio Calabria, Italy. E-mail: nicola.moraci@unirc.it.
P.S. Calabrò, Mechanics and Materials Department, Faculty of Engineering, Mediterranean University of Reggio Calabria, Reggio Calabria, Italy. E-mail: paolo.calabro@unirc.it.
P. Suraci, Mechanics and Materials Department, Faculty of Engineering, Mediterranean University of Reggio Calabria, Reggio Calabria, Italy. E-mail: paolo.suraci@unirc.it.
Submitted on June 8, 2010; Final Acceptance on October 5, 2010; Discussion open until December 30, 2011.

The probability of this barrier bypass is increased by the recent trend of adopting semi-permeable funnels (hydraulic conductivity only two or three orders of magnitude lower than PRB) in funnel and gate configurations; in fact, in these conditions, if gate permeability decreases, the plume of contaminated groundwater can flow through the funnels.

Furthermore, when the barrier bypass is not possible, since the natural gradient of groundwater remains relatively constant, a decrease of hydraulic conductivity causes a parallel reduction of discharge through the barrier, significantly modifying the hydrogeology downstream.

In this paper, in order to sustain hydraulic conductivity in the long term and to optimize the use of ZVI, which is rather expensive, the adoption in PRBs of granular mixtures of zero-valent iron and pumice (a volcanic rock with a spongy, vitreous structure), in different weight ratios, is proposed.

The experimental research on the efficiency of ZVI-pumice granular mixtures in the removal of heavy metals was carried out by column tests, using an aqueous solution of the nitrates of two different metallic contaminants (nickel and copper) at various concentrations.

2. Contaminants Removal Mechanisms In Zero-Valent Iron Permeable Reactive Barriers

Iron (Fe) is a chemical element with three possible oxidation states: 0, +2 and +3 (other oxidation states are rare); ZVI acts as a reducing agent (electron donor) and tends to be easily and quickly oxidized (Fe^0/Fe^{2+} - E0 = -0,44 V), as outlined below, Fe^{2+} also, in certain conditions, can be further oxidized.

The groundwater contaminants passing through the barrier, if their redox potential is higher than - 0.44 V, act as electron acceptors and may be reduced.

For a generic metal (Me) the reactions involved are as follows:

$$Fe^0 \rightarrow Fe^{2+} + 2e^- \text{ oxidation}$$

$$Me^{2+} + 2e^- \rightarrow Me \text{ reduction}$$

Moreover, metallic contaminants may also be involved in reactions with other chemical compounds normally present in groundwater (*e.g.* carbonates, sulphides, hydroxides) forming solid precipitates. However, since the solubility of these compounds is strongly dependent on the pH value, the barrier should operate in a given pH range, so that the precipitates formed are barely soluble and are not re-transformed in a soluble form. At the same time the accumulation of precipitates in the barrier pores progressively reduce hydraulic conductivity (NTUA, 2000; Vogan *et al.* 1999; Mackenzie *et al.*, 1999).

If the ZVI oxidation takes place in anaerobic conditions (generally prevalent in groundwater) ferrous hydroxides are formed according to the following reactions:

$$Fe^0 \rightarrow Fe^{2+} + 2e^-$$

$$2H_2O + 2e^- \rightarrow H_2 + 2OH^-$$

$$\underline{Fe^{2+} + 2OH^- \rightarrow Fe(OH)_2}$$

$$Fe^0 + 2H_2O \rightarrow Fe^{2+} + H_2 + 2OH^-$$

However, the rate of this reaction is slower than that involved in the removal of metallic cations (contaminants), while it is accelerated in aerobic conditions or when the metallic cations are removed from groundwater.

Furthermore, at high pH and high Fe^{2+}concentration, the ferrous ion will be further oxidized to the ferric state Fe^{3+}, precipitating as ferric hydroxide and potentially compromising the hydraulic conductivity of the barrier, according to the reaction:

$$Fe^{3+} + 3OH^- \rightarrow Fe(OH)_3$$

Therefore ZVI is easily corroded in an aqueous environment, even in the absence of contaminants; oxidation is not strictly detrimental to PRB performance, in fact, as a matter of fact, the contaminants reducing reactions imply ZVI corrosion.

Nevertheless, both iron corrosion and hydroxides formation have been generally believed to have a negative influence on the long-term effectiveness of the barrier, because corrosion implies a macroscopic dissolution of ZVI, thus reducing the reactive surface necessary to maintain contact with the contaminants, and because of the formation, on the reactive metal grains, of a thick layer of passivating oxidation products, the so-called “pseudo-protection” layer. According to the “traditional view” on ZVI PRBs, considering contaminants removal mainly due to oxidation-reduction reactions on the surface of ZVI grains, the presence of this “pseudo-protection” layer, preventing the water from coming into contact with virgin ZVI, prevents further oxidation of iron and subsequent reduction of metallic contaminants. A more complex mechanism for contaminants removal, directly involving corrosion products, has been recently proposed (Noubactep, 2008; Noubactep, 2006). According this new view, the heavy metals present in the contaminated solution are thus removed mainly through three possible processes (Noubactep, 2008; Noubactep, 2006; Rangsivek and Jekel, 2005; Wilkin and McNeil, 2003; Smith, 1996): reduction (direct reduction on the surface of ZVI or reduction through Fe^{2+} at the surface of corrosion products); adsorption onto corrosion products; and coprecipitation (precipitating corrosion products that can capture contaminants into their structure). Therefore contaminants removal is possible in three different places: on the ZVI surface, within the corrosion products film and on the surface of corrosion products.

According to Smith (1996), the SiOH sites that are present on the pumice surface are also able to remove the metals from the solution according to the reaction:

$$> SiOH + Me^{2+} \leftrightarrow (> SiO^{-} - Me^{2+})^{+} + H^{+}$$

where > represents the pumice surface.

Another mechanism for the removal of metals by pumice is the ionic exchange with alkaline and alkaline-earth metals present in the pumice structure. In fact according to information provided by the supplier of the pumice (Pumex spa, 2008) the bonds – Si – O–Me, where Me is an alkaline or alkaline-earth metal, are easily hydrolyzed to form the active group – Si – OH. Moreover, according to the results of the research activity carried out on the ZVI/Pumice granular mixtures (Moraci *et al.* 2010) it seems that Pumice can enhance ZVI performance due to its capacity of storing corrosion products in its pores thus augmenting the available reactive surface for the reactions and, at the same time, allowing the preservation of the hydraulic conductivity.

3. Materials and Methods

Pumice is a volcanic rock with a spongy, vitreous structure, characterized by a high internal porosity due to the expansion of magmatic gases during the effusion process by which it was generated. The pumice used in this research comes from the quarries of Lipari (Aeolian Islands, Sicily – Italy); it is a natural complex silicate (Pumex spa, 2008) constituted mainly by silica (SiO_2 – 71.75%) and by oxides of various elements (*e.g.* Al_2O_3 – 12.33%, K_2O – 4.47%, Na_2O – 3.59%, Fe_2O_3 – 1.98%, MgO – 0.12%, TiO_2 – 0.11%, MnO – 0.07%, FeO – 0.02%). In terms of morphology, the pumice presents irregularly shaped grains; three different grain size distributions were tested in the present research.

The average micropore diameter of pumice grains is lower than 5 μm (Rigano, 2007).

Pumice is generally considered chemically inert, since it is insoluble both in water and in acids or bases, except hydrofluoric acid (HF); it has, as already mentioned, a significant surface chemical activity due to the presence of – OH groups and mono and polyvalent ions in its chemical

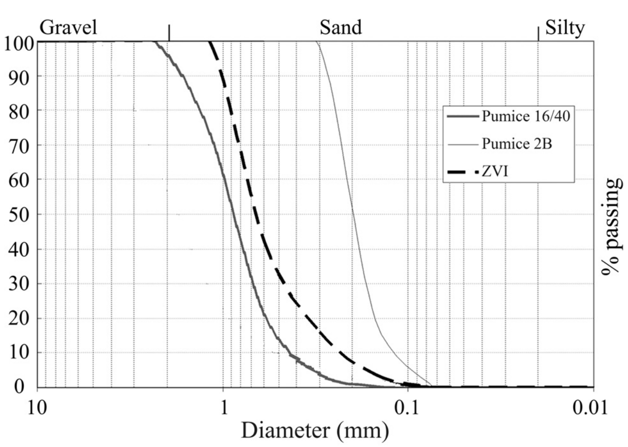

Figure 1 - Grain size distribution curves for Pumice and ZVI.

structure; therefore this material is able to form chemical bonds with organic and inorganic compounds. The pumice from Lipari with two different grain size distributions (called 16/40 and 2B) was used (Fig. 1). The uniformity coefficients, $C_u = D_{60}/D_{10}$, are, respectively, equal to 2.2 (Pumice 16/40) and 1.8 (Pumice 2B). The solid's unit weight, ρ_s, determined on the non-crushed grains of pumice was, respectively, equal to 16 kN/m^3 (Pumice 16/40) and 20 kN/m^3 (Pumice 2B). The same measurements carried out after the grains crushing revealed a solid's unit weight equal to 26 kN/m^3. The difference between the values is due to the internal porosity of pumice.

The ZVI used in this research is of the type FERBLAST RI 850/3.5, distributed by Pometon S.p.A., Mestre – Italy. The powder is composed mainly of ZVI (> 99.74%), with impurities constituted mainly of Manganese (about 0.26%) and traces of oxygen, sulphur and carbon. The grain size distribution is almost uniform (see Fig. 1) and the specific weight is of 78.5 kN/m^3 and the uniformity coefficients C_u is 2.4.

The solutions used in the column tests were obtained by mixing either copper nitrate or nickel nitrate with distilled water (Nickel(II) nitrate hexahydrate, purity 99.999; Copper(II) nitrate hydrate, purity 99.999; Sigma-Aldrich).

The assessment of the contaminant concentrations in the samples collected during the column tests was carried out by Atomic Absorption Spectrophotometry (AAS – Shimadzu AA – 6701F – method CNR-IRSA Q.no 64).

To evaluate the performance of the ZVI-Pumice granular mixtures column tests were carried out by letting a contaminated solution to flow through a polymethyl methacrylate (PMMA – Plexiglas) column (internal diameter = 5 cm; height = 100 cm) filled with the reactive medium. Each column had 9 sampling ports (Fig. 2), in correspondence with, respectively, the inlet and the outlet and the other 7 in between (*i.e.* 3, 8, 18, 28, 38, 58, 78 cm from the inlet).

The columns tests were performed with a constant upward flow (equal to 0.5 mL/min) using either a copper or a nickel solution. The constant flow was maintained during the test by using a precision peristaltic pump (Ismatec ISM 930). Five reactive media were used: ZVI; Pumice 16/40; three granular mixtures of ZVI and Pumice 2B (50:50, 30:70 and 10:90 weight ratio respectively). Pumice 2B was selected for granular mixtures according to the results of preliminary batch tests (not reported in this paper). The experimental program and the main characteristics of the different tests are reported in Table 1.

To assess the capacity of the mixtures to maintain an adequate long-term permeability, in the column tests carried out using the 10:90 ZVI-Pumice granular mixture, hydraulic conductivity was measured by constant head permeability tests. To make a direct comparison of the hydraulic performance of respectively ZVI and ZVI-Pumice granular mixture PRBs, the hydraulic conductivity was also

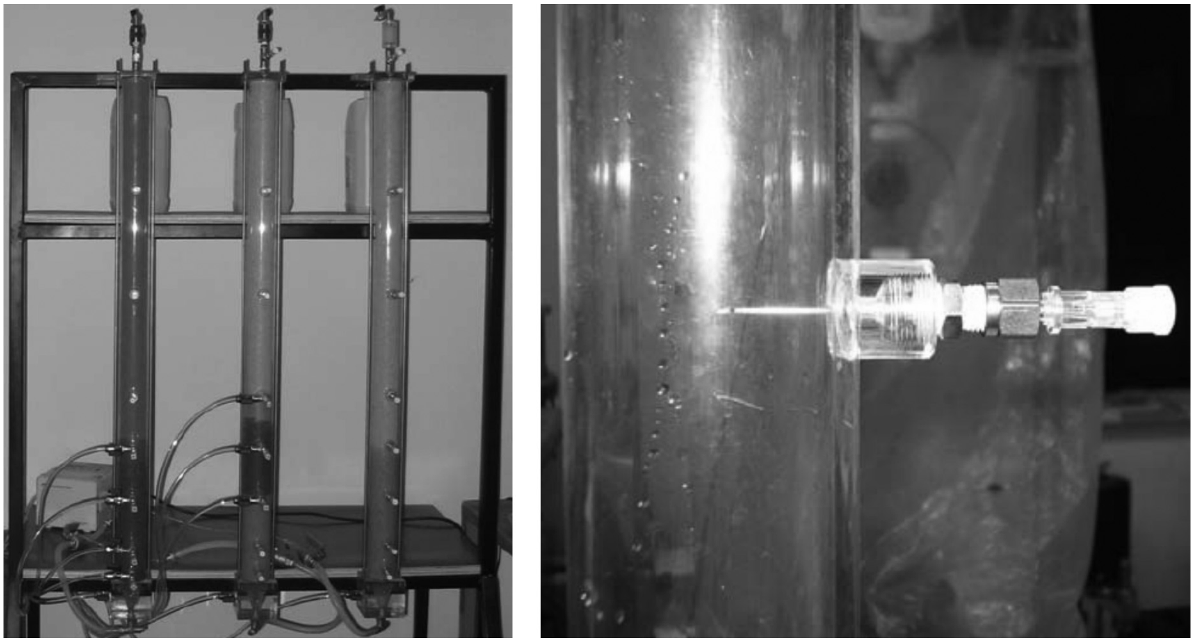

Figure 2 - Columns tests setup.

Table 1 - Column tests experimental program.

Contaminant	Initial concentr. (mg/L)	Reactive medium	Limit conc. Ground-water (mg/L)	ZVI (g)	Pumice (g)	PV (L)
Copper	50	ZVI	1	7850	-	0.97
Copper	50	Pumice 16/40	1	-	1015	1.33
Copper	50	ZVI-Pumice 2B; Weight Ratio 50:50	1	1240	1240	1.18
Copper	50	ZVI-Pumice 2B; Weight Ratio 30:70	1	595	1387	1.19
Copper	500	ZVI-Pumice 2B; Weight Ratio 10:90	1	155	1395	1.25
Nickel	5	ZVI	0.02	7850	-	0.97
Nickel	5	ZVI-Pumice 2B; Weight Ratio 50:50	0.02	1240	1240	1.18
Nickel	5	ZVI-Pumice 2B; Weight Ratio 30:70	0.02	595	1387	1.19
Nickel	40	ZVI-Pumice 2B; Weight Ratio 10:90	0.02	153	1374	1.26

measured in two columns filled with ZVI only and fed with the same contaminated solution of the 10:90 ZVI-Pumice granular mixture columns (see Table 1). Aqueous samples for chemical analyses were not collected from iron filled columns since they were used only as a benchmark for hydraulic conductivity tests.

In order to have a better understanding of the chemical mechanisms involved in the heavy metal removal, at the end of the test carried out on the columns filled with a granular mixture of ZVI and Pumice (weight ratio 10:90), a sample of the reactive medium was collected from the column inlet zone, the iron was magnetically separated from pumice and the two materials were dried in nitrogen atmosphere to prevent further reaction with the oxygen in the air. Nevertheless it was impossible to avoid air contact completely, especially during the extraction from the column, the drying and the preparation of the samples for the analyses. Furthermore, microscopic observation showed small pumice grains merged on the surface of iron grains while pumice samples appeared free of any iron inclusion.

Samples were analyzed using X-ray diffraction (XRD – Bruker D8 ADVANCE) and X-ray fluorescence (XRF – Bruker S2 RANGER).

4. Analysis of Experimental Results

The column tests results are shown in Table 2 and in Figs. 3 to 9. In particular, Figs. 3 to 6 present the tests results in terms of relative concentration (C/C_0, where C is the measured contaminant concentration in the samples collected and C_0 is the contaminant concentration at the inlet),

Table 2 - Column tests results.

Contaminant/ Initial conc.(mg/L)/ Reactive m.	Test duration (h)	Pollutant mass flowed (g)	Massic discharge (mg/s)	C_F (mg/L)	Specific removal (g cont./ g reac.m.)	Mass removal
Copper / 50 / ZVI	1032	1.548	$4.17*10^{-4}$	0.004	$1.97*10^{-4}$	99.993%
Copper / 50 / Pumice 16/40	528	0.792	$4.17*10^{-4}$	50*	$2.49*10^{-4}$§	18.970%
Copper / 50 / Mix ZVI-Pumice 2B; W. Ratio 50:50	1032	1.548	$4.17*10^{-4}$	0.007	$1.25*10^{-3}$	99.981%
Copper / 50 / Mix ZVI-Pumice 2B; W. Ratio 30:70	1032	1.548	$4.17*10^{-4}$	0.04	$2.6*10^{-3}$	99.901%
Copper/ 500 / Mix ZVI-Pumice 2B; W. Ratio 10:90	1500	22.555	$4.17*10^{-3}$	0.5	$1.45*10^{-2}/1.19*10^{-1}$§§	99.776%
Nickel / 5 / ZVI	1032	0.155	$4.17*10^{-5}$	0.002	$1.97*10^{-5}$	99.945%
Nickel / 5 / Mix ZVI-Pumice 2B; W. Ratio 50:50	1032	0.155	$4.17*10^{-5}$	0.003	$6.24*10^{-5}$	99.997%
Nickel / 5 / Mix ZVI-Pumice 2B; W. Ratio 30:70	1032	0.155	$4.17*10^{-5}$	0.005	$7.81*10^{-5}$	99.995%
Nickel/ 40 / Mix ZVI-Pumice 2B; W. Ratio 10:90	1500	1.612	$3.33*10^{-4}$	37.14**	$3.65*10^{-4}/5.19*10^{-4}$§§	30.759%

* Minimum concentration during the test equal to2.0 mg/L (measured at the outlet for T = 24 h).
** Minimum concentration during the test equal to 0.3 mg/L (measured at the outlet for T = 80,75 h).
§ Limit removal.
§§ Limit removal calculated for the sampling port at 8 cm from the inlet.

in time for ZVI-Pumice granular mixtures (weight ratio 30:70 and 10:90) for copper and nickel. Figures 7 and 8 show the trend of the contaminant specific mass removal (mass of contaminant removed for each gram of reactive medium) for the tests carried out using a granular mixture with a weight ratio of 10:90 for copper and nickel respectively. Figure 9 shows the variation in the hydraulic conductivity for the tests carried out using either the ZVI/Pumice granular mixture (weight ratio 10:90) or ZVI only.

The column tests results confirmed that granular mixtures of ZVI and Pumice, in different weight ratios (excepting the 10:90 granular mixture for nickel) have a significant remediation capacity for groundwater contaminated by either copper or nickel, reaching results both in terms of concentration and mass removed at the outlet of the column comparable (concentrations and mass removal at the outlet of the column are in the same order of magnitude) to those of the columns containing ZVI only but using a significantly lower amount of this reagent (see Table 2). In all columns tests the final pollutant concentration (C_F) reached values well below the limit stated in the Italian Regulation (Gazzetta Ufficiale della Repubblica Italiana, 2006); the only exception being constituted by the tests carried out using pumice alone or a granular mixture 10:90 and 40 mg/L nickel (Table 2), due, in the former, to the limited pumice efficiency and in the latter to the high contaminant concentration. The performance of granular mixtures with 30:70 and 50:50 weight ratio is very similar notwithstanding the higher ZVI content of the latter.

In the test carried out using a 50 mg/L Copper solution or a 5 mg/L Nickel solution (Figs. 3 and 4), both for the column using only ZVI as reactive medium and the mixture between ZVI and Pumice (weight ratio 30:70), the contaminant was almost completely removed in the first 3 cm of the column (Fig. 10). This circumstance is due to the fact that the mass of ZVI used in the columns greatly exceeds the amount necessary to remove the mass of contaminant flowing through the column during the test and to achieve the desired final concentration. This fact is proven by the evident corrosion only of the first layers of the filling material of the column, up to the first sampling port.

The fact that Figs. 3 and 4 present a steady trend is due to the limited duration of the transient period of the reaction that was probably already completed before the first sampling.

Table 2 clearly shows that the removal capacity of the pumice is limited and not sufficient alone to remedy severe contamination; in fact the column removal capacity was already exhausted after 528 h without reaching the allowed limit concentration.

The column tests carried out using ZVI-Pumice granular mixtures with weight ratio of 10:90 and highly contaminated solutions (Copper 500 mg/L and Nickel 40 mg/L, see Figs. 5 and 6) allowed the complete exhaustion of the reactive medium and the possibility to calculate the limit re-

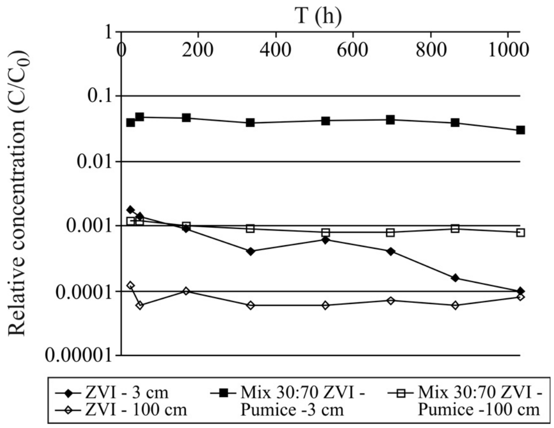

Figure 3 - Relative concentration *vs.* time for Copper (C_0 = 50 mg/L) in column tests with ZVI and ZVI – Pumice 2B granular mixture (weight ratio 30:70).

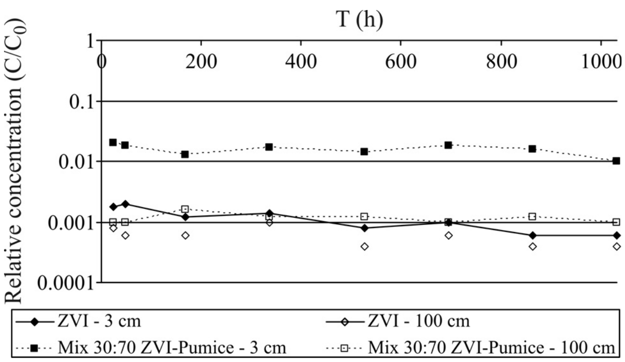

Figure 4 - Relative concentration *vs.* time for Nickel (C_0 = 5 mg/L) in column tests with ZVI and a ZVI – Pumice 2B granular mixture (weight ratio 30:70).

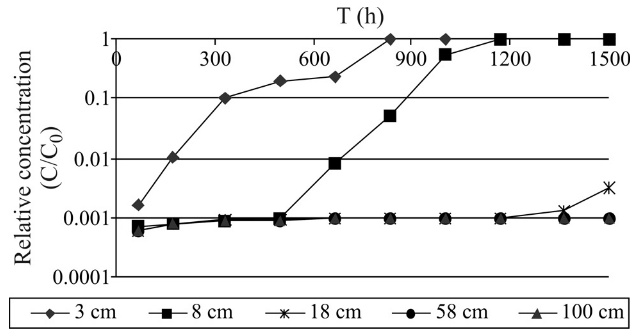

Figure 5 - Relative concentration *vs.* time for Copper (C_0 = 500 mg/L) in column test with a ZVI – Pumice 2B granular mixture (weight ratio 10:90).

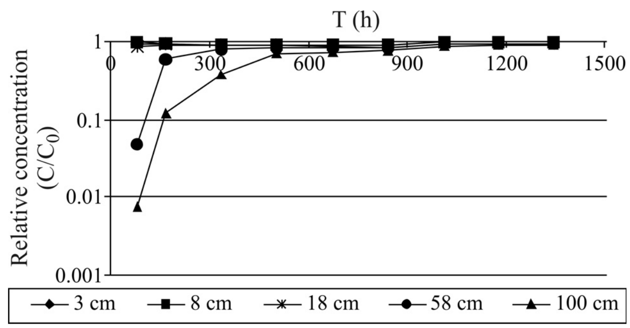

Figure 6 - Relative concentration *vs.* time for Nickel (C_0 = 40 mg/L) in column test with a ZVI – Pumice 2B granular mixture (weight ratio 10:90).

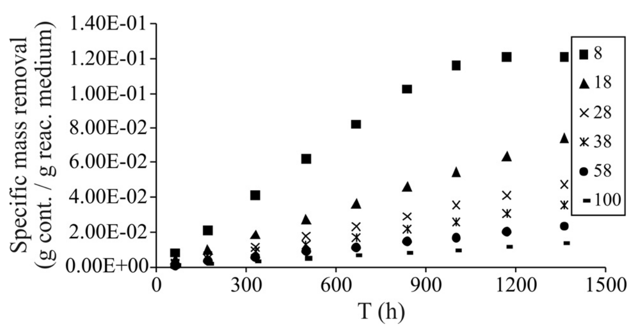

Figure 7 - Contaminant specific Mass Removal *vs.* time for Copper (C_0 = 500 mg/L) in column test with a ZVI – Pumice 2B granular mixture (weight ratio 10:90).

moval capacity. In particular, during the column test the removal capacity of the first 8 cm of the column solution tested with copper and nickel was completely annulated after respectively about 1200 and about 1000 h. The limit removal capacity of the reactive medium calculated for both the columns with reference to the first 8 cm differs for the two contaminants by more than two orders of magnitude (see Table 2), being higher for copper. Also, the trend of removal for the two pollutants is significantly different (Figs. 5 and 6).

The column removal capacity for copper (Fig. 7) was progressively exhausted and the separation between the part of the column involved in the removal and the zone still potentially active, indicated by the pollutant concentration and by the trend of specific removal is clear. On the other hand, the trend observed for nickel is different: after only 168 h of test duration the pollutant concentration at the outlet of the column was of the same order of magnitude as the one at the inlet, although more than 50% of the length of the column was still clearly active (pollutant concentration lower than 80% of the inflowing pollutant concentration and high residual specific removal capacity, Fig. 8). The different behaviors of the ZVI/Pumice granular mixtures concerning the two contaminants (see Table 2) might be linked to different removal mechanisms and chemical kinetics, in fact copper is more efficiently and rapidly removed than nickel.

As already mentioned, in order to assess the long-term hydraulic behavior of the different reactive media, the hydraulic conductivity was measured during column tests carried out in columns filled with a ZVI-Pumice 2B - 10:90 granular mixture and with ZVI only respectively, and flushed with contaminated solutions having a concentration of either 40 mg/L of nickel or 500 mg/L of copper (Fig. 9).

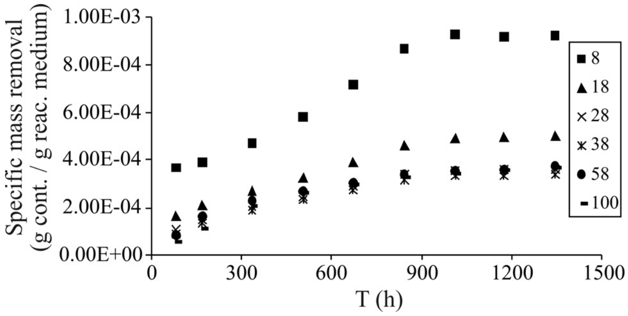

Figure 8 - Contaminant specific Mass Removal *vs.* time for Nickel (C_0 = 40 mg/L) in column test with a ZVI – Pumice 2B granular mixture (weight ratio 10:90).

At the beginning of the test the hydraulic conductivity was about 10^{-4} m/s for all the columns. At the end it was of the same order of magnitude (10^{-4} m/s) for the columns filled with the ZVI-Pumice mixture and for the one filled with ZVI only and flushed with the nickel contaminated solution, while it was more than four order of magnitude lower for the same column flushed with copper solution. This difference could be very probably be ascribed to the superior production of corrosion products in the column flushed with copper solution due to both the higher initial contaminant concentration and to the probable remarkable production of $Fe(OH)_3$ after complete metal removal (Moraci et. al., 2010). In fact, as already mentioned, metal removal and oxidation by water are probably competitive processes: the first is favored but when metal is removed the ZVI oxidation by water increases the pH and the related production of $Fe(OH)_3$ that precipitating increases clogging.

These results confirmed the efficiency of the granular mixtures in maintaining the hydraulic conductivity of the barrier in the long term while those filled with ZVI only present severe clogging problems (Fig. 9).

To give a more detailed analysis of the chemical mechanisms involved in contaminant removal, the results of XRD and XRF (Jeen *et al.*; 2007: Komnitsas *et al.*, 2007; Noubactep *et al.*, 2006; Rangsivek and Jekel, 2005; Furukawa *et al.* 2002) analyses carried out on the specimens from the samples collected from the columns after the test and on the same virgin materials are discussed below.

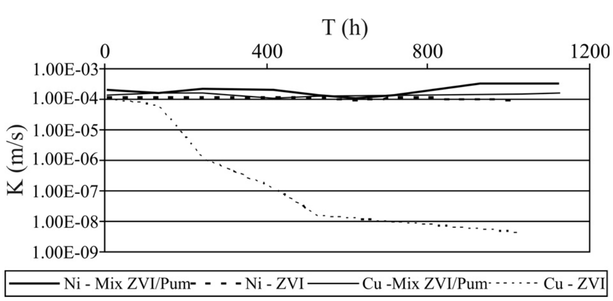

Figure 9 - Hydraulic conductivity *vs.* time in column test carried out using a either a ZVI – Pumice 2B granular mixture (weight ratio 10:90) or ZVI only and either Copper (500 mg/L) or Nickel (40 mg/L) contaminated solutions.

XRD tests allowed recognition of the crystalline compounds found in the iron and pumice specimens. The tests highlighted the presence of magnetite as the main oxidized form of ZVI; moreover, in the iron samples from the column fed with nickel, trevorite ($NiFe_2O_4$) was detected, while the presence of peaks due to traces of metallic nickel and bunsenite (NiO) cannot be confirmed with certainty. The presence of trevorite could be related to the coprecipitation of nickel and iron hydroxides (Pishch and Radion, 1996).

In the iron specimens collected from the column fed with copper, the main reaction products identified were copper hydroxide nitrate ($Cu_2(OH)_3NO_3$) and cuprite (Cu_2O); also in this case the presence of peaks due to trace of metallic copper cannot be confirmed. It is probable that cuprite derives from the oxidation, during sample preparation (pulverization by a mill), of Cu^0.

The XRD test carried out on pumice coming from the column fed with nickel does not reveal anything relevant, while the test carried out on the pumice taken from the copper column presents peaks attributable to copper hydroxide nitrate ($Cu_2(OH)_3NO_3$) and cuprite (Cu_2O).

The composition of the pumice samples given by XRF analyses is shown in Table 3; in the table, only compounds or elements present in concentrations higher than 1% have been reported since below this percentage the results are probably unreliable; however, the concentration of heavy metals present in the contaminated solution has been always reported.

From the analysis of these data, a rise in the concentration of iron and of the contaminant used during the test (copper or nickel, respectively) is evident. This fact is attributable to the contaminants removal performed by pumice and represents another demonstration that this material has a non negligible reactivity. The increase in iron concentration is similar for the two tests, while it seems that copper is more easily removed from the contaminated solution than nickel; nevertheless the concentration of the latter is

Table 3 - XRF analyses: Pumice composition after column tests using ZVI – Pumice 2B granular mixture (weight ratio 10:90) and Copper 500 mg/L and Nickel 40 mg/L contaminated solutions.

Compound	Pumice (contaminated solution Cu 500 mg/L)	Pumice (contaminated solution Ni 40 mg/L)
SiO_2	66.3%	69.9%
Cu	6.0%	-
Fe_2O_3	2.6%	3.4%
Al_2O_3	12.0%	12.6%
K_2O	4.0%	4.4%
Na_2O	5.8%	6.1%
MgO	2.0%	2.0%
Ni	-	0.3%

Figure 10 - ZVI filled column after the test.

only indicative, being close to the instrumental detection limit.

XRF analyses show that the amount of copper detected on the pumice sample is about 10% of that detected on the iron sample while for nickel this percentage is reduced to about 5%. This fact leads to the conclusions that for the 10:90 granular mixture flushed with copper contaminated solution, the removal imputable to ZVI is probably similar to the one imputable to Pumice, while for nickel it is approximately 50%. Moreover, it is likely that the amount of iron and contaminants found on pumice samples is also partly attributable to the accumulation of reaction products in the porous structure of pumice.

5. Conclusions

In this paper, in order to solve the problems related to the long term efficiency of ZVI PRBs in terms of permeability, the use of granular mixtures, in different weight ratios, of ZVI and pumice, a material never tested before for use in PRBs, has been proposed. The results of preliminary column tests, carried out using two different metallic contaminants (nickel and copper) in aqueous solution at different concentrations have been described, demonstrating that:

° The columns filled with iron-pumice mixtures presents a contaminant removal efficiency comparable to those filled with ZVI only;

° The most efficient compromise between efficiency (high metal removal) and efficient use of ZVI seems to be given by the granular mixture with 30:70 weight ratio.

° The permeability tests carried out during long term column tests using ZVI only, confirmed the possibility of problems related to PRBs clogging;

° The permeability tests carried out on the granular mixtures (ZVI-Pumice) confirmed the long term hydraulic efficiency of this material for use in PRBs and its capacity to maintain the aquifer flow.

Acknowledgments

The authors wish to thank Dott. Giuseppe Panzera (Ph. D.), Ing. Giulia Rigano (Ph. D.), and Ing. Stefania Bilardi (M. Sc.) for the indispensable help given during the research activity and to the Director and the Officials of the Environmental Protection sector of the Province of Reggio Calabria for the authorization to use the Atomic Absorption Spectrophotometer, property of the same Province.

References

Blowes, D.W.; Ptacek, C.J.; Benner, S.G.; McRae, C.W.T.; Bennett, T.A. & Puls, R.W. (2000) Treatment of inorganic contaminants using permeable reactive barriers. Journal of Contaminant Hydrology, 45:1-2, p. 123-137.

Cundy, B.; Hopkinson, L. & Whitby, R.L.D. (2008) Use of iron-based technologies in contaminated land and groundwater remediation: A review. Science of The Total Environment, v. 400:1-3, p. 42-51.

Furukawa, Y.; Kim, J.; Watkins, J. & Wilkin, R.T. (2002) Formation of ferrihydrite and associated iron corrosion products in permeable reactive barriers of zero-valent iron. Journal of Environmental Science and Technology, v. 36, p. 5469-5475.

Gazzetta Ufficiale della Repubblica Italiana (2006) Norme in materia ambientale (Environmental regulations). Gazzetta Ufficiale n. 88 del 14 aprile 2006. Poligrafico dello Stato, Roma.

Jeen, S.; Jambor, J.; Blowes, W. D. & Gillham, R. (2007) Precipitates on granular iron in solutions containing calcium carbonate with trichloroethene and hexavalent chromium. Journal of Environonmental Science and Technology, v. 41 p. 1989-1994.

Komnitsas, K.; Bartzas, G.; Fytas, K. & Paspaliaris, I. (2007) Long- term efficiency and kinetic evaluation of ZVI barriers during clean-up of copper containing solutions. Minerals Engineering, 20 p. 1200-1209.

Li, L.; Benson, C.H. & Lawson, E.M. (2006) Modeling porosity reductions caused by mineral fouling in continuous-wall permeable reactive barriers. Journal of Contaminant Hydrology, v. 83:1-2, p.89-121.

Li, L.; Benson, C.H. & Lawson, E.M. (2005) Impact of mineral fouling on hydraulic behavior of permeable reactive barriers. Ground Water, v. 43:4, p. 582-596.

Liang, L.; Moline, G.R.; Kamolpornwijit, W. & West, O.R. (2005) Influence of hydrogeochemical processes on zero-valent iron reactive barrier performance: A field investigation. Journal of Contaminant Hydrology, v. 78:4, p. 291-312.

Mackenzie, P.; Horney, D. & Sivavec, T. (1999) Mineral precipitation and porosity losses in granular iron columns. Journal of Hazardous Materials, v. 68:1-2, p. 1-17.

National Technical University of Athens (2000) Literature Review: Reactive Materials and Attenuation Processes for Permeable Reactive Barriers. Project on Long Term Performance of Permeable Reactive Barriers used for the Remediation of Contaminated Groundwater. Project Contract Number: EVK1-CT-1999-00035. Web Site: www.perebar. bam.de.

Moraci, N.; Calabrò, P.S. & Bilardi, S. (2010) Efficiency of zero valent iron/pumice granular mixtures in simultaneous removal of copper and nickel. Proceedings of Hazardous and Industrial Waste Management Conference, Chania.

Morrison, S.J.; Metzler, D.R. & Dwyer, B.P. (2002) Removal of As, Mn, Mo, Se, U, V and Zn from groundwater by zero-valent iron in a passive treatment cell: reaction progress modelling. Journal of Contaminant Hydrology, v. 56:1-2, p. 96-116.

Noubactep, C. (2006) Contaminant reduction at the surface of elemental iron: the end of a myth. Wissenschaftliche Mitteilungen, v. 31, p. 173-179.

Noubactep, C. (2008) A critical review on the mechanism of contaminant removal in Fe0-H_2O systems. Environmental Technologies, v. 29:8, p. 909-920.

Noubactep, C.; Schoner, A. & Meinrath, G. (2006) Mechanism of uranium removal from the aqueous solution by elemental iron. Journal of Hazardous Materials B, v. 132, p. 202-212.

Pishch, I.V.; Radion, E.V. (1996) A pigment based on coprecipitated iron(III) and nickel(II) hydroxides. Glass and Ceramics, v. 53:6, p.178-179.

Pumex spa (2008) Lipari Pumice. Website http://www.pumex.it/pumex%20inglese.pdf. Accessed October 1, 2008.

Rangsivek, R.& Jekel, M.R. (2005) Removal of dissolved metals by zero-valent iron (ZVI): Kinetics, equilibria, processes and implications for stormwater runoff treatment. Water Research, v. 39, p. 4153-4163.

Rigano, G. (2007) Studio dell'efficienza di Barriere Permeabili Reattive per la bonifica di acquiferi contaminati da metalli pesanti. Ph. D. Thesis Università degli Studi Mediterranea di Reggio Calabria.

Smith, E.H. (1996) Uptake of heavy metals in batch systems by a recycled iron-bearing material. Water Research, v. 30:10, p. 2424-2434.

Thiruvenkatachari, R.; Vigneswaran, S. & Naidu, R. (2008) Permeable reactive barrier for groundwater remediation. Journal of Industrial and Engineering Chemistry, v. 14:2, p. 145-156.

USEPA (1998) Permeable Reactive Barrier Technologies for Contaminant Remediation. EPA/600/R-98/125.

USEPA (2004) Evaluation of Permeable Reactive Barrier Performance. EPA 542-R-04-004.

Vogan, J.L.; Focht, R.M.; Clark, D.K. & Graham, S.L. (1999) Performance evaluation of a permeable reactive barrier for remediation of dissolved chlorinated solvents in groundwater. Journal of Hazardous Materials, v. 68:1-2, p. 97-108.

Wilkin, R.T. and McNeil, M.S. (2003) Laboratory evaluation of zero-valent iron to treat water impacted by acid mine drainage. Chemosphere, v. 53:7, p. 715-725.

Back Analysis of a Landslide in a Residual Soil Slope in Rio de Janeiro, Brazil

Denise Maria Soares Gerscovich, Eurípedes do Amaral Vargas Jr., Tacio Mauro Pereira de Campos

Abstract. After a short period of relatively intense rainfall, a deep-seated landslide occurred in a slope in Rio de Janeiro. On the following day, field inspection revealed full saturation of the failure mass, despite the inexistence of groundwater in the slope. A comprehensive experimental investigation was undertaken to determine the geotechnical parameters of the residual soil. A numerical modeling study of the infiltration processes revealed that the rainfall amount was insufficient to reproduce the saturation condition of the failure surface. This paper introduces the slope stability approach aiming to verify if the factor of safety would reflect a stable condition under the pluviometric records that occurred before the landslide. Therefore, 2D limit equilibrium analyses were accomplished, considering the different hydrological scenarios that were conceived for the flow simulations. The geotechnical parameters were defined according to laboratory test carried out on samples extracted from the slide surface and from an undisturbed site. Pore pressure distributions were obtained from previous results of flow simulations. Regardless of the geometry of the failed mass, the analyses indicated that the landslide could not be triggered solely by rain infiltration. Amongst various alternatives, a preferential flow through the bedrock fractured layer revealed to be the only feasible scenario that could reproduce not only the saturated condition, but also a FS value close to 1. Despite the usual approach of identifying the landslide as a rainstorm-induced mechanism, it appears to be more complex and other infiltration sources may play an essential role.

Keywords: unsaturated soil, residual soil, transient flow, rainfall, stability analysis, landslide.

1. Introduction

Rio de Janeiro city is located in the southeastern region of Brazil. Its mountainous landscape associated to a tropical humid climate results in slopes of unsaturated residual soil with thickness that may vary from a few centimeters to dozen of meters. Rain-induced soil and/or rock mass movements are quite frequent, during or immediately after periods of intense rainfall.

Despite the considerable progress in the understanding of the behavior of unsaturated soils, it is actually very difficult to predict when or where a landslide may happen. Nevertheless, it is recognized that rainfall-induced landslides are caused by changes in pore water pressures.

Many authors have attempted to address the probable causes of landslides (*e.g.* Kim *et al.*, 2004; Capra *et al.*, 2003; Gasmo *et al.*, 2000; Au, 1998; Costa Nunes *et al.*, 1989; Wolle & Hachich, 1989; Vargas *et al.*, 1986). Shallow failures may be attributed to the deepening of a wetting front into the slope, which results in a decrease of matric suction or to the development of the weathering process of steep slopes. Large landslides and debris flows usually result from the development of positive pore pressures that comes along with fully saturation of the soil mass. This scenario may be achieved when infiltrating water encounters a low permeability soil layer and a transient perched water table occurs (Capra *et al.*, 2003) or when water infiltrates through fractured layers of the bedrock (Dietrich *et al.*, 1986; Wilson, 1988; Vargas Jr. *et al.*, 1990). Further studies have also illustrated that positive pore pressure generation along the failure surface may be produced by the crushing of soil grains resulting in a liquefied soil condition (Wang & Sassa, 2003) or as a consequence of soil contraction that originates at the sliding surface and spreads to the unsaturated soil mass (Capra *et al.*, 2003).

In February 1988, a considerable number of soil/rock slides occurred in various slopes in Rio de Janeiro city. Most of them were shallow and quite long in extension (100-150 m) and were classified as being amongst the largest that have occurred in the city. The pluviometric data corresponding to 21 days indicated an accumulated amount of 515.6 mm, with a rain peak of 85.4 mm in a single day.

Nine months later, in November, a deep-seated slide occurred in a re-vegetated slope (Fig. 1) after a period of a medium intensity rainfall. After 21 days, the accumulated rainfall amount was 246.3 mm, with a maximum rain peak of 57.5 mm (Fig. 2). The failure caused structural and material damages to an adjacent building, with the shearing of one pillar and complete destruction of one apartment. Sev-

Denise Maria Soares Gerscovich, Departamento de Estruturas e Fundações Universidade do Estado do Rio de Janeiro, Rio de Janeiro, RJ, Brazil. e-mail: deniseg@uerj.br.
Eurípedes do Amaral Vargas Jr., Departamento de Engenharia Civil, Pontifícia Pontifícia Universidade Católica do Rio de Janeiro, Rio de Janeiro, RJ, Brazil. e-mail: vargas@civ.puc-rio.br.
Tacio Mauro Pereira de Campos, Departamento de Engenharia Civil, Pontifícia Universidade Católica do Rio de Janeiro, Rio de Janeiro, RJ, Brazil. e-mail: tacio@civ.puc-rio.br.
Submitted on July 15, 2010; Final Acceptance on January 11, 2011; Discussion open until December 30, 2011.

Figure 1 - Slope view on the day after.

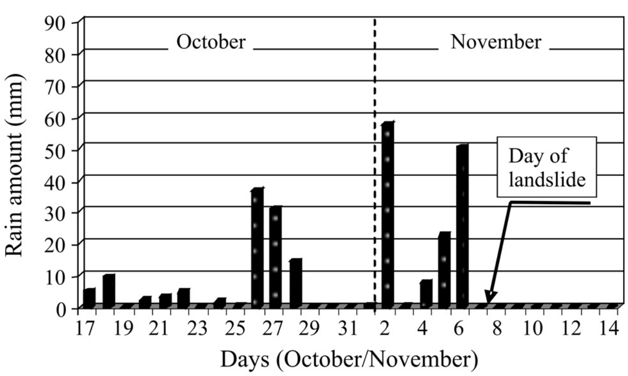

Figure 2 - Daily pluviometric data.

eral cars in external and internal building parking areas were also damaged. Fortunately, nobody was injured. Despite no evidence of groundwater within the slope, on the following day and continuously for the following week after the slide, there were clear indications of full saturation of the failure surface, with groundwater springs in its upper region.

Figure 3 shows a schematic topographic plan of the site before the landslide. The slope crest has a maximum elevation of 384 m and surface inclinations ranging from 30° to 55°. At the toe of the slope there was a gravity wall aligned with an anchored wall, located at the rear of Building A. The superficial drainage system, located in the upper region of the slope, was presumably malfunctioning, since blockage of the channel adjacent to the slide was observed during field inspections.

Preliminary analyses disregarded the hypothesis of failure of the retaining wall structure as the shape of the failure surface suggested a major tendency of soil movement over the wall crest. There was also no evidence that the accumulated rainfall could have raised the water table, which was located at a considerable depth below ground level. Using a simple one-dimensional water balance, one can prove that a large amount of water would be required to achieve soil saturation. Considering, for example, the average depth of the sliding mass to be approximately 5 m, fully drained condition and typical values of porosity (n = 0.38) and volumetric water content ($\theta = V_w/V = 0.1$), then the difference between both parameters gives the available volume of voids to be filled. Therefore, full saturation of the profile would require at least 1400 mm of infiltrating water. Besides this unrealistic value, the actual volume of water that infiltrates, compared to the rainfall rate, depends, among other factors, on the initial soil moisture condition, slope angle, vegetation type, etc. Consequently, the amount of infiltration would be less than the values predicted by the pluviometers data. Nevertheless, the triggering mechanism was undoubtedly associated to changes in the pore water

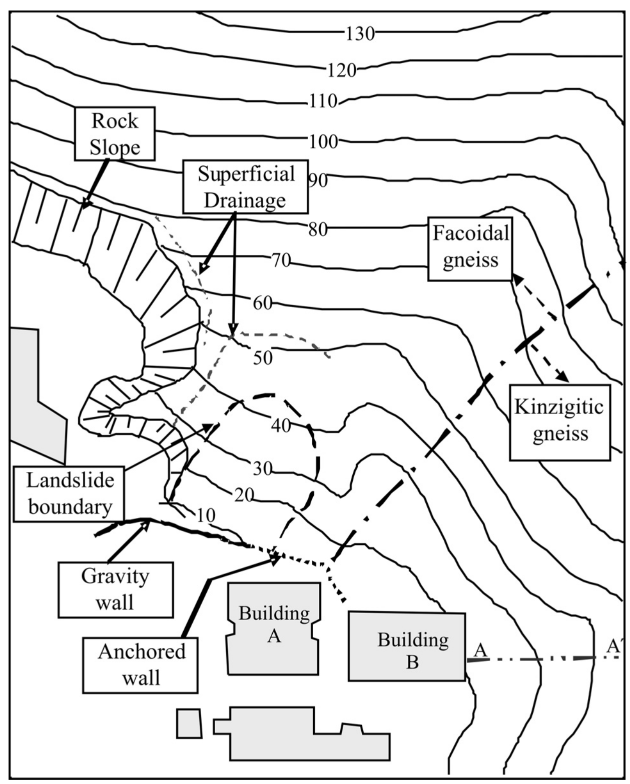

Figure 3 - Schematic site plan before landslide.

pressure and it was likely that complex changes of the slope hydrogeology might have occurred.

Numerical 3D-FEM transient flow analyses were carried out to identify the infiltration process that could explain field evidence of complete saturation of the failure surface. Different boundary conditions were conceived and the results revealed that only major changes of the slope hydrogeology could justify the deep-seated slope failure (Gerscovich *et al.*, 2006).

This paper describes the investigations that were carried out after the slope failure in order to define soil stratigrafy and the geotechnical parameters of the residual soils. Slope stability analyses were also performed with pore water meshes previously obtained from transient flow simulations.

2. Geotechnical Investigation

A comprehensive series of field and laboratory tests was carried out to determine soil profile and geotechnical and hydrological parameters. Field investigation comprised seismic refraction surveys, percussion and rotary drillings. Twenty-one holes were drilled for the installation of fifteen piezometers and six slope indicators, outside the slide area. Maxima piezometers (Brand, 1985) were also installed at the soil-rock interface to record maximum transient water pressure levels A pluviometric station was installed on the roof of the building, as well. For more details regarding field instrumentation refer to Gerscovich *et al.* (2006).

The soil profile showed depths varying from 0 to 15 m and was originated from a gneissic metamorphic rock that outcropped at the upper and left sides of the landslide boundary. The weathering profile was composed of a superficial mature clayey sand residual soil, with an average thickness of 1 m, underlain by a layer of a sandy matrix young residual soil (saprolitic soil), with a well defined inherited mineral alignment from the parent rock. The transition between the sound rock and the saprolitic soil is a highly fractured and weathered rock with a thickness varying within 4 m to 10 m. The mechanical soundings did not indicate the presence of a groundwater level within the soil mass. However, water level was observed in some rotary drillings within the fractured rock layer. Figure 4 illustrates the a cross section of the slope behind building B (section AA' - see Fig. 3).

Topographic plans that were generated before and after the slide, aero photos taken between 1966 and 1975, and logging profiles were used to restore the original geometry of the whole area as well as to define the landslide surface. The failure surface presented an ellipse shape with the relationship width (perpendicular to the movement) and length (along the direction of the movement) of approximately 0.6. Figure 5 displays the reconstructed 2D central section of the slope and the 3D geometry along with boundaries description.

Block samples were extracted from the slope failure surface and from a trench located 50 m away from the failure zone. The laboratory investigation comprised geotechnical characterization, determination of hydraulic parameters (hydraulic conductivity and water retention curve) and shear strength tests.

2.1. Soil characterization

Table 1 shows a summary of the characterization tests with the average physical indexes. Two different materials appeared at the failure surface: an apparently homogeneous and isotropic red-colored mature residual soil, and a grey saprolitic soil, with a well-defined mineral alignment. At the trench, only the saprolitic soil was extracted and it was coarser and denser than the one from the slip surface.

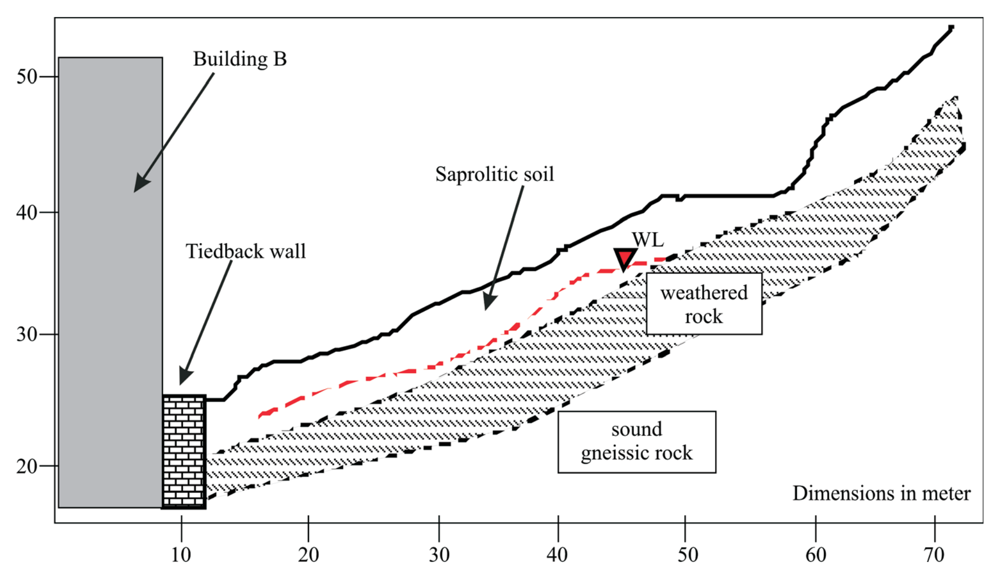

Figure 4 - Cross section behind building B.

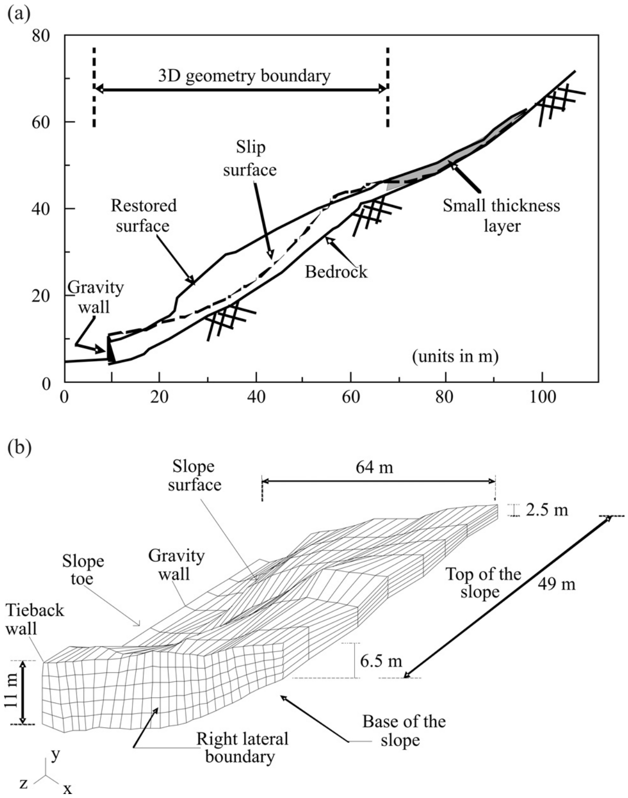

Figure 5 - Restored geometry. (a) Central section of the slope. (b) 3D geometry and boundaries description.

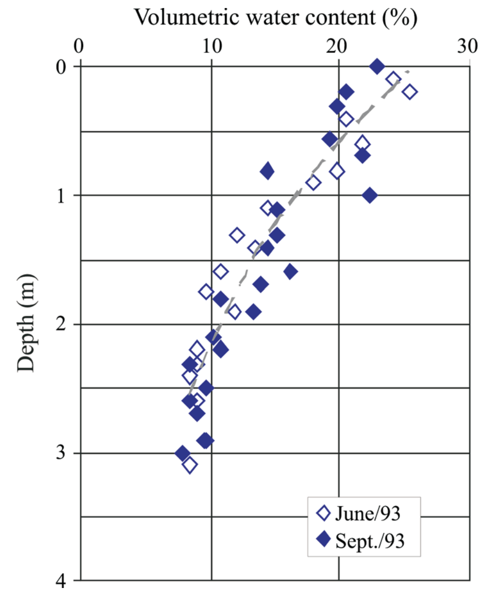

Figure 6 - Volumetric water content profiles of the saprolitic soil from the trench.

Table 1 - Soil characterization.

Location	Slip surface		Trench
Soil type	Saprolitic soil	Mature soil	Saprolitic soil
Sand (%)	63.0	56.0	82.0
Silt (%)	27.5	34.0	9.8
Clay (%)	9.5	10.0	8.2
ω_L (%)	38.2	39.5	-
ω_P (%)	NP	24.7	-
ω (%)	19.0	21.2	6.4
θ (%)	22.4	25.5	10.3
G_s	2.64	2.63	2.66
e	1.19	1.14	0.62
n	0.54	0.53	0.38
γ_t (kN/m^3)	14.0	14.6	17.1

Notes: ω_L = liquid limit; ω_L = plasticity limit; ω = water content; θ = volumetric water content; G_s = specific gravity of grains; e = voids ratio, n = porosity, γ_t = in situ density.

The volumetric soil moisture profile of the saprolitic soil extracted from the trench, located behind Building B, is shown in Fig. 6. The results indicated volumetric water content around 25% on the surface and a gradual reduction with depth. Below 2 m deep, this value is approximately constant and equal to 9%.

2.2 Shear strength parameters

Isotropically consolidated drained triaxial tests (CID) were performed on saturated 100 mm-diameter undisturbed samples of the saprolitic soil extracted from the trench. The specimens were molded with the xistosity plane inclined around 30° with the horizontal plane. The consolidation stress levels ranged from 25 to 200 kPa and the shearing velocity was 0.0122 mm/min. The triaxial chamber allowed for the use of internal devices for automatic measurement of axial and radial strains and volume changes (water and total volume). The variations of air volume were mechanically monitored by a bubble trap device (Aguilar, 1990).

Conventional direct shear tests were carried out on soil samples extracted from the slip surface. The saprolitic soil specimens were molded with the shearing plane parallel and perpendicular to the plane of xistosity. In spite of the apparent isotropic condition, the mature soil samples were also prepared according to perpendicular angles. The samples were initially saturated, prior to the consolidation stage, under normal stresses ranging from 22 to 135 kPa. The shearing velocity was 0.036 mm/min and the shear box was assembled with an opening of 0.5 mm between the two halves.

Figure 7 shows the shear strength test results of the saprolitic soil and Table 2 summarizes the mean values of strength parameters, with no influence of the shear plane angle with respect to the xistosity orientation having been observed. The results revealed a reasonable agreement between the direct shear and the triaxial tests of the saprolitic soil, despite the differences on soil characterization.

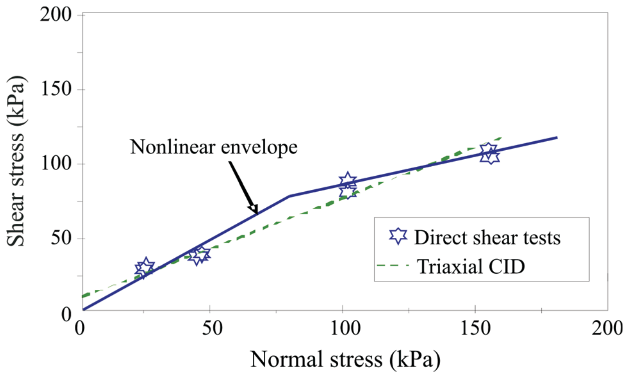

Figure 7 - Shear strength of saprolitic soil – saturated condition.

The Mohr-Coulomb strength envelope of the saprolitic soil could be fitted by a straight line with effective cohesion and friction angle equal to 13 kPa and 33°, respectively. However, due to the relatively high percentage of sand, it would be expected a null cohesion within the range of low confining stresses. For that reason, the Mohr-Coulomb strength envelope would better defined by a bi-linear curve that is also plotted in Fig. 7. The small thickness mature residual soil provided lower values of strength parameters as a result of a more intense weathering process.

The shear strength response of the residual soil under unsaturated condition was determined by direct shear tests with suction control. The tests were carried out on samples extracted from the slip surface, according to a multi stage technique (Ho & Fredlund, 1982), following the wetting path (Fonseca, 1991; Carrillo *et al.* 1994). Similarly to the saturated tests, specimens were molded with shearing planes parallel and perpendicular to the plane of xistosity. The samples were initially consolidated under a vertical stress of 50 kPa, and then submitted to decreasing suctions from 200 to 15 kPa (de Campos *et al.*, 1994). The shearing velocity was equal to 0.0366 mm/min.

The shear strength of unsaturated soils is based on the Mohr-Coulomb criterion and, according to Fredlund *et al.* (1978), can be expressed by:

$$\tau = c' + (u_a - u_w)\mathrm{tg}\phi^b + (\sigma - u_a)\,\mathrm{tg}\phi' \qquad (1)$$

where u_a and u_w are the pore air and pore water pressures, respectively, σ is the total normal stress; c' and ϕ' are effective strength parameters and ϕ^b is the angle indicating the rate of increase in shear strength relative to the matric suction. ϕ^b is equal to ϕ' at low matric suction, and decreases to a lower value at high matric suctions (Tekinsoy *et al.*, 2004).

Figure 8 shows the shear strength results with respect to soil suction. Similar to the saturated soil response, no influence of xistosity plane on the soil strength was observed. The nonlinear relationship between the shear strength and soil suction was fitted by a bi-linear curve with $\phi^b = 33°$, for soil suction up to 115 kPa, and equal to 20°, for higher values. For low soil suctions values, the ϕ^b value was equivalent to ϕ'.

The similarity between ϕ^b and ϕ', for low values of matric suction, was also observed by Rahardjo *et al.* (1995) in triaxial tests on residual soils of Singapore. Following a drying path, the authors obtained ϕ^b equal to 26°, for matric suctions up to 400 kPa, which was equal to the soil effective friction angle ϕ'.

It is worth to note that the relatively high ϕ^b values revealed the strong influence of the matric suction on the shear strength; thus, any infiltration process promotes a substantial reduction of the shear strength.

Table 2 - Saturated strength parameters.

Test soil	Conventional direct shear test		Triaxial test
	Saprolitic soil	Mature soil	Saprolitic soil
c'(kPa)	14.6	4.8	9.6
ϕ'(°)	31.8	27.5	34.0

Notes: c' = effective cohesion; ϕ' = effective friction angle.

2.3. Hydraulic parameters

The hydraulic conductivities profiles were obtained by laboratory tests on 100 mm-diameter samples and in the field by means of Guelph permeameter tests (Reynolds & Elrick, 1987). The results in Fig. 9 reveal a sharp decrease of the relative hydraulic conductivity (k/k_{sat}) with the increase of matric suction, within the first 3 m of the soil profile. Below this depth, the hydraulic conductivity parameters were considered constant.

Soil-water retention curves (SWCC) were obtained from the saprolitic soil samples from the slip surface, following drying and wetting paths. The results, shown in Fig. 10, indicated no significant deviation between the wetting and drying curves. Characterization of the saprolitic soil of the slip surface (Table 1) indicates that the saturated

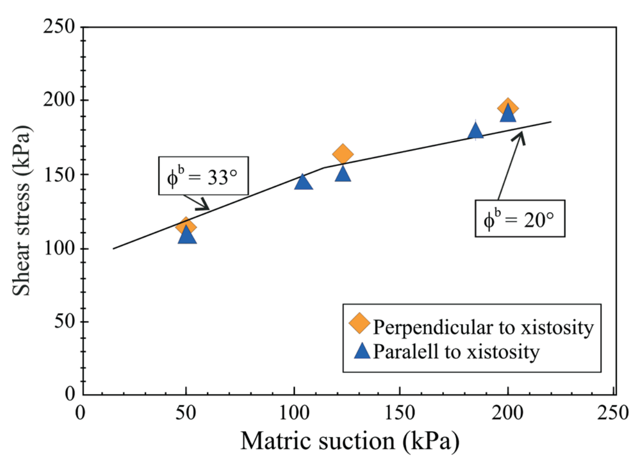

Figure 8 - Unsaturated strength envelope.

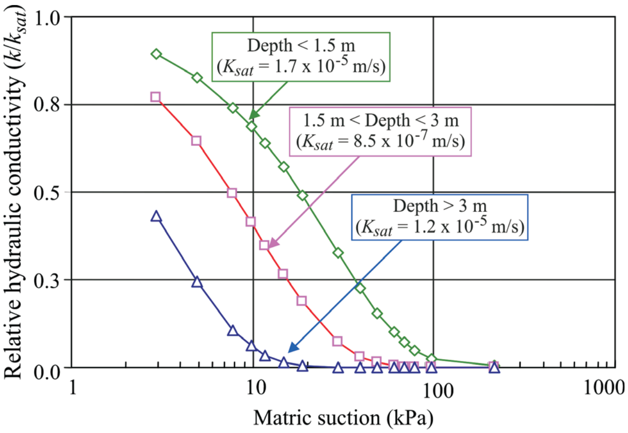

Figure 9 - Prescribed relative hydraulic conductivity curves.

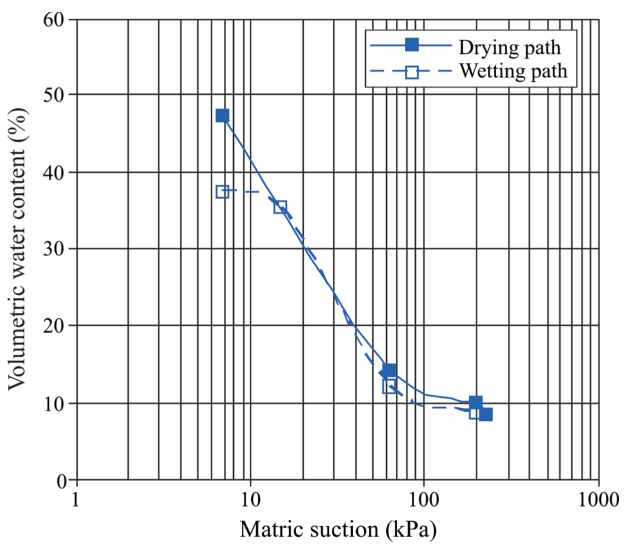

Figure 10 - Soil-water retention curve of the saprolitic soil from the slip surface.

volumetric water content ($\theta_s = n$ x S) is equal to 54%. However, the results suggests a lower value, around 40% that is mainly attributed to entrapped air effects. A more detailed description regarding the hydraulic parameters tests and data interpretation are presented in Gerscovich *et al.* (2006).

3. Transient Flow Simulations

The general equation that controls steady-unsteady state flow problems through 3-D saturated-unsaturated porous media, usually referred to as Richards' equation, may be written as:

$$\frac{\partial}{\partial x_i}\left[k_{ij}^s K_r \frac{\partial h_p}{\partial x_i} + k_{ij}^s K_r\right] = \left[C(\psi) + \frac{\theta(\psi)}{n} S_s\right]\frac{\partial h_p}{\partial t} \qquad (2)$$

where h_p is the pressure head, ψ is the matric suction, θ is the volumetric water content (V_w/V), k_{ij}^s is the tensor of hydraulic conductivity at saturation; K_r is the relative hydraulic conductivity, which is defined as the relationship between unsaturated and saturated hydraulic conductivities (k/k_{sat}); K_r is a scalar function of the degree of saturation ($K_r(S)$) that varies between 0 and 1; $C(\psi)$ is the volumetric water retention capacity ($\partial\theta/\partial\psi$), given by the tangent to the SWCC, n is the porosity and S_s is the coefficient of specific storage. S_s physically represents the volume of water that a unit volume of porous media releases from storage under a unit decline in hydraulic head (Freeze & Cherry, 1979). [$K_r k_{ij}^s$] represents the effect of the elevation head, since the equation is written in terms of pressure head.

A finite element program (FLOW3D) was specially developed (Gerscovich, 1994) to solve the general flow equation to evaluate flow processes that might have happened within the slope. Its code was derived from FPM500 finite element program (Taylor & Brown, 1967), which performs flow modeling within saturated soil media. The major modifications were based on the paper by Neuman (1973), in order to incorporate the unsaturated and transient conditions.

The mathematical development of the flow equation, built-in in the FLOW3D code, assumes that: i) flow is laminar and Darcian; ii) inertial forces, velocity heads, temperature gradients and chemical concentration gradients are all negligible; iii) soil is linearly elastic and isotropic; iv) hydraulic properties are not affected by volume changes; v) the air phase is continuous and always in connection with the constant, external atmospheric pressure; vi) the hysteretic behaviour of the SWCC is negligible; vii) the effect of soil compressibility on the storage of water under unsaturated conditions is quite small.

FLOW3D was tested for various steady and unsteady state flow conditions and geometries. 1D steady-state state response was evaluated by prescribing constant pressure heads at the boundaries of an unsaturated soil profile and comparing the results with the exact solution. 1D transient flow condition was evaluated by computing the volume of infiltrating water and comparing it with Buchanan *et al.* (1980) results. 2D steady state condition was evaluated by simulating flow infiltration through a homogeneous earth dam until the development of a phreatic surface that remained fixed and similar to Kozeny's solution. The 3D transient flow condition was evaluated by reproducing a 3D model experiment run by Akai *et al.* (1979). Detailed description of flow tests referrer to Gerscovich *et al.* (2006).

3.1. Slope geometry and boundary conditions

The 3D mesh comprised 1820 elements and 2436 nodes, as shown in Fig. 5b. The small thickness layer, located at the top of the slope (Fig. 5a), was disregarded in order to avoid excessive mesh discretization. It is worthwhile to mention that a 2D analysis of the center cross section of the slope revealed that the amount of the rainfall rate was sufficient to fully saturate the small thickness layer. Consequently, its effect was indirectly incorporated by prescribing pressure heads at nodes located at the top boundary.

The lateral boundaries, bottom of the slope, as well as the slope toe were considered as impervious surfaces. At the slope surface, daily rainfall events were simulated by prescribing flow velocities at the surface nodes, according to the amounts registered at a pluviometric station, located 4 km away from the slope.

The time dependent characteristic of the transient flow through unsaturated soil requires the knowledge of the initial distribution of matric suction (or soil moisture), previous to the simulation period. Flow modeling assumed null suction at the slope surface and a progressive increase of matric suction with depth. Below 2 m-depth the soil suction was taken as constant and equal to 200 kPa. These values were assumed by evaluating both the water content profile of the saprolitic soil (Fig. 6) and the soil water retention curve (Fig. 10).

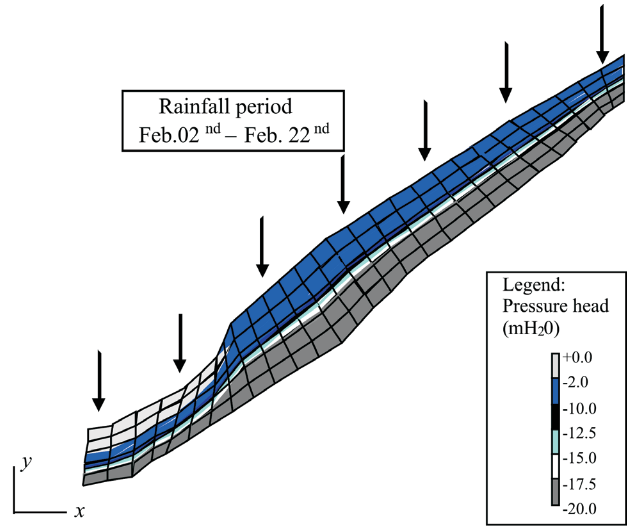

Figure 11 - Pressure head distribution at the central section of the slope - 3D Analysis (Gerscovich *et al.*, 2006).

3.2. Flow simulation results

Different scenarios of flow infiltration were analyzed in an attempt to reproduce the full saturation of the slope that was observed the day after the landslide, despite the inexistence of groundwater within the soil mass (Gerscovich *et al.*, 2006).

3.2.1. Case 1: Flow pattern predicted after 21 days of rainfall recorded in February, 1988

The influence of rainfall intensity was initially evaluated by analysing flow patterns considering a more intense rainfall that occurred few months before the landslide. In this period, the accumulated rainfall was approximately 2 times greater than the registered in November, 1988, prior to the landslide. The results, shown in Fig. 11, indicated slight changes in pressure head distributions, but no development of positive pore pressures within the soil slope. This pore-water pressure distribution is in disagreement to field observation after the landslide, since water was springing from the failure surface. This result, therefore, suggests that rain infiltration solely would not be sufficient to produce significant pore-water changes.

3.2.2. Case 2: Flow pattern predicted after 19 days of rainfall recorded in November, 1988, with an extra pressure head imposed at the top of the slope

The effect of disregarding the small thickness layer, located at the top of the slope, was evaluated by analysing its response to rain infiltration. Thus, a 2D flow analysis of this varying thickness layer (Fig. 5a) was carried out and revealed that 17 days of rainfall, prior to November 2nd (landslide day), could easily induce its complete saturation. In this study, the initial matric suction was set constant and equal to 10 kPa, the lower and bottom boundaries were impervious and null pressure heads were prescribed at the upper boundary.

The effect of the saturation of the upper layer was incorporated in the 3D numerical analysis by prescribing hydrostatic pressure heads at the top boundary nodes. In this study, flow velocities imposed at the nodes of the slope surface comprised 19 days of rain events, from October 19th to November 7th. Figure 12 presents the pressure head distribution predicted at the central section of the slope. Despite the generation of positive pore pressure at the upper zone, mainly due to the progress of a saturation front, this result still did not reproduce the saturation condition of the failure surface that was verified after the slide.

An additional numerical analysis was carried out in an attempt to evaluate if geometry changes of the slope, produced by the displacement of the soil mass after the landslide, could accelerate the progression of the saturation front. This hypothesis was tested by performing a 2D nu-

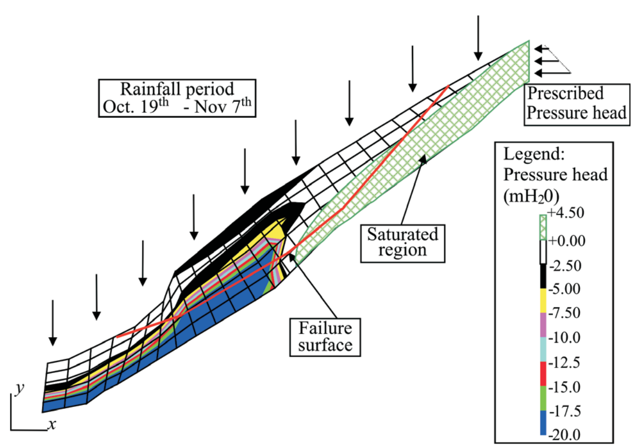

Figure 12 - Pressure head distribution in the central section of the slope; prescribed heads at the top of the slope - 3D Analysis (Gerscovich *et al.*, 2006).

merical simulation of the central section of the slope, including the small thickness layer, located at the top of the slope. In this analysis, a high value of saturated hydraulic conductivity ($k_{sat} = 1$) was used for the soil above the failure surface and null pressure heads were prescribed at the nodes at failure surface. The initial moisture conditions where equivalent to the ones predicted after 19 days of rain simulation (Fig. 12) and the remaining boundary conditions were unchanged. The results confirmed that few hours were sufficient to nearly cause a saturation of the whole soil mass and could be a feasible explanation for the saturation condition of the failure surface. However, it could not explain the landslide, since it was likely that large positive pore-water pressures would be required to reduce shear strength and cause the soil mass to fail.

3.2.3. Case 3: Flow pattern generated by a rainfall period of 5 days prior to the landslide and pressure heads prescribed at the top and at the base of the slope

Field investigations indicated the existence of a 4 to 10 m thick highly fractured rock layer at the transition of the sound rock and saprolitic soil. Maxima piezometers measured water levels restricted to this transition layer and confined to a small area.

The major role of the bedrock in generating high pore-water pressures have already been pointed out by other researchers (Dietrich *et al.*, 1986; Wilson, 1988; Vargas Jr. *et al.*, 1990). On the other hand, in the current engineering practice, it is very difficult not only to identify the existence of layers with high transmissivities but also to conceive an adequate mathematical model for this condition. Nevertheless, the influence of an eventual preferential flow through the fracture systems was roughly evaluated by prescribing positive pressure heads at 13 nodes, located along a transversal line of nodes at the base of the 3D mesh, as shown in Fig. 13. At each node, the magnitude of pressure head was equivalent to the vertical distance between the node coordinate and the highest point of the slope mesh. This simulation was carried out for a time of approximately 6 days, from November 2nd to November 7th. Boundary conditions and initial soil suction were similar to the ones used in the previous analysis. The numerical simulation (Fig. 13) showed that the whole soil mass nearly reached full saturation, with high levels of positive pore pressure been achieved and confirmed the major influence of water sources when they occur at the base of the slope.

4. Slope Stability Analyses

The stability analyses were carried out using the code SLOPE/W (GEO-SLOPE International Ltd – 2003), which allows for the computation of safety factors under in 2D conditions.

The slope profile consisted of a superficial mature residual soil and a variable thickness saprolitic soil layer. Due to the small thickness of the mature residual soil, this layer

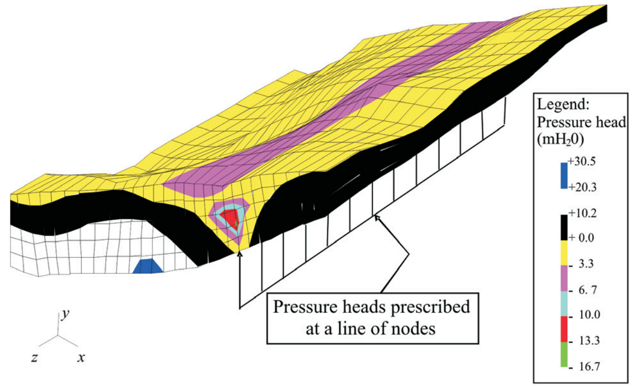

Figure 13 - Pressure head distribution – prescribed heads at the top and at the base of the slope- 3D Analysis (Gerscovich *et al.*,

was disregarded and the stability analyses were carried out considering a homogeneous material.

The geotechnical parameters were obtained from laboratory tests and are listed in Table 3. The non-linearity of the effective strength envelope, obtained from Fig. 7, was adjusted by two straight lines crossing at a confining stress equal to 80 kPa. Due to limitations of the computer program, the unsaturated strength parameter (ϕ^b) was assumed constant and equal to the average value of the experimental results.

It is worthwhile to mention that the strength parameters correspond to peak values, as the stress-strain curves did not show any loss of strength for high strain levels.

The stability analyses were undertaken for the different scenarios of flow infiltration previously described. The pore-water pressure distributions at the central section of the slope were incorporated in the SLOPE/W program through a mesh of 46 nodes, as the program presents a limitation of the maximum number of nodes (50 nodes). The effect of pore air pressure was disregarded.

4.1. Case 1: Flow pattern predicted after 21 days of rainfall recorded in February, 1988

Figure 14 displays the set of results of Morgenstern & Price method for a slip surface similar to the one observed in situ (FS = 4.1) and for a potential failure surface derived

Table 3 - Geotechnical parameters.

Soil Parameter	Shear stress level (kPa)	
	≤ 80.0	> 80.0
γ_t (kN/m^3)	17.5	17.5
c' (kPa)	0	44.2
ϕ' (°)	43.7	22
ϕ_b (°)	25	25

Notes: ϕ^b = rate of increase in shear strength relative to the matric suction.

from center grid search (FS = 3.5). Both analyses provided high factors of safety and the potential failure surface showed an higher initiation point and a larger volume of the displaced soil mass.

Shear tests with unsaturated samples indicated a bi-linear relationship between shear strength and matric suction and relatively high ϕ^b values. The influence of the matric suction on the safety factor was evaluated by performing analyses with $\phi^b = 0$. The factors of safety obtained were relatively high and equal to 1.53 and 1.67, for the circular search and field surfaces, respectively.

Stability analyses were also carried out in order to identify the likely range of shear strength parameters that would result in a FS close to 1. The smallest factors of safety (FS = 1.13 and 1.17, for the circular search and field surfaces, respectively) were computed by disregarding the influence of the matric suction and using the effective strength parameters obtained in the saturated CID tests.

It is worthwhile to emphasize that the analyses were carried out considering a plane strain condition. The 3D feature of the landslide would undoubtedly provide higher factors of safety.

The computed FS revealed that an ordinary amount of rain infiltration would not be sufficient to trigger the slope failure. These results are in accordance to the conclusions derived from the numerical simulations of rain infiltration, since it did not reproduce the saturated condition of the failure surface.

4.2. Case 2: Flow pattern predicted after 19 days of rainfall recorded in November, 1988, with an extra pressure head imposed at the top of the slope

The small thickness layer at the top of the slope (Fig. 5a) was disregarded to improve 3D mesh discretization. However, full saturation of this region could actually have happened and imposed an additional boundary condition. 2D flow simulation of this layer (Fig. 5a) subjected to 17 days of rain infiltration, prior to the landslide day, resulted in complete saturation of this soil.

This alternative was taken in account in the 3D flow analysis by prescribing hydrostatic pressure heads at the nodes located at the upper boundary of the mesh. The 3D numerical flow simulation revealed a localized positive pore pressure generation at the upper zone, mainly due to the progress of a saturation front. At the failure surface the soil mass remained unsaturated and, therefore, did not reproduce field condition.

Stability analyses, corresponding to the observed field surface and potential failure surface provided values of FS higher than 1.5, as shown in Fig. 15. Thus existence of a water source at the top of the slope promoted an increase of the pore water pressure mesh, which was definitely not sufficient to trigger the landslide.

4.3. Case 3: Flow pattern generated by a rainfall period of 5 days prior to the landslide and pressure heads prescribed at the top and at the base of the slope

The results of the 3D numerical simulations of different flow scenarios pointed out that, besides rain infiltration, other mechanisms might played a major role on the slope hydrological pattern. Field investigations have indicated the existence of a highly fractured rock layer at the transition between the saprolitic soil and the sound rock. This layer was, therefore, incorporated in the flow analyses assuming that preferential flow paths through the fractures could act as deep water sources at different positions of the base of the slope. The 3D flow simulation of 6 days of rain infiltration resulted in an almost full saturation condition of the whole soil slope (Gerscovich *et al.*, 2006). The loss of soil suction followed by generation of positive pore pressure appeared as an ideal condition for the landslide. In fact,

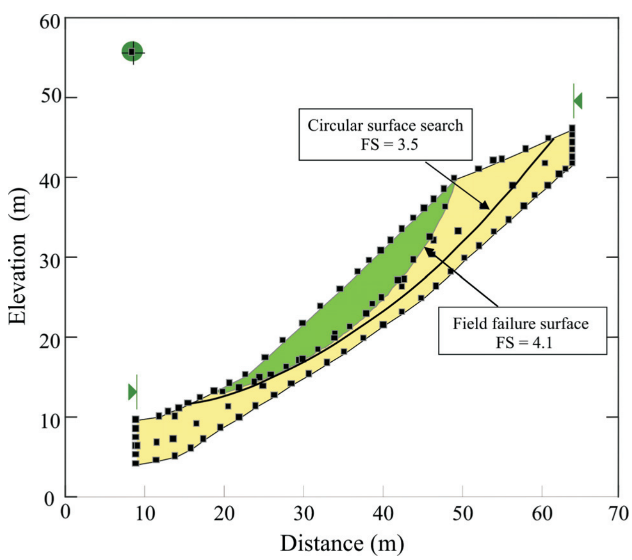

Figure 14 - Failure surfaces and Factors of Safety – Case 1.

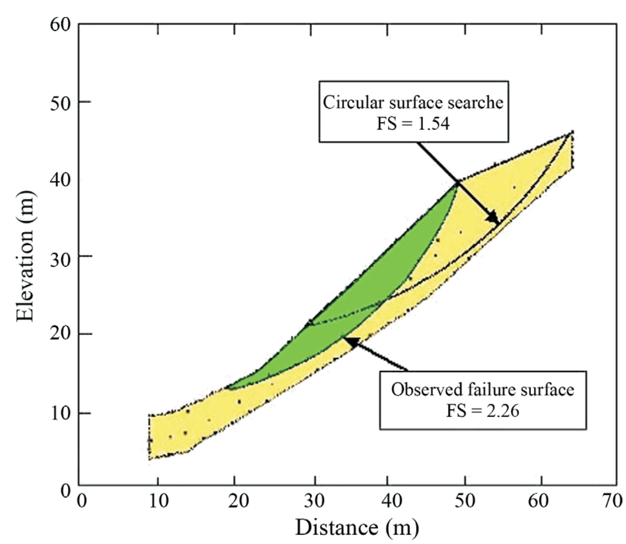

Figure 15 - Failure surfaces and Factors of Safety – Case 2.

the use of a pore water pressure mesh that reproduced this scenario, resulted in FS values less than 1 (Fig. 16) and, confirmed the assumption that the rainfall amount itself would not sufficient to justify the soil failure.

5. Conclusions

In an attempt to identify the triggering mechanism of the deep-seated slide of a slope, in Rio de Janeiro, Brazil, a comprehensive experimental investigation, 3D numerical flow analyses and stability analyses were undertaken. The landslide occurred after a rainfall period and despite the unsaturated soil condition, on the following day and even one week after the slide full saturation of the failure surface, with groundwater sprouting at its upper region, was clearly observed.

The slope consisted of a varying thickness layer of a residual soil overlying a gneissic rock that outcropped at the upper and left sides of the landslide boundary. The transition between the sound rock and the saprolitic soil was densely fractured.

A 3D-FEM transient/unsaturated flow program was used to simulate various flow scenarios in an attempt to assess the suitable condition that could promote the generation of positive pore water pressure within the slope. The flow analyses not only considered different rainfall rates, but also the influence of the soil saturation at the upper part of the slope, as a result of the malfunction of a surface drainage system, and an eventual development of a preferential flow paths through the fractured rock layer. The studies revealed that the existence of a water source at the base of the slope appeared to be the only feasible scenario that could explain the hydrological condition after the landslide.

A series of shear strength laboratory tests, carried out under saturated and unsaturated soil conditions revealed that a single strength envelope could be used for the entire slope. These strength parameter were used with the different pore water pressure meshes, which were conceived from the results of flow simulations.

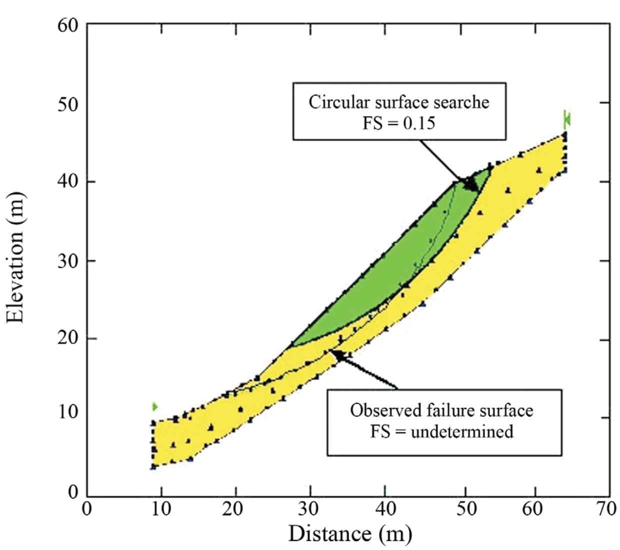

Figure 16 - Failure surfaces and Factors of Safety – Case 3.

The stability analyses of the central section of the landslide, indicated high values of FS, except for the most severe flow condition that assumed water sources at different positions of the failure surface; *i.e.*, the rainfall amount that reached slope surface before the landslide was not sufficient to trigger slope failure. These slope stability results agreed with the 3D flow simulations, since full saturation of the failure surface was only predicted if mechanisms other than rain infiltration were prescribed.

The authors consider that the main conclusion of this study is that, despite the development of experimental and numerical techniques to address the behavior of unsaturated soils, the understanding of the complex phenomenon of rainstorm-induced landslides is still a challenge among geotechnical engineers. Besides, except for extreme and unpredictable rainfall amounts, landslides are probably triggered by a combination of mechanisms. Therefore, geotechnical engineers must call attention to the complexity of landslides in unsaturated residual soils, and always try to answer a simple question that many times arises: why the landslide did not occur during a more intense event or why it did not occur few meters away?

Acknowledgments

The authors acknowledge the financial support from the International Development Center (IDRC), Canada, the National Council for Research (CNPq) and the Rio de Janeiro Research Support Agency (FAPERJ), Brazil. The authors are also grateful to all graduate students that participated in this research project.

References

Akai, K.; Ohnishi, Y. & Nishigaki, M. (1979) Finite element analysis of three-dimensional flow in saturated-unsaturated soils. Proc. 3rd Int. Conf. Numerical Methods in Geomechanics, Aachen, pp. 227-239.

Au, S.W.C. (1998) Rain-induced slope instability in Hong Kong. Engineering Geology, v. 51:1, p. 1-36.

Brand, E.W. (1985) Geotechnical engineering in tropical residual soils. Proc. 1st Int. Conf. on Geomechanics in Tropical Lateritic and Saprolitic Soils, Brasília, v. 3, pp. 23-100.

Buchanan, P.; Savigny, K.W. & de Vries, J. (1980) A method for modeling water tables at debris avalanche headscarps. Journal of Hydrology, 113, p. 61-68.

Capra, L.; Lugo-Hubp, J. & Borselli, L. (2003) Mass movements in tropical volcanic terrains: the case of Teziulán (Mexico). Engineering Geology, 69, p. 359-379.

Carrillo, C.W.; Fonseca, E.C. & de Campos, T.M.P. (1994) Suction controlled direct shear device. Proc. 2nd Symp. on Unsaturated Soils, Recife, pp. 67-78 .

Costa Nunes, A.J.; Couto Fonseca, A.M.M.C.; Couto Fonseca, de M.; Fernandes, C.E. & Craizer, W. (1989) Intense rainstorm and ground slides. Proc. 12th Int. Conf. Soil Mech. and Found. Engn, v. 3, pp. 1627-1630.

de Campos, T.M.; Andrade, M.H.N.; Gerscovich, D.M.S. & Vargas Jr., E.A. (1994) Analysis of the failure of an unsaturated gneissic residual soil slope in Rio de Janeiro, Brazil. Proc. 1st. Pan Am. Symp. of Landslides, Guayaquil, v. 1, pp. 201-213.

Dietrich, W.E.; Wilson, C.J. & Reneau, S.L. (1986) Hollows, colluvium, and landslides in soil mantled landscapes. A.D. Abrahams (ed) Hillslope Processes, Allen & Unwin Ltd, pp. 361-368.

Fonseca, E.C. (1991) Ensaio de Cisalhamento Direto com Sucção Controlada em Solos Não Saturados. MSc. Thesis. Departamento de Engenharia Civil, Universidade Católica do Rio de Janeiro.

Fredlund, D.G.; Morgenstern, N.R. & Widger, R.A. (1978) The shear strength of unsaturated soils. Canadian Geotechnical Jour., 15, p. 228-232.

Freeze, R.A. & Cherry, J.A. (1979) Groundwater. Prentice-Hall, Inc., Englewood Cliffs.

Gasmo, J.M.; Rahardjo, H. & Leong, E.C. (2000) Infiltration effect son stability of a residual soil slope. Computers and Geotechnics, 26, p. 145-165.

GEO-SLOPE International Ltd. (2001). SLOPE/W for slope stability analysis, version 5.0.

Gerscovich, D.M.S. (1994) Fluxo em Meios Porosos Saturados e Não Saturados Modelagem Numérica com Aplicações ao Estudo da Estabilidade de Encostas do Rio de Janeiro. DSc. Thesis, Departamento de Engenharia Civil, Universidade Católica do Rio de Janeiro.

Gerscovich D.M.S.; de Campos T.P.P. & Vargas Jr., E.A. (2006) On the evaluation of unsaturated flow in a residual soil slope in Rio de Janeiro Brazil. Engineering Geology, 88, p. 23-40.

Ho, D.Y.F & Fredlund, D.G. (1982) The increase in shear strength due to soil suction for two Hong Kong soils. Proc. ASCE Geotech. Conf. on Engn. Construction in Tropical and Residual Soils, Honolulu, pp. 263-295.

Kim, J.; Jeong, S.; Park, S. & Sharma, J. (2004) Influence of rainfall-induced wetting on the stability off slopes in weathered soils. Engineering Geology, 75, p. 251-262.

Neuman, S.P. (1973) Saturated-unsaturated seepage by finite elements. Journal of Hydraulics Division, 99 (HY12), p. 2233-2250.

Rahardjo, H.; Lim, T.T.; Chang, M.F. & Fredlund, D.G. (1995) Shear strength characteristics of a residual soil. Canadian Geotechnical Journal, 32, p. 60-77.

Reynolds, W.D. & Elrick, D.E. (1987) A laboratory and numerical assessment of the Guelph permeameter method. Soil Science, v. 144:4, p. 282-292.

Taylor, M.E. & Brown, C.B. (1967) Darcy's flow solution with free surface. Journal of Hydraulics Division, HY2, p. 25-33.

Tekinsoy, M.A.; Kayadelen, C.; Keskin, M.S. & Soylemez M. (2004) An equation for predicting shear strength envelope with respect to matric suction. Computers and Geotechnics, v. 31, p. 589-593.

Vargas Jr., E.A.; Costa Filho, L.M. & Prado Campos, L.E. (1986) A study of the relationship between stability of the slopes in residual soils and rain intensity. Proc. Int. Symp. on Environmental Geotechnology, pp. 491-500.

Vargas Jr., E.A.; Velloso, R.C.; de Campos, T.M.P. & Costa Filho, L.M. (1990) Saturated-unsaturated analysis of water flow in slopes of Rio de Janeiro, Brazil. Computers and Geotechnics, v. 10:3, p. 247-261.

Wang, G. & Sassa, K. (2003) Pore-pressure generation and movement of rainfall-induced landslides: effects of grain size and fine-particle content. Engineering Geology, 69, p. 109-125.

Wilson, C.J. (1988) Runoff and Pore Pressure Development in Hollows. PhD Thesis, Department of earth and Planetary Science, California University, Berkeley.

Wolle, C.M. & Hachich, W. (1989) Rain-induced landslides in south-eastern Brazil. Proc. 12th Int. Conf. Soil Mech. and Found. Engn., v. 3, p. 1639-1644.

List of Symbols

G_s: specific gravity of grains
S: degree of saturation
n: porosity
e: voids ratio
ψ: matric suction
γ_t: in situ density
θ: volumetric water content
ω: water content (in weight)
V_w: volume of water
V: total volume
ω_{LL}: liquid limit
ω_{LP}: plasticity limit
c': effective cohesion
ϕ': effective friction angle
ϕ^b: rate of increase in shear strength relative to the matric suction
u_a: pore air pressure
u_w: pore water pressure
$(u_a - u_w)$: matric soil suction

Technical Note

Soils and Rocks
v. 34, n. 2

Settlement of Floating Bored Piles in Brasilia Porous Clay

W. Patrick Stewart, Renato P. Cunha, Neusa M.B. Mota

Abstract. The geotechnical graduate program of the University of Brasilia maintains a research site on the campus (to be discontinued for a new place). The site is underlain by the typically partly-saturated and potentially collapsible "porous clay" of the Federal District of Brazil. The soil conditions have been thoroughly evaluated using laboratory and *in situ* geotechnical tests (DMT, CPT, SPT, and PMT). Five bored piles were installed and tested at the site. Simplified analyses have been used so that the results of the tests can be easily compared. The various soil tests were used to estimate the pile settlements which were compared to the measured values and the results are discussed. It has been shown that simple elastic models can be routinely used in practice for the estimation of the settlement of bored floating piles on tropical unsaturated soils. Besides, the results tend to indicate that PMT tests provide the best ratios between predicted and measured data.

Keywords: *in situ* testing, Brasilia porous clay, pile settlement, elastic theory.

1. Introduction

Brasilia, the capital city of Brazil, was a pre-designed city, built to accommodate the federal government and the supporting population of staff and workers. Recently the size of the city has increased in both population and developed properties. Given the particular conditions of the local tropical subsoil, specific local solutions have been developed for foundation design. Recently more research-based solutions and techniques have been developed with the support of the University of Brasília "Foundation Group" (www.geotecnia.unb.br/gpfees), a joint academic-industry group. The good academic-industry interaction has not only allowed a better knowledge of the existing technologies, but also has stimulated a pioneering use of advanced *in situ* tests (such as the DMT, CPT, the standard penetration test with torque measurement, SPTT, and PMT) in the tropical soil of the city.

Brasília is located in the Central Plateau of Brazil, and is portrayed in Fig. 1 by an "airplane" shape like form. The University of Brasília (UnB) campus is located within the city of Brasília. The UnB foundation and *in situ* testing research site is marked on this figure.

Within the Federal District extensive areas are covered by a weathered latosoil of Tertiary-Quaternary age. This latosoil has been extensively subjected to a laterization process and has a variable thickness throughout the District, varying from a few centimetres to around 40 m. In this latosoil there is a predominance of the clay mineral kaolinite, and oxides and hydroxides of iron and aluminum (giving it a distinct reddish colour). The variability of the properties depends on several factors, such as the topography, the vegetation cover, and the parent rock. In localized areas of the Federal District the latosoil overlays a saprolitic/residual soil with a strong anisotropic mechanical behaviour and high (SPT) penetration resistance. The saprolite originated from a weathered, folded and foliated slate, the typical parent rock of the region.

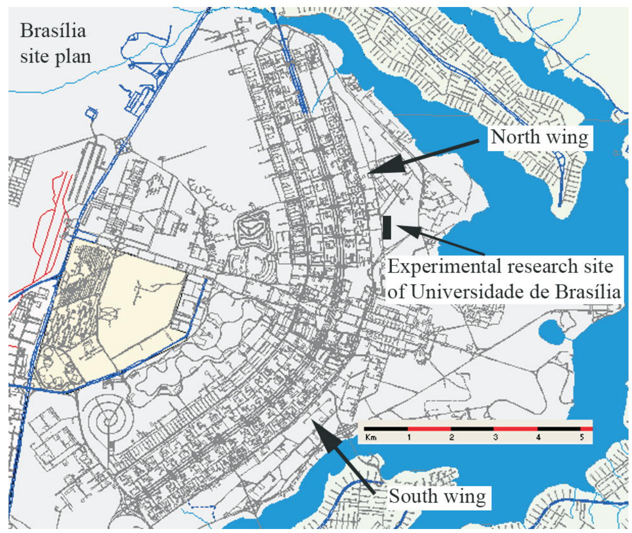

Figure 1 - Site plan of Brasilia showing the research site of the UnB geotechnical group.

2. Site Characterization

The superficial latosoil is locally known as the Brasília "porous clay", forming a lateritic horizon of low unit weight and high void ratio, and often an extremely high coefficient of collapse (Cunha *et al.*, 1999). However the soil can vary from clay to silt and in the upper portion of this site, silty sand. By breaking down the structure with a

W.P. Stewart, Department of Civil Engineering, British Columbia Institute of Technology, Burnaby, BC, Canada.
R.P. Cunha, Department of Civil and Environmental Engineering, University of Brasilia, Brasilia, DF, Brazil. e-mail: rpcunha@unb.br.
N.M.B. Mota, BMS Engenharia Ltda., Brasilia DF, Brazil.
Submitted on April 6, 2010; Final Acceptance on February 3, 2011; Discussion open until December 30, 2011.

deflocculating agent, the grain size curve of this soil shows a greater concentration of clay-size particles.

Figure 2 contains a simplified profile of the deposit, characterized by a superficial lateritic layer overlying a transition zone and a saprolite formed by the native rock of the region. The figure also presents the average results of SPT blow counts, torque measurements, CPT tip resistance and lateral sleeve friction, for each meter depth at the site. Table 1 presents the geotechnical characterization of the site, based on soil classification tests, including

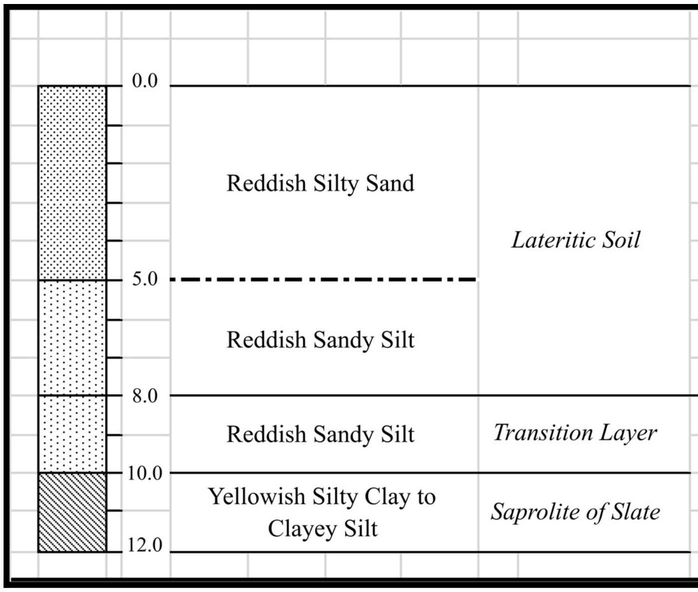

N_{avg}	T_{avg} (kgf-m)	qc_{avg} (MPa)	fs_{avg} (MPa)
-	-	-	-
3	1.4	1.5	0.02
2	3.5	0.7	0.05
3	6.7	0.8	0.08
3	7.2	0.8	0.09
4	9.0	1.0	0.11
6	9.8	1.6	0.19
7	7.9	2.3	0.24
8	6.4	3.0	0.27
11	10.7	3.7	0.35
19	22.2	34.0	0.35
16	24.0	3.9	0.35

Figure 2 - Simplified profile of the soil at the UnB research site.

Table 1 - Geotechnical characterization of the soil of the UnB experimental site.

Parameter	Depth (m)									
	1	2	3	4	5	6	7	8	9	10
γ_s (kN/m^3)	26.9	26.8	26.1	25.9	26.9	25.8	26.5	26.2	27.1	27.6
γ_d (kN/m^3)	10.2	10.4	11.5	11.5	12.0	12.0	12.8	13.9	13.8	13.3
γ (kN/m^3)	13.3	13.7	14.7	14.5	15.0	14.4	15.4	18.0	17.8	17.5
γ_{sat} (kN/m^3)	16.5	16.5	17.1	17.0	17.5	17.3	17.8	18.6	18.8	18.5
G_s	2.7	2.7	2.7	2.7	2.7	2.6	2.7	2.7	2.8	2.8
e	1.6	1.57	1.27	1.27	1.25	1.15	1.07	0.89	0.96	1.08
n (%)	61.6	61.1	56.0	55.9	55.6	53.5	51.7	47.2	49.0	51.9
Gravel ND[1]	0.2	0.2	0.7	0.8	1.4	2.1	4.3	3.6	0.6	0.0
Sand ND	56.2	56.2	53.2	53.0	49.2	34.9	30.1	42	10.2	1.4
Silt ND	51.4	35.9	34.2	43.1	48.6	61.4	61.9	51.9	86.8	79.5
Clay ND	2.2	7.7	11.9	3.1	0.8	1.6	3.7	2.5	2.4	19.1
Gravel WD[2]	0.2	0.2	0.7	0.8	1.4	2.1	4.3	3.6	0.6	0.0
Sand WD	41.5	41.5	41.6	33.7	31.6	25.7	22.7	33.8	10.2	3.4
Silt WD	24.9	29.2	25.7	26.3	26.5	22.9	24.6	27.4	80.4	93.2
Clay WD	33.4	29.1	32.0	39.2	40.5	49.3	48.4	35.2	8.8	3.4
w_L (%)	38	36	39	41	45	44	46	43	44	46
w_P (%)	28	26	29	29	34	33	35	34	26	30
PI (%)	10	10	10	12	11	11	11	9	18	16

[1]Gravel portion with no deflocculating agent. [2]Gravel portion with deflocculating agent.

grain size proportions both without and with a deflocculating agent.

3. Field and Laboratory Tests

In support of the foundation testing, a series of field and laboratory tests have been completed at the site (for more details see Mota, 2003). Table 2 summarizes the field tests. Figure 3 presents the layout of the field testing and test piles.

The dilatometer tests (DMT) were carried out with a standard Marchetti apparatus pushed into the soil with a 200 kN hydraulic field rig (until the maximum resistance was met). The tests were done in accordance with ASTM D-6635-01, using nitrogen gas to expand the membrane. Measurements were done at 20 cm intervals, and the dilatometer was pushed at 2 cm/s. The measured pressures were corrected using lab calibrations. Typical examples are shown in Fig. 4.

Table 2 - Summary of field tests at UnB experimental site.

Test type	Total no. of borings	Depths (m) at end of test	Comments
DMT	12	12.0-18.2	Hydraulic Field Rig
CPT	17	12.1-18.0	Hydraulic Field Rig
SPT-T	5	10.5-12.5	Manual Procedure
PMT	3	7.6-9.6	Done in sequence together with SPT's

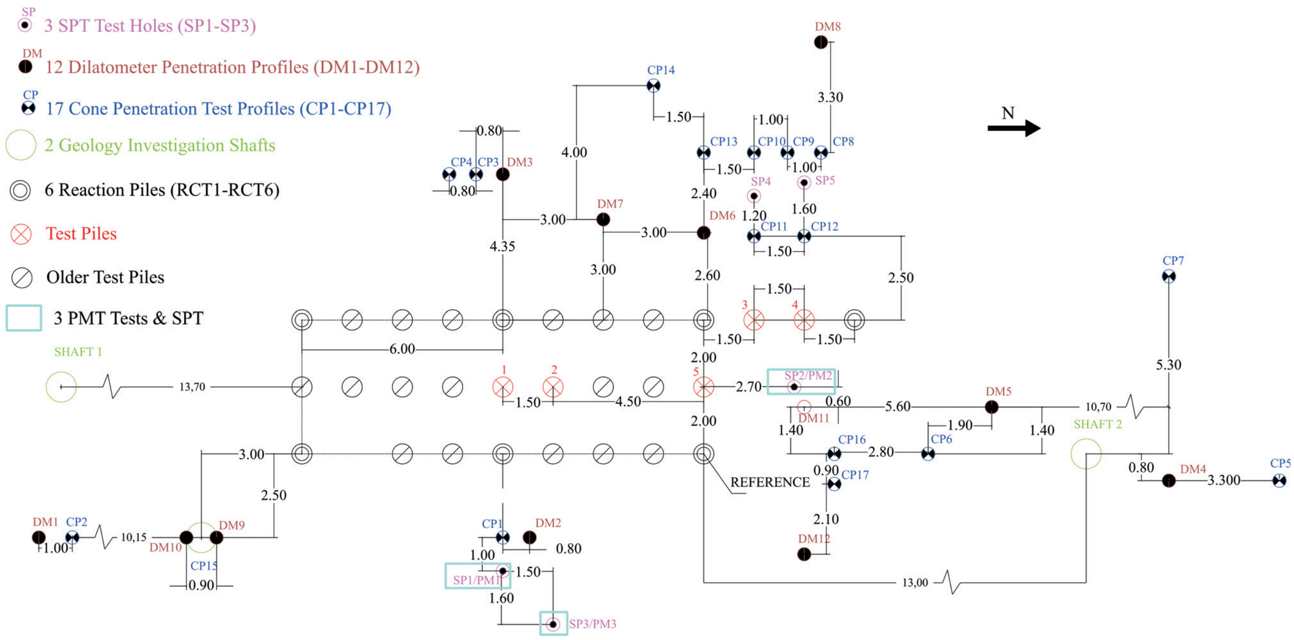

Figure 3 - Layout of *in situ* testing and test piles.

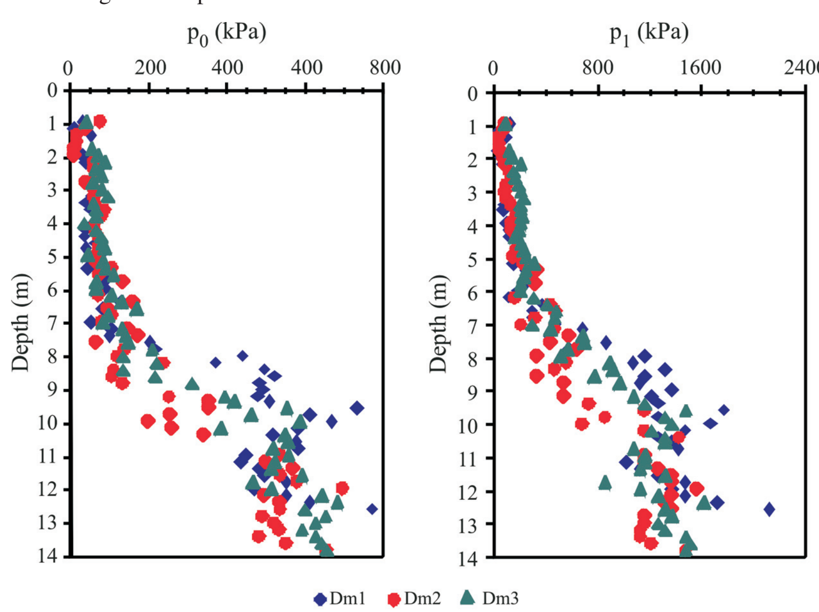

Figure 4 - Typical DMT results.

The cone penetration tests (CPT) were advanced with the same hydraulic rig. CPTs 1-14 were conducted with a standard electronic cone - 60° tip with area of 10 cm^2 - and CPTs 15-17 were conducted with a piezocone. The tests were conducted with a penetration rate of 2 cm/s (ASTM D-5778). The inclination was measured and the test was stopped if it became excessive (above 15 degrees). The cones were calibrated at the national Laboratory of Furnas in Goiânia-GO. Results of 4 CPT tests are given in Fig. 5.

The standard penetration tests (SPT-T) were conducted according to NBR-6484, and a manual hammer was used. The test used a four-legged frame with a winch on one side. The hammer was a long (H ≈ 2D) pin-guided type that was raised by 2 labourers pulling on the cables used to lift the hammer. After the SPT, the torque was measured with a calibrated torque wrench at a set rate (for both the peak and residual values) as presented for the typical peak result in Fig. 2. Results of the number of blow counts of all SPT tests are presented in Fig. 6.

The Menard pressuremeter tests (PMT) were conducted according to ASTM D-4719 to obtain a pressure-deflection curve and gave the strength and deformability parameters of the soil, as well as the insitu horizontal stress. The test was usually run in increments of 25 kPa. An example test is shown in Fig. 7, based on a "curve matching" procedure (see Mota, 2003 and Fontaine *et al.* 2005).

Two shafts were excavated for geological investigations of the soil profile as depicted in Fig. 3. Triaxial tests were conducted earlier on block samples from depths of 3 m, 6 m, and 9 m. At each depth CK_oD tests were conducted at cell pressures of 50 kPa, 100 kPa, and 200 kPa and the values of the initial modulus E_i and the tangent modulus at 50% of the failure stress E_{50} were found. These values were interpolated to the stress conditions at each depth. For this paper these three values were averaged, giving E_i = 6.6 MPa and E_{50} = 3.7 MPa.

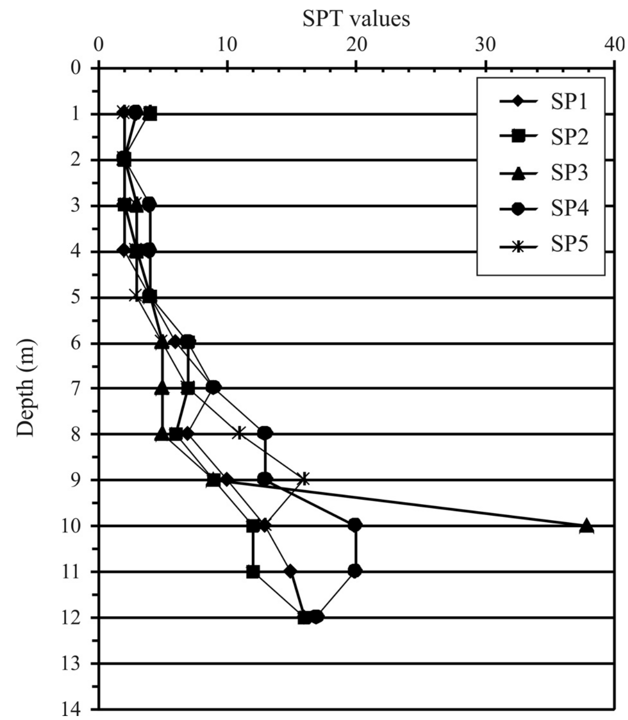

Figure 6 - Summary of SPT blow count results.

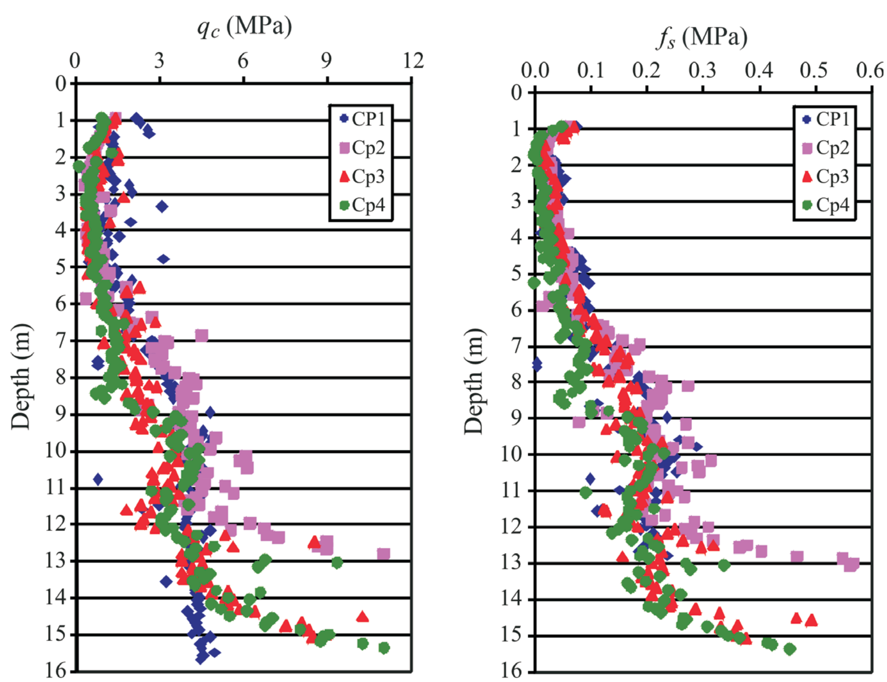

Figure 5 - Results of four CPT profiles.

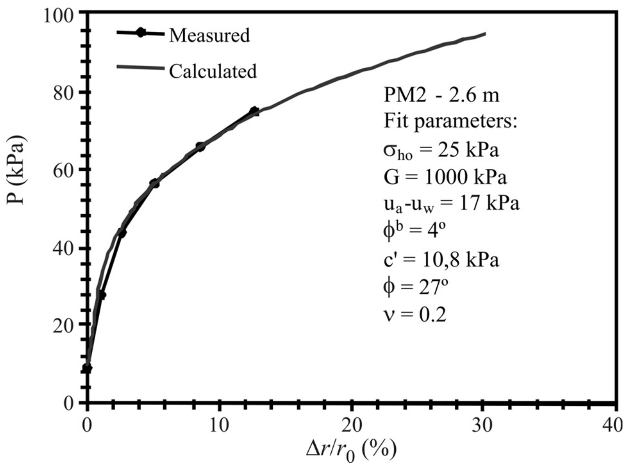

Figure 7 - Example PMT test result and analytical fitting analysis.

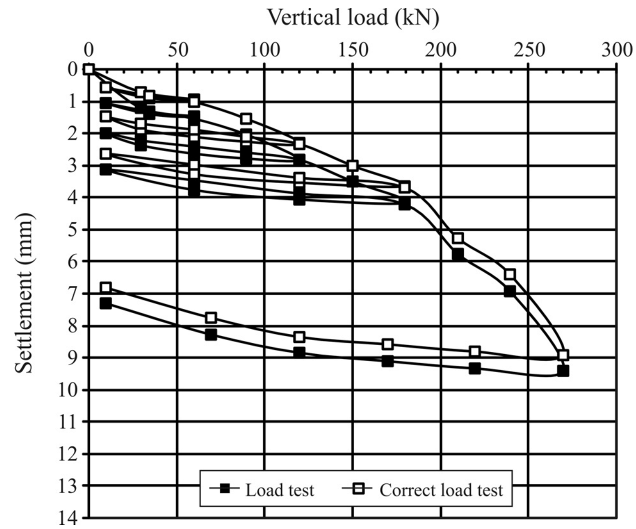

Figure 8 - Example of load-settlement curve of test pile.

4. Pile Load Tests

An earlier series of test piles had been conducted at this site, also following the NBR-12131. For this paper a series of five piles were constructed and are noted as E-1 to E-5 on Fig. 3. It was planned to install internal instrumentation (strain gauges in all of the piles and load cells at the base of E-1, 2 & 4). However the soil squeezed inwards at the base of piles E-2 & 4, and the instrumentation could not be installed. The difficulties have been noted for later tests. For piles E-3 & 5, the instrumentation was not installed. The instrumentation in pile E-1 provided reasonable results, proving that this pile, and by analogy the others, behaved as a *floating* foundation.

The soil was excavated with mechanical augers to a diameter of 30 cm. The pile lengths were 7.25-7.85 m. After a re-bar cage was installed, the borings were filled with ready-mix concrete. Cylinder samples were obtained for later testing. After the concrete had hardened, a smooth-faced concrete block was installed at the top of each pile. Pile Echo tests (PET) with a new acquired equipment were recently conducted on each of the piles to confirm the absence of voids or reductions in cross-section.

Reaction piles with a diameter of 0.5 m and depth of 10 m were installed to hold the metal beams that provided the support for the load tests. For the tests a hydraulic jack, a load cell and extensometers were attached to the head of the pile. Six extensometers were used, each with a travel of 0.05 m and a sensitivity of 10^{-5} m. Static load tests were carried out in progressive stages. The load-settlement plots were manually adjusted for any apparent settlement of the loading equipment. A typical example is shown in Fig. 8.

5. Analysis of Pile Settlement

Modulus values were selected for each type of field test. The values of the field measurements varied with depth, but were averaged (neglecting extreme values). Most correlations consider sand and clay values separately. Since the soil is partly saturated, undrained (clay) values were not used. Many authors consider sand correlations to vary widely depending on stress history and age of the sand deposit. The soil dates from Tertiary-Quaternary era and is aged soil. The water table is below the pile depth and the soil is likely somewhat overconsolidated due to variations in the soil suction. Simple correlations were adopted from references:

• Baldi *et al.* (1986) indicate that theoretically $E_{25} = (1 - \nu^2)E_D$, but gave an empirical relation of $E = 0.88E_D$, where E_D is the dilatometer modulus.

• Robertson and Campanella (1988) suggested $E = 6$ to $10q_c$ and a value of $8q_c$ was used, where q_c is the cone tip resistance.

• Poulos (1998) related SPT N-values to the modulus along and below a pile as 3 N, where N is the SPT blow counts for 30 cm.

• After standard corrections, the PMT data was plotted and curve "matched" via the methodology and cavity expansion model proposed by Cunha (1996). This original model was later modified for cohesive-frictional materials by Fontaine *et al.* (2005), and the model used herein is this modified version. Hence, a number of soil parameters were fit into their model and were adjusted to match the field curve, giving a modulus value, E, for each test. This modulus is derived from the shear modulus G obtained for the elastic zone around the pressurementer. The E values were averaged for the pile analysis.

• Values of E_i and E_{50} from the triaxial tests were used directly in the analysis.

As required, the averaged field data were converted to E values, using the correlations and techniques given in Table 3.

These modulus values for each soil test were then used in the Poulos & Davies (1990) solution to calculate

Table 3 - Correlations & techniques used for moduli assessment.

Test	Reference	Formulation
DMT	Baldi *et al.* (1986)	$E_{25} = 0.88E_D$
CPT	Robertson & Campanella (1988)	$E = 8q_c$
SPT	Poulos (1998)	E(MPa) = 3 N
PMT	Fontaine *et al.* (2005)	Curve fitting
Laboratory	Triaxial CK0D tests	E_i and E_{50}

settlement. The predicted values were then compared to the measured values. The ratio of the predicted values to the measured values are presented in Table 4 (together with working loads and settlements) and plotted in Fig. 9.

The simple (elastic) model used allowed a straightforward comparison of the settlement predictions. In Table 4, it can be seen that the pressuremeter and SPT modulus values seem to provide the best estimates of the pile settlements, followed by the CPT. The DMT and lab values over-predict considerably the pile settlements.

6. Conclusions

Simple elastic models can be routinely used in practice for the estimation of the settlement of bored floating piles on tropical unsaturated soils. Although limited in terms of data, the results tend to indicate that PMT tests provide the best ratios between predicted and measured data. As a general conclusion it can be said that more research emphasis must be placed on this matter, so that this versatile *in situ* tool becomes more readily used in practice.

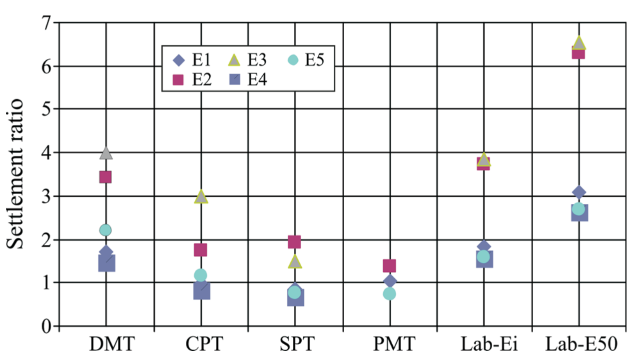

Figure 9 - Plot of settlement ratio for various tests used for modulus.

Acknowledgments

The authors acknowledge the financial support from both CNPq and CAPES organizations on the scholarships provided to the University of Brasília. Grant provided by MCT/CNPq 14/2009 Research fund proposal, to buy the PET equipment, is also acknowledged and valued. Prof. Stewart would like to acknowledge the professional development grant provided by BCIT. This grant provided the time for him to visit the University of Brasília, develop knowledge of local practices, and prepare this paper.

References

ABNT (2001) NBR 6484. Solo – Sondagens de Simples Reconhecimentos com SPT – Método de Ensaio (Soil – Standard Penetration Test – SPT- Soil Sampling and Classification – Test Method). ABNT Brazilian Association of Technical Standards, 17 pp.

ABNT (2006) NBR12131. Estacas – Prova de Carga Estática – Método de Ensaio (Piles – Piles – Static Load Test – Method of Test). ABNT Brazilian Association of Technical Standards, 8 pp.

ASTM (2007) Suggested method for performing the flat dilatometer test: D-6635-01. Geotechnical Testing Journal, v. 9:2, p. 93-101.

ASTM (2007) Standard test method for pressuremeter testing in soils: D-4719. American Society for Testing and Materials, 9 pp.

ASTM (2007) Standard test method for performing electronic friction cone and piezocone penetration tests of soil: D-5778. American Society for Testing and Materials, 19 pp.

Baldi, G.; Belloti, R.; Ghionna, V.; Jamiolkowski, M.; Marchetti, S. & PasqualiniI, E. (1986) Flat dilatometer tests in calibration chambers. Proceedings of *In situ*'86

Table 4 - Measured and predicted settlements using Poulos & Davies (1990) solution.

Pile	P_{load} (kN)	$\delta_{measured}$ (mm)	Settlement ratio (predicted/measured)					
			DMT	CPT	SPT	PMT	Lab-E_i	Lab-E_{50}
E1	135	2.4	1.72	0.98	0.86	1.03	1.82	3.08
E2	180	1.56	3.43	1.73	1.92	1.39	3.73	6.31
E3	135	1.13	3.99	3.00	1.49	-	3.86	6.53
E4	130	2.70	1.47	0.84	0.66	-	1.56	2.63
E5	155	3.14	2.21	1.15	0.75	0.72	1.59	2.70
Average			2.56	1.54	1.14	1.05	2.51	4.25

Note: P_{load} = working load, $\delta_{measured}$ = measured settlement at working load.

ASCE Speciality Conference on Use of *In situ* Tests in Geotechnical Engineering, Virginia Tech, Blacksburg, v. 6, pp. 431-441.

Cunha, R.P.; Jardim, N.A. & Pereira, J.H.F. (1999) *In situ* Characterization of a Tropical Porous Clay via Dilatometer Tests. Geo-Congress 99 on Behavorial Characteristics of Residual Soils, ASCE Geotechnical Special Publication 92, Charlotte, pp. 113-122.

Cunha, RP. (1996) A new cavity expansion model to simulate selfboring pressuremeter tests in sand. Solos e Rochas, v. 19:1, p. 15-27.

Fontaine, E.; Cunha, R.P. & David, C. (2005) A simplified analytical manner to obtain soil parameters from Ménard pressuremeter tests on unsaturated soils. 50 Years of Pressuremeters International Symposium – ISP5, Paris, v. 1, pp. 289-295.

Mota, N.M.B. (2003) Ensaios Avançados de Campo na Argila Porosa Não Saturada de Brasília: Interpretação e Aplicação em Projetos de Fundação (Advanced *in situ* Tests in the Brasília Unsaturated Porous Clay: Interpretation and Foundation Design Application). Ds.c. Thesis. Departamento de Engenharia Civil, Universidade de Brasília, Brasília, Pub. G.TD-013A/03, 336 pp.

Poulos, H.G. (1998) The pile-enhanced raft – An economical foundation system. Proceedings of XI Brazilian Congress of Soil Mechanics and Geotechnical Engineering, Brasilia, v. 5, pp. 27-43.

Poulos, H.G. & Davies, E.H. (1990) Pile Foundation Analysis and Design. R.E. Krieger Publishing Company.

Robertson, P.K. & Campanella, R.G. (1988) Guidelines for using the CPT, CPTU, and Marchetti DMT for geotechnical design. Federal Highway Administration, Report No. FHWA PA-87-023+84+24, v. 2.

Case History

Evaluation of Rockfall Hazard Along Brazil Roads

Guilherme José Cunha Gomes, Frederico Garcia Sobreira, Milene Sabino Lana

Abstract. The Brazilian road network is constructed in a highly heterogeneous geological environment and some stretches cross through discontinuous rock masses that have uncertain or even ignored geotechnical characteristics. Rock slopes are potentially unstable surfaces and as such are susceptible to rockfalls that affect the highway's user safety, transportation infrastructure and surrounding environment. The geomechanical behavior of rock masses and also the geometric and traffic conditions of highways are fundamental aspects of rockfall evaluation. This research presents a case study of rockfall evaluation for slopes bordering highway sections, aiming to classify them and determine a hierarchy for intervention, based on defined criteria. The presented method could be used as a first step in the study of stabilization techniques for problems caused by rockfalls from highway slopes. In order to use this approach, field investigations including geomechanical classification of rock mass are necessary. In this context, twelve slope sections containing rock slopes in Espirito Santo's road network were investigated. The slopes were analyzed individually and the influence of each parameter in the global rating was evaluated. Parameter effectiveness in the proposed method was also evaluated. The slopes were classified to define priority measures to minimize roadway problems in each place.

Keywords: rockfall, slope, highway.

1. Introduction

The Brazilian road network is constructed in a relatively heterogeneous geological environment, amidst different kinds of discontinuous rock masses with uncertain or even ignored geotechnical characteristics. The user safety and environmental preservation require tools to ascertain an acceptable degree of rockfall hazard along highway slopes, based on rational methodology.

In the highway engineering context, rock slopes are potentially unstable surfaces and as such are susceptible to rockfalls that affect highway user safety, transportation infrastructure and the surrounding environment.

Due to the seriousness of the problem and the difficulties encountered in investigating and analyzing rockfall along hundreds of kilometers of mountainous highways, several countries have developed classification systems for slopes that could be obtained through field investigations and simplified calculations. The objective of these classifications is to identify and distinguish particularly dangerous places requiring urgent stabilization measures or further studies, and therefore, enabling agencies or highway departments to take remedial action.

Rockfall evaluation methods along highways are important tools to monitor potentially unstable slopes. These methods use studies and investigations of directly linked characteristics to the events. Analyses of road sections with great geotechnical and geometric problems, allied to an elaborated database obtained in a discerning way, can be helpful for road managers to choose remedial measures in places of potential hazard.

2. Highway Rockfalls

A rockfall corresponds to the detachment of a block rock mass from a steep or scarp slope (Giani, 1992), with little or no shear failure (Hoek & Bray, 1981), without structurally controlled planar and wedge failures. The displacements are rapid, and usually involve free fall, rolling or bouncing (Ahrendt, 2005). Individual blocks subjected to falls have varied geometric dimensions, and can be in the form of cubes, plates, among others (ISRM, 1978; Palmström, 1995).

According to Giani (1992), the beginning of a rockfall phenomenon at a slope involves initially unstable conditions, which cause the movement of a mass induced by slope failure. The main factors in slope instability induction are: joint pore pressure, earthquakes or vibrations due to blasting, joint pressure due to ice formation and excavation.

Ritchie (1963) studied various factors that influence block trajectory during a rockfall event. Some of them were: block size and shape, slope height and angle, hill surface characteristics, joint pattern and rock type. He carried out pioneer research about rockfalls onto roads by studying highways in Washington, USA. His work included the observation of hundreds of falls from rock slopes and highway talus, measuring and recording block paths and the distances they reached beyond the slope. The study culmi-

Guilherme José Cunha Gomes, M.Sc., Engenheiro Ambiental Rodoviário, Departamento de Estradas de Rodagem do Estado do Espírito Santo, Vila Velha, ES, Brazil. e-mail: guilhermejcg@yahoo.com.br.
Frederico Garcia Sobreira, D.Sc., Associate Professor, Campus Universitário do Morro do Cruzeiro, Escola de Minas, Universidade Federal de Ouro Preto,Ouro Preto, MG, Brazil. e-mail: sobreira@degeo.ufop.br.
Milene Sabino Lana, D.Sc., Associate Professor, Departamento de Engenharia de Minas, Universidade Federal de Ouro Preto, Ouro Preto, MG, Brazil.
Submitted on March 3, 2010; Final Acceptance on September 21; Discussion open until December 30, 2011.

nated in developing a practical design criterion to estimate the width of rockfall catchment areas based on rock slope height, rock slope angle and depth of the catchment area. A rockfall catchment area is defined as the area between the highway edge of the pavement and the base of a road slope that is designed to avoid rockfalls from reaching the roadway (Pierson *et al.*, 2001).

Ritchie's design criteria has become a practical method for estimating ditches in rock cuts, frequently used by roadway engineers, mainly in North America, even though it was proposed four decades ago (Pierson *et al.*, 2001). Later, this criteria was modified to a chart form (Fig. 1), published by the Federal Highway Administration – FHWA (1989), improving data manipulation by roadway engineers.

Geomechanical slope behavior is constantly being evaluated by geotechnical engineers, using data concerning slope stability, orientation and shape of discontinuities and

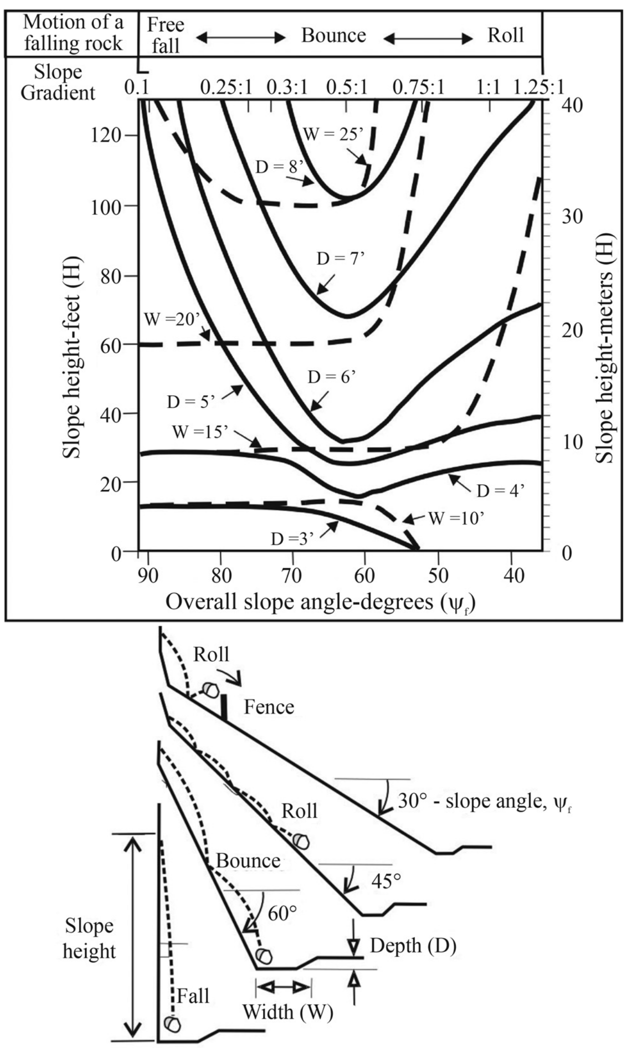

Figure 1 - Modified Ritchie's design chart to determine required width (*W*) and depth (*D*) of rock catchment areas in relation to height and slope angle (after FHWA, 1989; Hoek, 1998).

infilling material. Rock mass geomechanical classifications can be used for this evaluation. Gomes (1991) restated the concept that geomechanical classifications are oriented systems seeking to separate rock masses into classes with similar geomechanical characteristics. He did this by allotting ratings for them, based on geological, mechanical and geotechnical parameters, and in doing so, homogenized segments with the same behavior.

From among the main geomechanical classifications, the Bieniawski (1973, 1989) and Romana (1985) systems became the base for the development of highway rock slope classifications. *RMR* (Rock Mass Rating), proposed by Bieniawski (1973, 1989), includes six parameters that are used to classify a rock mass: strength of intact rock material; drill core quality or rock quality designation (*RQD*); spacing of discontinuities; condition of discontinuities; groundwater and discontinuity orientation. *SMR* (Slope Mass Rating) proposed by Romana (1985) is obtained from an adjustment of Bieniawski's *RMR*, to which is added a factorial term dependent on the slope – joint orientations and the excavation method.

Block size is a very important index for rock mass quality evaluation, but its determination is not an easy task. This dimension is calculated through discontinuity spacing and persistence, as well as from the number of joint sets that delimit potentially unstable blocks (ISRM, 1978). Palmström (1995) also affirms that there are many ways to calculate block volume in a rock mass. Beyond field observations, Palmström (1995) describes some relationships to estimate block volume in rock masses with different joint sets.

Traffic and geometric characteristics of road sections also must be considered in highway rockfall evaluation. Among these characteristics, average traffic per day represents the average number of vehicles traveling on a roadway section per day (DNIT, 2006). The posted speed limit, defined in the road project, is the larger speed allowed in this segment with appropriate safety conditions, even with wet pavement, without traffic influence. Another roadway characteristic, sight distance, can be understood as a vision pattern given to the driver, in a way that there is always time to safety decisions.

The first inventory of problematical rockfall areas was developed by Brawner & Wyllie (1975). Since then, highway rock slope classifications have been developed in order to assist in the management of critical roadway areas.

In the beginning of the 90's, a highway rock slope classification system was developed by Pierson *et al.* (1990), based on a previous study, and named *Rockfall Hazard Rating System* (RHRS). This method, implanted in the State of Oregon (USA), has proved to be an important tool for analysis and prevention of rockfall problems involving roads. It has provided significant innovation by improving the identification, evaluation and mitigation processes of potentially unstable rock masses. The RHRS system is a highly-used technique employed for quickly establishing which rock slopes offer risks for the users. The nine categories of this system are framed in four different ratings. Categories between the established ratings can be interpolated. The criterion to interpolate ratings increases exponentially from 3 to 81, making it possible to distinguish which slopes are more problematic or dangerous. Slopes with the largest ratings need priority intervention.

Budetta (2004) evaluated the rockfall problems of Italian roads based on the RHRS method (Pierson *et al.*, 1990). The author modified the method, adapting it to the geological and road context of that country. The main modification proposed by Budetta (2004) was the incorporation of the *SMR* (Romana, 1985) into the geological evaluation of rock masses.

Several other authors also have studied highway rockfalls all over the world, for example, Bunce *et al.* (1997), Hadjin (2002), Hopkins *et al.* (2003), Rose (2005), Eliassen & Springston (2007), among several others.

3. Work Development

This research developed and applied a method for rockfall evaluation of slopes bordering highway sections, aiming to classify them and determine a priority intervention hierarchy. For this, existent data, as well as collected data in the area, was analyzed. This resulted in the definition of a field investigation area involving twelve highway-bordering rock slopes in the State of Espirito Santo, Brazil (Fig. 2). Due to map scale, two investigated slopes that are very close do not appear in figure.

The applied rockfall hazard evaluation method then used the data from the geological and geotechnical slope investigation, as well as traffic and geometrical highway section assessment. Geomechanical rock mass classification systems were applied as a geotechnical tool for evaluating the slopes, adjusting rockfall hazard assessment methods internationally proposed for Espírito Santo roads. Slopes with the highest intervention priority were defined.

The application of the methodology, added to professional's experience in problem diagnosis, represents a contribution to highway departments for road safety increment

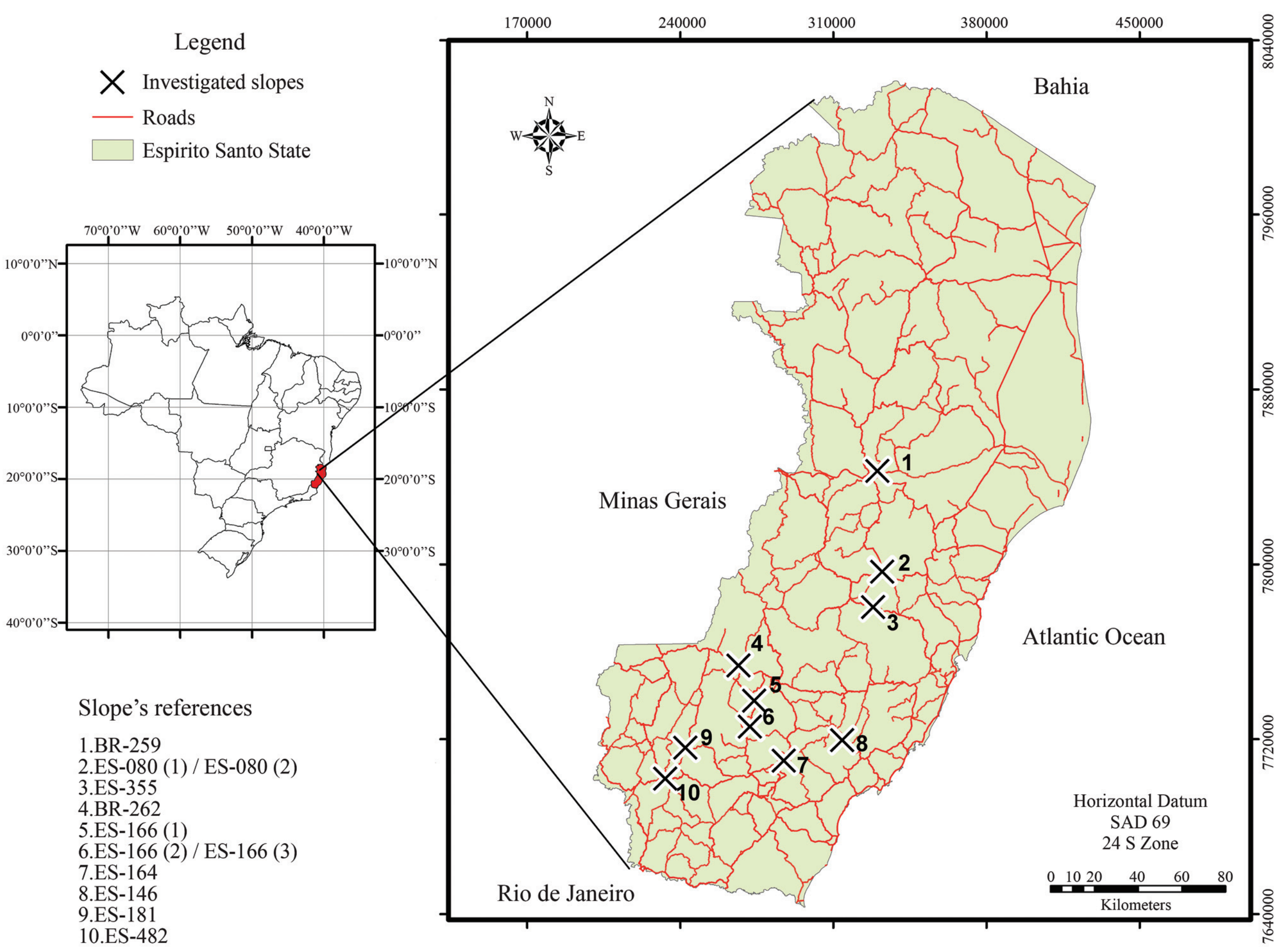

Figure 2 - Investigated rock slopes distribution (Espirito Santo State, Brazil).

when adding the acquired results to roadway rehabilitation and improvement projects.

In this method, pavement widths, posted speed limit, decision sight distance, slope height and extension, catchment area and the longitudinal ramp of slope extension are determined in order to characterize the traffic conditions along the road sections and the geometry of each studied area.

For the characterization of the basic structural model for each slope, an overall rock mass analysis is performed and the surveyed data registered in a standard field sheet. The geological and geotechnical characterization is achieved by surveying the physical and geometric characteristics of rock mass discontinuities, as proposed by Bieniawski (1973, 1989), ISRM (1978), Romana (1985), Pierson & van Vickle (1993) and Palmström (1995).

For the discontinuity characterization, the following parameters are used: orientation, spacing, persistence, roughness, opening, infilling, water flow, joint sets and block size.

The collected information in the field of jointing rock mass was treated to obtain values concerning geomechanical quality of the slopes studied. The application of classification Bieniawski (1989) was conducted from field surveys and in literature data. Initially, we defined the most important families of discontinuities that control rock mass behavior.

As the characteristics of the rock masses studied were composed by crystalline rocks (granites and gneisses), values between 100 and 250 MPa for strength of rock material were considered, in accordance with Palmström (1995) and Bieniawski (1984) work's. It may also be added that due to operational conditions no samples were collected for uniaxial compression test. Therefore, ISRM (1978) proposal was used and as a result, the rocks were considered as very resistant, requiring many hammer blows in order to be fractured.

For RQD index, as no borehole was available, Priest & Hudson (1976) proposals were used. This method correlates RQD with joint spacing by using the following equation:

$$RQD = 110\, e^{-0.1/S} \left[\left(\frac{0.1}{S} \right) + 1 \right] \tag{1}$$

being S the average spacing between discontinuities in meters.

The joint spacing average of every family was taken into account in each slope. Joint condition, which involves opening characteristics, persistence, roughness, alteration in the walls and filling material conditions, it was calculated by averaging the magnitudes analyzed. For the influence of groundwater, a year length visual observations were made mostly during the rainy season, in order to define the state conditions such as the dry, damp, wet, dripping and flowing occurrences.

Bieniawski joint orientation was not considered in *SMR* classification, as proposed by Romana (1985). In this case, the joint and slope dip and dip direction were recorded for application of the *SMR* model.

4. Slope Rating Evaluation Methodology

Eight parameters are adopted for the evaluation of the slopes, as shown in Table 1. Each parameter receives a rating ranging from 3 to 81, where the smallest values correspond to the best highway safety conditions.

Pierson & van Vickle (1993) have proposed a practical field method for the calculation of average slope heights. Due to access difficulties to the top of most of the slopes, the cut height is obtained with a measuring tape and

Table 1 - Parameters for classification of the evaluated rock slopes.

Parameter	Criteria and rating			
	3 points	9 points	27 points	81 points
Slope height	6.0 m	12.0 m	18.0 m	24.0 m
Ditch effectiveness	Good catchment + Ritchie's chart conformity + protection	Moderate catchment + Ritchie's chart conformity	Limited catchment + Ritchie's chart disconformity	No catchment
Average vehicle risk	25% of time	50% of time	75% of time	100% of time
Percent of sight distance (DV)	100% (Appropriate DV)	75% (Moderate DV)	50% (Limited DV)	25% (Very limited DV)
Roadway width	13.2 m	10.8 m	8.4 m	6.0 m
Block size	0.30 m	0.60 m	0.90 m	1.2 m
Climate condition	Low annual rainfall < 1,150 mm	Medium annual rainfall 1,150-1,450 mm	Large annual rainfall 1,450 - 1,750 mm	High annual rainfall > 1,750 mm
Geologic characteristic (*SMR*)	80	70	60	50

a clinometer, using the relationship between the angle formed by the observation point and the slope surface:

$$H = X * \tan\alpha + AC \tag{2}$$

where X is the distance, in meters, of the measurement point (pavement edge); α is the angle measured by clinometer and AC is the clinometer height. Slope height is a fundamental characteristic in stability analyses. This parameter has shown to be effective in the geometric diagnosis of slopes, because a high slope will probably have discontinuity occurrences that induce rockfalls. The values of 6, 12, 18 and 24 meters shown in Table 1 were defined according to the variation of slope heights found on the worked area, aiming at establishing an adequate indicator to this category.

The ditch effectiveness parameter measures the efficiency of the catchment area to prevent rockfalls from reaching the roadway pavement (Ritchie, 1963). This highway section characteristic have been rated from Budetta (2004), that modified Pierson & van Vickle's (1993) qualitative evaluation, improving the pioneering geometric aspects proposed by Ritchie (1963).

According to Pierson & van Vickle (1993), the average vehicle risk (RV) measures the percentage of time that vehicles have been exposed to a dangerous rockfall zone. The percentage is obtained from equation below. Average vehicle risk meaning is similar to that used by the RHRS method.

$$RV = \frac{ADT \times CE}{PSP} \tag{3}$$

where ADT is average daily traffic (cars/h), CE is the cut extension (km) and PSP is the posted speed limit (km/h). Average vehicle risk is determined in percentage terms. In this case, the smaller the percentage of vehicles in rockfall hazard areas is, the smaller the index rating of the road section under consideration will be.

Percentage of sight distance (DV) is used to determine the highway length available to the driver for taking an instantaneous decision. This category is considered critical when roadway obstacles are difficult to notice, or when an unexpected move is requested (Pierson & van Vickle, 1993). Percentage of sight distance is an important parameter for evaluating rockfall hazard. This is because it is intimately related to the probability of the occurrence of automobile collision with any object present on the road. The calculation is based on the relationship between actual sight distance (ASD) and designed sight distance (DSD), measured in meters:

$$DV = \frac{ASD}{DSD} \times 100\% \tag{4}$$

DSD is designed by engineering project, usually established by the highway department. ASD is obtained in the field, changing in each road meter. Due to several operational reasons involving technical and financial resources, some road extensions are built without considering project sight distance. This fact is perceptible in highways that transpose mountainous or sinuous extensions.

The parameter roadway width represents the paved band extension, including the shoulder, and is measured perpendicularly to the central road line. It represents the space a driver has to maneuver. Most highway rockfall evaluation methods, based on Pierson *et al.* (1990) proposal, maintain the pavement width as an essential category or parameter because this is considered an important geometric aspect for safety.

In the investigated sections, frequently less than 3 joint sets were identified, so the calculation of the equivalent block volume proposed by Palmström (1995) was considered convenient, see Eq. (5). This relationship determines block volume from the volumetric joint count (J_v) and block shape factor (β), which is a function of the largest and the smallest joint spacing ($S_{máx}$ e S_{min}) and the number of joint set indexes (n_j):

$$Vb = \beta \times J_V^{-3} \tag{5}$$

$$\beta = 20 + 7\left(\frac{S_{max}}{S_{min}}\right)\left(\frac{3}{n_j}\right) \tag{6}$$

In which n_j = 3,0 to 3 joint sets; n_j = 2,5 to 2 joint sets and random sets; n_j = 2,0 to 2 joint sets; n_j = 1,5 to 1 joint sets and random sets; n_j = 1,0 to 1 single joint set.

The J_v index, according to Palmström (1995), is equal to the number of joints in a unitary rock mass volume. After calculation of Vb, Budetta's proposal (2004) is used to calculate block size (Db), measured in meters:

$$Db = \sqrt[3]{Vb} \tag{7}$$

Several methods of rockfall hazard evaluation in roadway rock slopes, especially those adopted in developed countries, use combinations between the period when there is water in the slope and when it snows. But, as the presence of snow would be a rare event and the slope water condition has been already used in SMR classification, this parameter is rated as a function of incident annual rainfall in the studied places. The most important climatic factor in Brazilian slopes is the rainfall, because the water, flowing on discontinuities, leads to rock mass shear strength reduction (Bieniawski, 1984 and Palmström, 1995), among other aspects. As this aspect has already been considered in the RMR classification, Budetta's proposal (2004) was adopted, which uses annual rainfall values for the studied areas. Then values of rainfall were obtained from historical series of Espirito Santo state. Low annual rainfall (< 1.100 mm) represents points of minor influence of water on the slope. On the other hand, high annual rainfall (> 1.750 mm) represents water's major contribution to slope instability.

Due to the geotechnical characteristics of the investigated slopes, the geological characteristic adopted by Pierson and Van Vickle (1993) was not used. The author's method, as quality is concerned, is better suited for regions on wich lithologic structure vary greatly (Gomes & Sobreira, 2008).

The geological characteristic parameter is evaluated according the *SMR* index (Romana, 1985). Budetta (2004) proposed *SMR* incorporation, whose value is inversely proportional to the Pierson *et al.* (1990) rating. *SMR* values have been adjusted in this work to provide a better understanding about the mechanical behavior of the slope. Values of *SMR* smaller than 50 can be considered critical, hence they have a high value in this parameter.

The parameter ratings are exponential, according to the Pierson *et al.* (1990) proposition. Slopes with a larger rating are hazardous and they must be given priority for immediate interventions. All parameters, except ditch effectiveness, can be put in equation form, according to Ritchie (1963), ISRM (1978), Romana (1985); Bieniawski (1989), Pierson & van Vickle (1993), Palmström (1995), Budetta (2004) and DNIT (2006). The equations to aid the parameter calculations and the symbology adopted are presented in the Table 2.

After the calculation of the parameter values for each slope, a value that represents the rockfall hazard index (I_{QB}) is determined by de equation:

$$I_{QB} = I_{AT} + I_{AC} + I_{RV} + I_{DV} + I_{LP} + I_{DB} + I_{CC} + 2I_{CG} \quad (8)$$

where I_{AT} = slope height parameter; I_{AC} = ditch effectiveness parameter; I_{RV} = average vehicle risk parameter; I_{DV} = sight distance parameter; I_{LP} = roadway width parameter; I_{DB} = block size parameter; I_{CC} = climate condition parameter; I_{CG} = geologic characteristic parameter. The I_{CG} index was multiplied by a weight of 2 in order to value the influence of geological-geotechnical characteristic in instability rockfall processes.

5. Results and Discussions

The slope sections selected for the study are located in different areas to encompass the aspects desired for the analysis. Places with differences in the traffic conditions, ramps, geometry, speed limit, among other intrinsic road project aspects were chosen, since the geological characteristics in the studied area didn't vary significantly. Twelve slopes were selected, two of which are federal highways subject to larger loads and greater traffic. The other ten are regional highways.

Table 2 - Symbols and equations used to each parameter of slope evaluation.

Parameters	Symbol	Equation
Slope height (*H*)	I_{AT}	$I_{AT} = e^{0.1831.H}$
Ditch effectiveness	I_{AC}	-
Average vehicle risk (*RV*)	I_{RV}	$I_{RV} = e^{0.0439.RV}$
Percent of sight distance (*DV*)	I_{DV}	$I_{DV} = 243e^{-0.0439.DV}$
Roadway width (*LP*)	I_{LP}	$I_{LP} = 1262.7e^{-0.4578.LP}$
Block size (*Db*)	I_{DB}	$I_{DB} = e^{3.662.\mathrm{Db}}$
Climate condition (*P*)	I_{CC}	$I_{CC} = 0.0048e^{0.0054.P}$
Geologic characteristic (*SMR*)	I_{CG}	$I_{CG} = 243e^{-0.055.SMR}$

Basically, the rock masses are highly metamorphic crystalline rocks (Meneses & Paradella, 1978). There is also gneiss, essentially composed of quartz, feldspar, biotite and garne that is well-oriented by the centimetric alternation of the banding. The foliation presents concordance with the banding.

Each slope was evaluated, increasing the understanding of the most problematic places per parameter. The rating of each parameter, following the model developed by Pierson *et al.* (1990), varied exponentially (see Table 1). The graphs in Fig. 3 show the indexes versus parameters rating relation.

Fig. 3 (h) shows the relationship between the I_{CG} index and the *SMR* value, as well as the distribution of the values obtained for each slope. It can be noticed that the I_{CG} rating is inversely proportional to the *SMR* index.

From Fig. 3 (h), it is possible to observe that *SMR* values above 60 result in low values of I_{CG}. Therefore, a rock slope must have a low value of *SMR* to present a significant influence on the I_{CG} index in the method proposed by Budetta (2004). On the other hand, if the I_{CG} value is multiplied by 2, the geological-geotechnical characteristic will have a larger contribution in the determination of I_{QB}.

Table 3 presents the summary of index values and total rating for each slope analyzed. The most problematic slopes in relation to rockfall hazards have larger values of I_{QB}.

In spite of the high *SMR* values, it is observed that four slopes can be considered less stable: ES-080 (1), ES-146, ES-164 e BR-259. As previously informed, the distinction between the geological characteristic indexes was only possible due to *SMR* use, which is more sensitive to changes in relation to the initial proposal of RHRS for that parameter. The RHRS original rating was modified due to two basic aspects: its evaluation is merely qualitative and it's difficult to distinguish between the crystalline rock mass being investigated. Gomes and Sobreira (2008) went into detail about this discussion.

As it can be seen in Table 3, the slope ES-164 was considered the most critical concerning rockfalls, receiving the largest I_{AT}. Besides the highway's geometric factor, due to the absence of ditch or catchment area in the basis of the slope, geotechnical factors were decisive for its classification in a critical category. The large slope height, with rockfall hazard, was the first geotechnical aspect considered in the rock mass evaluation.

The slope ES-164 has a jointing pattern that leads to loss of support at its base, favoring instability of the upper blocks. The 30° dip average of the main joint set, formed by

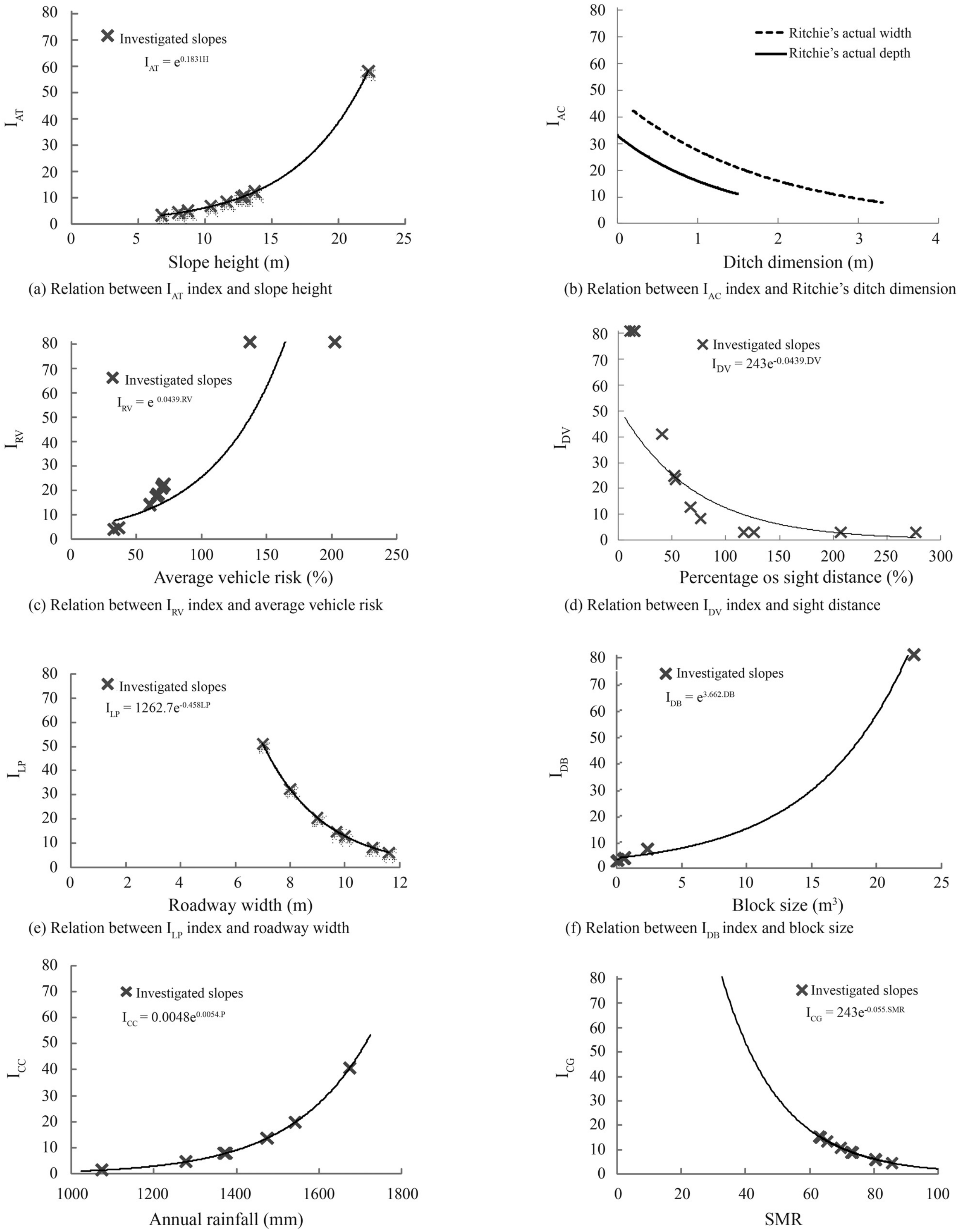

(a) Relation between I_{AT} index and slope height

(b) Relation between I_{AC} index and Ritchie's ditch dimension

(c) Relation between I_{RV} index and average vehicle risk

(d) Relation between I_{DV} index and sight distance

(e) Relation between I_{LP} index and roadway width

(f) Relation between I_{DB} index and block size

(g) Relation between I_{CC} index and climate condition

(h) Relation between I_{CG} index and SMR

Figure 3 - Relation of the eight parameters adopted in the investigated slopes. The smallest value of indexes corresponds to the best highway safety conditions.

gneiss rock banding that dips into the rock mass slope, frequently becomes smaller, due to folds or layers of different strength in the slope. However, due to different erosion rates of materials in the rock mass, several points below loosened blocks suffer erosion, creating ideal conditions for the beginning of falls. In spite of the fact that the main discontinuities, originating from gneiss banding, dip favorably (inside the slope face), there are some jointswith a dip smaller than the slope face, dipping inside it. This is relevant because this latter discontinuity pattern creates support loss for some blocks, and due to the lack of a catchment ditch, any rockfall tends to reach the pavement. Fig. 4(a) shows detail from the ES-164 slope.

Table 3 - Index values for each investigated slope.

Slope	I_{AT}	I_{AC}	I_{RV}	I_{DV}	I_{LP}	I_{DB}	I_{CC}	I_{CG}	I_{QB}
ES - 080 (1)	3.4	27.0	4.2	12.7	51.2	18.2	8.0	18.5	143.2
ES - 080 (2)	12.3	27.0	4.2	81.0	51.2	20.1	8.0	3.0	206.8
ES - 146	8.4	9.0	18.6	23.6	20.5	81.0	20.0	19.2	200.3
ES - 164	58.3	81.0	22.6	24.8	20.5	3.0	41.0	14.8	266.0
ES - 166 (1)	4.9	27.0	17.6	41.1	8.2	3.0	8.0	3.0	112.8
ES - 166 (2)	5.7	27.0	14.1	8.4	8.2	3.0	8.0	3.8	78.2
ES - 166 (3)	6.5	27.0	21.9	3.0	8.2	10.5	8.0	5.3	90.4
ES - 181	4.3	27.0	4.9	3.0	14.9	81.0	8.0	3.0	146.1
ES - 355	10.2	27.0	21.2	81.0	51.2	3.0	8.0	6.1	207.7
ES - 482	6.7	27.0	14.3	81.0	32.4	3.7	5.0	6.4	176.5
BR - 259	4.9	9.0	81.0	3.0	6.2	3.9	3.0	18.4	129.4
BR - 262	10.6	9.0	81.0	3.0	13.0	81.0	14.0	9.2	220.8

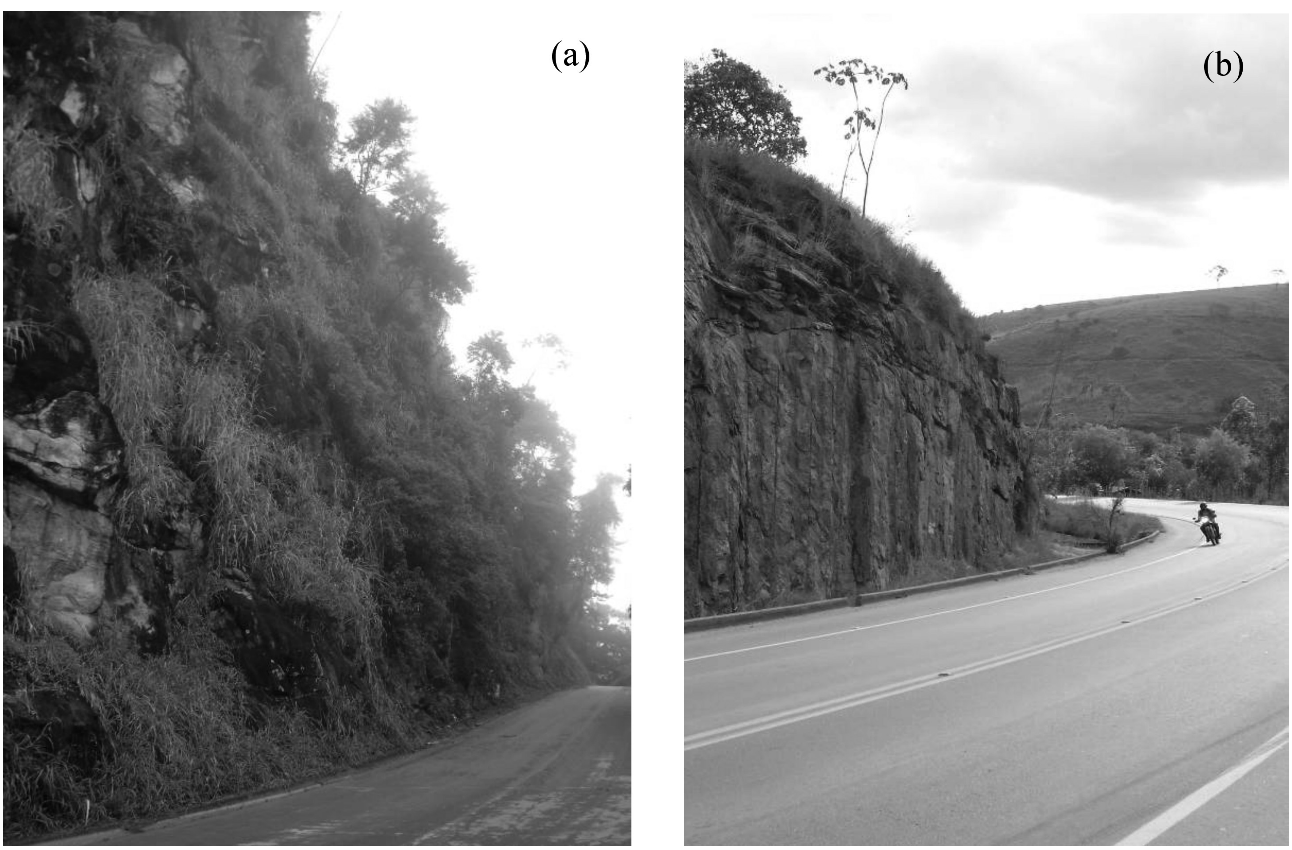

Figure 4 - (a) ES-164 slope. Due to the lack of a catchment ditch, any rockfall tends to reach the pavement. (b) BR-259 slope. Ditch designed according Ritchie's chart.

Due to a geotechnical problem, most of the catchment areas were not sized according to the Ritchie criterion for road safety. In relation to depth, only the two federal highways match Ritchie's chart. It can be observe in Fig. 4(b).

In slope ES-146, there is an abundant presence of water, even in dry periods, and its large block volumes can generate problems (Fig. 5 (a)). At the base of slope ES-355, several blocks in the ditch indicates regular rockfall problems (Fig. 5 (b)). The beginning of the slope is close to a horizontal curve and considering the traffic near the rock mass will result in high I_{DV} values.

Table 3 also displays other road segments with a high I_{QB} index. Slope ES-080 (2) has good geotechnical properties, but presents a high value for I_{QB}, related to inadequate driver-visibility distance and to unfavorable geometric characteristics.

The average dimensions of the blocks in each slope were systematized in the Table 4.

The block size index, I_{DB}, in spite of being an estimate, expressed the rockfall danger of big block failure in BR-262 slope. In this slope the only identified joint set has a large spacing. In case of another slopes, the less spaced fractures and the largest number of joint sets result in smaller block volumes, consequently the I_{DB} index decreased. Fig. 6 shows block format found in ES-166 (2) slope.

Table 4 - Values obtained for dimension of blocks and adopted terminology.

Slope	Block volume (m^3)	Description (Palmström, 1995)
ES - 080 (1)	0.496	Very large blocks
ES - 080 (2)	0.550	Very large blocks
ES - 146	2.358	Very large blocks
ES - 164	0.023	Moderate blocks
ES - 166 (1)	0.002	Small blocks
ES - 166 (2)	0.026	Moderate blocks
ES - 166 (3)	0.266	Large blocks
ES - 181	2.358	Large blocks
ES - 355	0.002	Small blocks
ES - 482	0.045	Moderate blocks
BR - 259	0.052	Moderate blocks
BR - 262	22.867	Very large blocks

Figure 5 - (a) ES-146 slope. Presence of water is constant even in dry periods. (b) ES-355 slope. Several blocks in the ditch indicates regular rockfall problems.

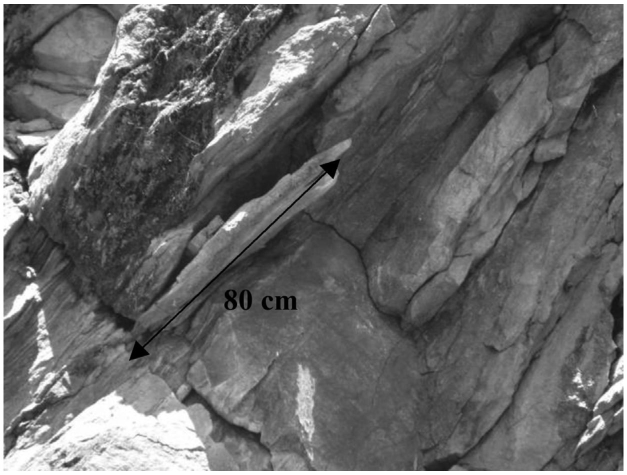

Figure 6 - Format of block in ES-166 (2) slope.

6. Proposition of Priority Interventions

The results of the classification presented in this paper can be used as a tool for road administration. Larger values of RHRS mean that the slopes must have priority in intervention measures. The proposed classification also allows ranking, for practical purposes, of the highway's characteristics that need to be improved or remedied when seeking user safety. The summary of the most critical aspects, besides interventions proposed for each rockfall section, is presented in the Table 5.

The measures to be taken were simply proposed as a way of minimizing the main problems observed in the field and confirmed after determination of the values for each parameter. The suggested measures include:

- Removal or stabilization of unstable blocks;
- Geometric improvements of the road and platform;
- Vertical warnings close to unstable slopes;
- Elaboration and execution of a rock mass stabilization project;
- Kinematic analysis for definition of potential failures.

7. Conclusions

The evaluation method proposed in this work is a preliminary tool for identifying hazardous points in highways as related to rockfall. It permits specific geotechnical diagnostics and is the first step towards problem correction in highway slopes when the problem is related to rockfalls.

Field investigations, including the application of geomechanic classification systems to crystalline rock masses that constitute the rock types studied, were very important. The geomechanical behavior of the slopes was similar, indicating that the intact rock had good geotechnical properties, in spite of the fact that most of the discontinuity orientations were unfavorable to slope stability.

The determination of the traffic and geometric characteristics of the road sections in this study was fundamental for the evaluation of the rockfall hazards. Highway rock slopes with high traffic or inadequate sight distance due to sinuous geometry should be studied carefully by the government, and appropriate interventions should be implemented in these places. This is the case of the slopes investigated in ES-355 and ES-482 roads that need geomet-

Table 5 - Summary of the most critical aspects and priority interventions proposed.

Slope	Critical(s) parameter(s)	Priorities in interventions
ES - 080 (1)	• geological characteristic	• removal or stabilization of unstable blocks
ES - 080 (2)	• decision distance	• geometric improvements of the road and platform
ES - 146	• geological characteristic • average vehicle risk • climatic condition	• removal or stabilization of unstable blocks • vertical warnings close to slopes
ES - 164	• geological characteristic • slope height • ditch effectiveness • climatic condition	• elaboration and execution of a rock mass stabilization project • geometric improvements of the road and platform • vertical warnings close to slopes
ES - 166 (1)	• ditch effectiveness	• geometric improvements of the road and platform
ES - 166 (2)	• ditch effectiveness	• geometric improvements of the road and platform
ES - 166 (3)	• ditch effectiveness	• geometric improvements of the road and platform
ES - 181	• geological characteristic	• removal or stabilization of unstable blocks
ES - 355	• sight distance	• geometric improvements of the road and platform
ES - 482	• sight distance	• geometric improvements of the road and platform
BR - 259	• geological characteristic	• removal or stabilization of unstable blocks
BR - 262	• block size	• kinematic analysis

ric improvements that would provide a safe sight distance for users.

A factor of great influence in rockfall mitigation is the existence of a ditch (catchment area). Even when the structure is not appropriately constructed, as in the vertical slopes studied, there is a great tendency for blocks to be captured by the structure between the limit of the pavement and the slope base. Road projects should contemplate a budget for the construction of that structure, which also has the important function of superficial drainage.

Rock block volume determination of the slopes can be considered the most arduous task during field surveys. It is difficult to identify some joint sets because of fractures caused during rock mass excavation. This influences the determination of joint spacing and the block shape. However, empirical relationships were used seeking the calculation of the average block dimensions because this characteristic is fundamental for rockfall hazard evaluation.

Another problem faced in this work, that is also an obstacle for most geotechnical investigations, was the difficulty of expressing a rock mass quality with a single index, due the variability of the structures, materials, etc. The studied slopes are heterogeneous, with distinct behavior in some places. Therefore, many times, it was necessary to represent the overall rock mass quality or, in some cases, the worst observed scenario. Although the index used may take into account many factors, it is not an easy task to have represented all of the rock massif complexity through one sole number, as the environment variability admits, sometimes, different values when rating the parameters which compose this index.

The method used in this research (rating system) satisfactorily represented the slope characteristics related to rockfall problems. The intervention hierarchy of the slopes matched the conditions observed in the field. The alterations proposed aimed to adapt internationally used criteria to the geotechnical and road characteristics encountered. In addition, the proposed alterations contributed to eliminate a certain subjectivity of some of the parameters.

The investigated slopes are placed in the same geological and climatic environment. This is fundamental for the viability of the application of the rockfall hazard evaluation method proposed in this research. Even though this methodology is not being used in Brazil, a highway rockfall assessment system could be adapted for the geological-geotechnical and climatic aspects presented in the area. Besides, geometric and traffic characteristics of the highway are essential parameters for these analyses, and should always be considered.

After obtaining the list of problematic roadway slopes, the government needs to implement this methodology, so that during the rehabilitation services or road restoration, the costs of improvement can be estimated.

Other geotechnical methods of slope classification can be used in the evaluation of the rockfall hazard along highways providing they are in accord with the rock mass structural model and failure conditions. Standard methods in engineering geology, like RMR and SMR, can be adapted for peculiar geomechanical conditions.

Acknowledgements

We are grateful to the Pos-graduate Program in Geotechnics of Ouro Preto Federal University (NUGEO) and to Espirito Santo Highway State Department (DER-ES) for providing the development of this study. Likewise, we are deeply grateful to CNPq for financial our research. Finally, we are grateful to the technical reviewers of this work and, last but not least, to Mr. E. Gomes for his English language review.

References

Ahrendt, A. (2005) Gravitational Mass Movements – Proposal of a Forecast System: Application in the Urban Area of Campos do Jordão – SP.DSc Thesis, Universidade de São Paulo, São Carlos, 360 pp (in Portuguese).

Bieniawski, Z.T. (1973) Engineering classification of jointed rock masses. Trans. S. Afr. Inst. Civ. Eng., v. 15:12, p. 355-3344.

Bieniawski, Z.T. (1989) Engineering Rock Mass Classifications, Wiley, New York, 251 pp.

Brawner, C.O. & Wyllie, D.C. (1975) Rock slope stability on railway projects. Proc. Am. Railway Engng Assoc., Regional Meeting, Vancouver, BC.

Budetta, P. (2004) Assessment of rockfall risk along roads. Natural Hazard and Earth System Sciences, v. 4:1, p. 71-81.

Bunce, C.M.; Cruden, D.M. & Morgenstern, N.R. (1997) Assessment of the hazard from rockfall on a highway, Can. Geotech. J., v. 34:3, p. 344-356.

National Department of Transportation (DNIT) (2006) Traffic Manual Study. IPR. Publ. n. 723, Rio de Janeiro, 384 pp. (in Portuguese).

Eliassen, T.D. & Springston, G.E. (2007). Rockfall Hazard Rating of Rock Cuts on U.S. and State Highways in Vermont. Vermont Agency of Transportation, Montpelier.

Federal Highway Administration (FHWA) (1989) Rock Slopes: Design, Excavation, Stabilization. Publication No. FHWA-TS-89-045, Turner-Fairbanks Highway Research Center, McLean, VA.

Giani, G.P. (1992) Rock Slope Stability Analysis. A.A. Balkema Publishers, Rotterdam, Netherlands.

Gomes, G.J.C. & Sobreira, F.G. (2008) Geomechanics rock slope characterization of Espirito Santo's highways, with emphasis in rockfall risk evaluation. 12° Engineering geology and environmental national congress, Ipojuca, Pe. São Paulo, v. CD ROM (in Portuguese).

Gomes, R.C. (1991) Classificação Geomecânica de Maciços Rochosos. Material Didático da Escola de Engenharia de São Carlos, Universidade de São Paulo, 37 pp.

Hadjin, D.J. (2002) New York State Department of Transportation Rock Slope Rating Procedure and Rockfall Assessment, Transportation Research Record 1786, Paper number 02-3978.

Hoek, E. (1998) Analysis of rockfall hazards. Rock Engineering, Course notes. Available at http://www.rockeng.utoronto.ca/hoekcorner.htm. Acessed January 8th, 2009.

Hoek, E. & Bray, J.W. (1981) Rock Slope Engineering. 3rd ed. IMM, London, 358 pp.

Hopkins, T.C.; Beckham, T.L.; Sun, L. & Butcher, B. (2003) Highway Rock Slope Management Program. Kentucky Transportation Center, University of Kentucky.

International Society of Rock Mechanics (ISRM) (1978) Suggested methods for the quantitative description in rock masses. Int. J. Rock Mech. Min. Sci. & Geomech. Abstr., v. 15:6, p. 319-368.

Meneses, P.R. & Paradella, W.R. (1978) Preliminar geological sintesys of Espirito Santo south part. Proc. I Brazilian National Congress of Remote Sensing, São José dos Campos, SP, v. 2 pp. 479-499 (in Portuguese).

Palmström, A. (1995) RMi – A Rock Mass Characterization System for Rock Engineering Purposes. PhD Thesis, Oslo University, Norway, 400 pp.

Pierson, L.A.; Davis, S.A. & Van Vickle, R. (1990) Rockfall Hazard Rating System – Implementation Manual, Federal Highway Administration (FHWA), Report FHWA-OR-EG-90-01, FHWA, U.S. Dep. of Transp.

Pierson, L.A. & Van Vickle, R. (1993) Rockfall Hazard Rating System, Transportation Research Record N° 1343, National Research Board, Washington, D.C., pp. 6-19.

Pierson, L.A.; Gullixon, C.F. & Chassie, R.G. (2001) Rockfall Catchment Area Design Guide Final Report. Spr-3 (032). Technical Report Form DOT F 1700.7 (8-72). Oregon, U.S.

Priest, S.D. & Hudson, J.A. (1976) Discontinuity spacing in rock. International Journal of Rock Mechanics, Mining Science & Geomechanics, cap. 13, p. 134-153.

Ritchie, A.M. (1963) Evaluation of rockfall and its control, U.S. Department of Commerce, Bureau of Public Roads, and theWashington State Highway Commission.

Romana, M. (1985) New adjustment ratings for application of Bieniawski classification to slopes. International Symposium on the Role of Rock Mechanics, Zacatecas, pp. 49-53.

Rose, B.T. (2005) Tennessee Rockfall Management System. PhD Thesis, Faculty of Virginia Polytechnic Institute and State University, Blacksburg, 100 pp.

List of symbols

AC: Clinometer height (L)
ADT: Average daily traffic
ASD: Actual sight distance (L)
CE: Cut extension (L)
D: Depth of rock catchment areas (L)
Db: Block size (L)
DSD: Designed sight distance (L)
DV: Percent of sight distance
H: Slope height (L)
I_{AC}: Ditch effectiveness parameter
I_{AT}: Slope height parameter
I_{CC}: Climate condition parameter
I_{CG}: Geologic characteristic parameter
I_{DB}: Block size parameter
I_{DV}: Sight distance parameter
I_{LP}: Roadway width parameter
I_{QB}: Rockfall hazard index
I_{RV}: Average vehicle risk parameter
J_V: Volumetric joint count (L^{-1})
LP: Roadway width (L)
n_j: Number of joint set indexes
P: Annual rainfall (L)
PSP: Posted speed limit (LT^{-1})
RV: Average vehicle risk
RMR: Rock mass rating
SMR Slope mass rating
RQD: Rock quality designation
S: Average joint spacing (L)
$S_{máx}$: Largest joint spacing (L)
S_{min}: Smallest joint spacing (L)
X: Distance of the measurement point (pavement edge) (L)
W: Width of rock catchment areas (L)
α: Angle measured by clinometer
β: Block shape factor

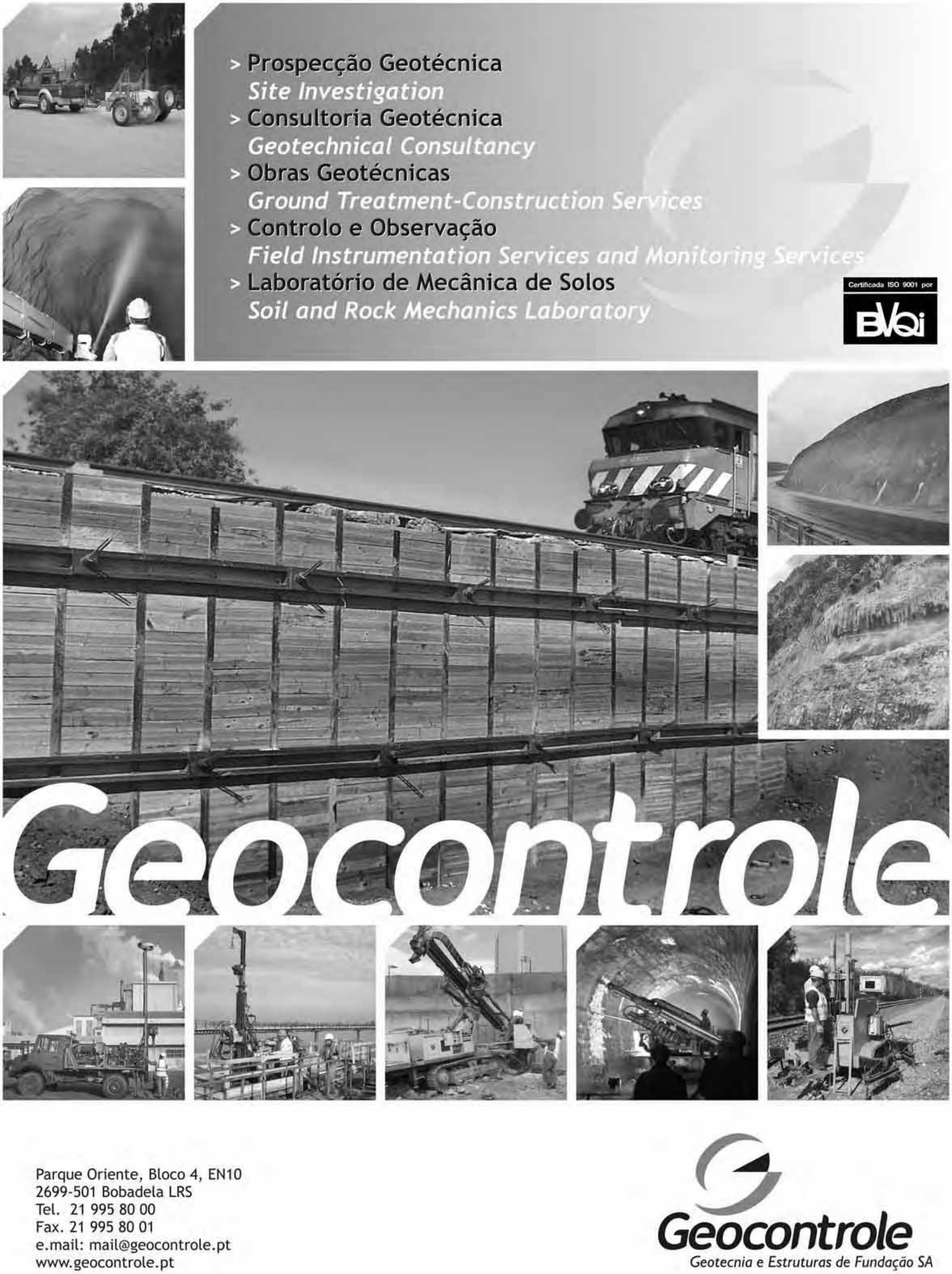
> Prospecção Geotécnica
Site Investigation
> Consultoria Geotécnica
Geotechnical Consultancy
> Obras Geotécnicas
Ground Treatment-Construction Services
> Controlo e Observação
Field Instrumentation Services and Monitoring Services
> Laboratório de Mecânica de Solos
Soil and Rock Mechanics Laboratory
Certificada ISO 9001 por
BVQi
Geocontrole
Parque Oriente, Bloco 4, EN10
2699-501 Bobadela LRS
Tel. 21 995 80 00
Fax. 21 995 80 01
e.mail: mail@geocontrole.pt
www.geocontrole.pt
Geocontrole
Geotecnia e Estruturas de Fundação SA


SPECIALISTS IN GEOTECHNICAL IN-SITU TESTS AND INSTRUMENTATION
GEOTECHNICAL SERVICES (onshore and offshore)
IN-SITU TESTS
Seismic CPT
Cone Penetration Testing Undrained-CPTu (cordless system)
Vane Shear Testing (electrical apparatus)
Pressuremeter Testing (Menard)
Flat Dilatometer Test-DMT (Machetti)
Standard Penetration Test-SPT-T
INSTRUMENTATION
Instrumentation, installation and direct import
Routine Monitoring
Operation and Maintenance
Engineering analyses
Consultancy, design & geotechnical engineering services
SAMPLING
Soil sampling and monitoring
Groundwater sampling and monitoring
Field and laboratory testing
ENVIRONMENTAL
Environmental Services
Soil and groundwater sampling and monitoring
Field and laboratory testing
0800 979 3436
São Paulo: +55 11 8133 6030
Minas Gerais: +55 31 8563 2520 / 8619 6469
www.deltageo.com.br deltageo@deltageo.com.br
DeltaGeo
Geotechnics


Geotechnic and Rehabilitation

SOILS and ROCKS
An International Journal of Geotechnical and Geoenvironmental Engineering

Publication of
ABMS - Brazilian Association for Soil Mechanics and Geotechnical Engineering
SPG - Portuguese Geotechnical Society
Volume 34, N. 2, May-August 2011

Author index

Instructions to Authors

Category of the Papers

Soils and Rocks is the scientific journal edited by the Brazilian Association for Soil Mechanics and Geotechnical Engineering (ABMS) and the Portuguese Geotechnical Society (SPG). The journal is intended to the divulgation of original research works from all geotechnical branches.

The accepted papers are classified either as an Article paper, a Technical Note, a Case Study, or a Discussion according to its content. An article paper is an extensive and conclusive dissertation about a geotechnical topic. A paper is considered as a technical note if it gives a short description of ongoing studies, comprising partial results and/or particular aspects of the investigation. A case study is a report of unusual problems found during the design, construction or the performance of geotechnical projects. A case study is also considered as the report of an unusual solution given to an ordinary problem. The discussions about published papers, case studies and technical notes are made in the Discussions Section.

When submitting a manuscript for review, the authors should indicate the category of the manuscript, and is also understood that they:

a) assume full responsibility for the contents and accuracy of the information in the paper;

b) assure that the paper has not been previously published, and is not being submitted to any other periodical for publication.

Manuscript Instructions

Manuscripts must be written in English. The text is to be typed in a word processor (MS Word or equivalent), using ISO A4 page size, left, right, top, and bottom margins of 25 mm, Times New Roman 12 font, and line spacing of 1.5. All lines and pages should be numbered. The text should be written in the third person.

The fist page of the manuscript is to include the title of the paper in English, followed by the names of the authors with the abbreviation of the most relevant academic title. The affiliation, address and e-mail is to be indicated below each author's name. An abstract of 200 words is to be written in English after the author's names. A list with up to six keywords at the end of the abstract is required.

Although alteration of the sequence and the title of each section may be required, it is suggested that the text contains the following sections: Introduction, Material and Methods, Results, Discussions, Conclusion, Acknowledgements, References and List of Symbols. A brief description of each section is given next.

Introduction: This section should indicate the state of the art of the problem under evaluation, a description of the problem and the methods undertaken. The objective of the work is to be clearly presented at the end of the section.

Materials and Methods: This section should include all information needed to the reproduction of the presented work by other researchers.

Results: In this section the data of the investigation should be presented in a clear and concise way. Figures and tables should not repeat the same information.

Discussion: The analyses of the results should be described in this section. **Conclusions**: The text of this section should be based on the presented data and in the discussions.

Acknowledgenments: If necessary, concise acknowledgements should be written in this section.

References: References to other published sources are to be made in the text by the last name(s) of the author(s), followed by the year of publication, similarly to one of the two possibilities below:

"*while Silva & Pereira (1987) observed that resistance depended on soil density*" or "*It was observed that resistance depended on soil density (Silva & Pereira, 1987).*"

In the case of three or more authors, the reduced format must be used, *e.g.*: Silva *et al.* (1982) or (Silva *et al.*, 1982). Two or more citations belonging to the same author(s) and published in the same year are to be distinguished with small letters, *e.g.*: (Silva, 1975a, b, c.). Standards must be cited in the text by the initials of the entity and the year of publication, *e.g.*: ABNT (1996), ASTM (2003).

Full references shall be listed alphabetically at the end of the text by the first author's last name. Several references belonging to the same author shall be cited chronologically. Some examples are listed next:

Papers: Bishop, A.W. & Blight, G.E. (1963) Some aspects of effective stress in saturated and unsaturated soils. Géotechnique, v. 13:2, p. 177-197.

Books: Lambe, T.W & Whitman, R.V. (1979) Soil Mechanics, SI Version, 2nd ed. John Wiley & Sons, New York, p. 553.

Book with editors: Sharma, H.D.; Dukes, M.T. & Olsen, D.M. (1990) Field measurements of dynamic moduli and Poisson's ratios of refuse and underlying soils at a landfill site. Landva A. & Knowles, G.D. (eds) Geotechnics of Waste Fills - Theory and Practice, American Society for Testing and Materials - STP 1070, Philadelphia, p. 57-70.

Proceedings (printed matter or CD-ROM): Jamiolkowski, M.; Ladd, C.C.; Germaine, J.T & Lancellotta, R. (1985) New developments in field and laboratory testing of soils. Proc. 11th Int. Conf. on Soil Mech. and Found. Engn., ISSMFE, San Francisco, v. 1, pp. 57-153.(specify if CD – ROM)

Thesis and dissertations: Lee, K.L. (1965) Triaxial Compressive Strength of Saturated Sands Under Seismic Loading Conditions. PhD Dissertation, Department of Civil Engineering, University of California, Berkeley, 521 p.

Standards: ASTM (2003) Standard Test Method for Particle Size Analysis of Soils - D 422-63. ASTM International, West Conshohocken, Pennsylvania, USA, 8 p.

Internet references: Soils and Rocks available at http://www.abms.com.br.

On line first publications must also bring the digital object identifier (DOI) at the end.

Figures shall be either computer generated or drawn with India ink on tracing paper. Computer generated figures must be accompanied by the corresponding digital file (.tif, .jpg, .pcx, etc.). All figures (graphs, line drawings, photographs, etc.) shall be numbered consecutively and have a caption consisting of the figure number and a brief title or description of the figure. This number should be used when referring to the figure in text. Photographs should be black and white, sharp, high contrasted and printed on glossy paper.

Tables shall be numbered consecutively in Arabic and have a caption consisting of the table number and a brief title. This number should be used when referring to the table in text. Units should be indicated in the first line of the table, below the title of each column. Abbreviations should be avoided. Column headings should not be abbreviated. When applicable, the units should come right below the corresponding column heading. Any necessary explanation can be placed as footnotes.

Equations shall appear isolated in a single line of the text. Numbers identifying equations must be flush with the right margin. International System (SI) units are to be used. The symbols used in the equations shall be listed in the List of Symbols. It is recommended that the used symbols be in accordance with Lexicon in 8 Languages, ISSMFE (1981) and the ISRM List of Symbols.

The text of the submitted manuscript (including figures, tables and references) intended to be published as an article paper or a case history should not contain more than 30 pages formatted according to the instructions mentioned above. Technical notes and discussions should have no more than 15 and 8 pages, respectively. Longer manuscripts may be exceptionally accepted if the authors provide proper explanation for the need of the required extra space in the cover letter.

Discussion

Discussions must be written in English. The first page of a discussion paper should contain:

• The title of the paper under discussion in the language chosen for publication;

• Name of the author(s) of the discussion, followed by the position, affiliation, address and e-mail. The discusser(s) should refer himself (herself, themselves) as "the discusser(s)" and to the author(s) of the paper as "the author(s)".

Figures, tables and equations should be numbered following the same sequence of the original paper. All instructions previously mentioned for the preparation of article papers, case studies and technical notes also apply to the preparation of discussions.

Editorial Review

Each paper will be evaluated by reviewers selected by the editors according to the subject of the paper. The authors will be informed about the results of the review process. If the paper is accepted, the authors will be required to submit a version of the revised manuscript with the suggested modifications. If the manuscript is refused for publication, the authors will be informed about the reasons for rejection. In any situation comprising modification of the original text, classification of the manuscript in a category different from that proposed by the authors, or refusal for publication, the authors can reply presenting their reasons for disagreeing with the reviewers' comments

Submission

The author(s) must submit for review:

1. A hard copy of the manuscript to Editors - Soils and Rocks, Av. Prof. Almeida Prado, 532 – IPT, Prédio 54 – DEC/ABMS, 05508-901 - São Paulo, SP, Brazil. The first page of the manuscript should contain the identification of the author(s), or

2. The digital file of the manuscript, omitting the authors' name and any information that eventually could identify them, should be sent to **abms@ipt.br**. The following must be written in the subject of the e-mail message: "*Paper submitted to Soils and Rocks"*. The authors' names, academic degrees and affiliations should be mentioned in the e-mail message. The e-mail address from which the digital file of the paper was sent will be the only one used by the editors for communication with the corresponding author.

Follow Up

Authors of manuscripts can assess the status of the review process at the journal website (www.soilsandrocks.com.br) or by contacting the ABMS secretariat.

Volume 34, N. 2, May-August 2011

Table of Contents